Chapter 7B. Analysis of Imaging Spectrometer Data for the Haji-Gak Area of Interest

By K. Eric Livo and Stuart A. Giles

Abstract

Imaging spectrometer data of the Haji-Gak area of interest (AOI) in the central-northeastern part of Afghanistan were analyzed using spectrum matching techniques to identify the distribution of selected materials at the surface. Characteristic absorption features (absorption bands) in the HyMap data were compared to a library of spectral standards. Wallrock mineralogy was detected in the HyMap data that is permissive for hosting iron ores and barite mineralization.

A sequence of Proterozoic and Paleozoic age rocks hosts known iron deposits. Spectrally mapped minerals within the host rock associated with this iron mineralization may be traced from the Haji-Gak deposits on the southwest extending northeastward through the AOI. Barite is associated with a group of spectrally mapped minerals within Ordovician age rocks in the northeastern part of the AOI.

7B.1 Introduction

Previous U.S. Geological Survey (USGS) analyses of existing geologic data of Afghanistan revealed numerous areas with indications of potential mineral resources of various types (Peters and others, 2007). From these areas of interest, several were selected for follow-on studies using modern hyperspectral remote sensing data to characterize surface materials. One of those areas is the Haji-Gak area in central-northeastern Afghanistan.

The Haji-Gak area of interest (AOI) is in the Bamyan and Wardak Provinces and extends northeastward into the Parwan Province (fig. 7B–1). The AOI contains Middle Proterozoic sedimentary rocks that host the Haji-Gak iron-oxide deposit and have the potential for iron, barite, lead-zinc, limestone, and sandstone deposits (Abdullah and others, 1977; Peters and others, 2007).

To help assess these potential resources, high-resolution imaging spectrometer data were analyzed to detect the presence of selected minerals that may be indicative of past mineralization processes. This report contains the results of those analyses and identifies numerous sites within the Haji-Gak area that merit further investigation, especially detailed geological mapping and geochemical studies.

7B.1.1 Hyperspectral Data Collection and Processing

In 2007, imaging spectrometer data were acquired over most of Afghanistan as part of the USGS project "Oil and Gas Resources Assessment of the Katawaz and Helmand Basins." These data were collected to characterize surface materials in support of assessments of resources (coal, water, minerals, and oil and gas) and earthquake hazards in the country (King and others, 2010). Imaging spectrometers measure the reflectance of visible and near-infrared light from the Earth's surface in many narrow channels, producing a reflectance spectrum for each image pixel. These reflectance spectra can be interpreted to identify absorption features that arise from specific chemical transitions and molecular bonds that provide compositional information about surface materials. Imaging spectrometer data can only be used to characterize the upper surface materials and not subsurface composition or structure. However, subsurface processes can be indicated by the distribution of surface materials that can be detected using imaging spectroscopy data.

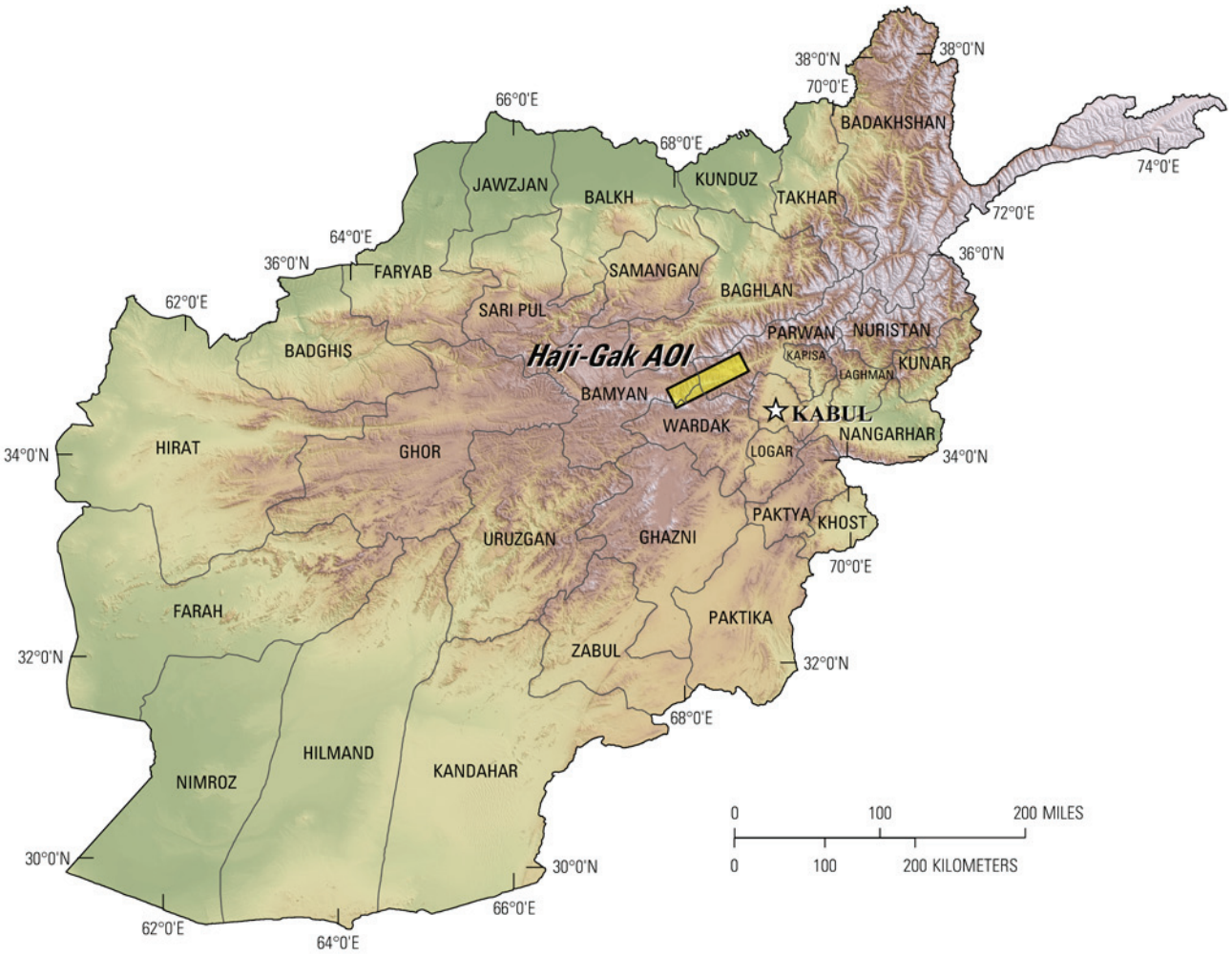

Figure 7B–1. The Haji-Gak area of interest is located about 100 kilometers west of Kabul in Bamyan, Wardak, and Parwan Provinces.

7B.1.2 Collection of Imaging Spectrometer Data

The HyMap imaging spectrometer (Cocks and others, 1998) was flown over Afghanistan from August 22 to October 2, 2007 (Kokaly and others, 2008). HyMap has 512 cross-track pixels and covers the wavelength range 0.43 to 2.48 micrometers (μm) in 128 channels. The imaging spectrometer was flown on a WB-57 high-altitude aircraft at approximately 50,000 ft. There were 207 standard data flight lines and 11 cross-cutting calibration lines collected over Afghanistan for a total of 218 flight lines, covering a surface area of 438,012 km^2 (Kokaly and others, 2008). Data were received in scaled radiance form (calibrated to National Institute of Standards and Technology reference materials). Before processing, four channels that had low signal-to-noise ratios and (or) were in wavelength regions overlapped by adjacent detectors were removed from the Hymap data (image cubes). Each flight line was georeferenced to Landsat base imagery in UTM projection (Davis, 2007).

7B.1.3 Calibration Process

HyMap data were converted from radiance to reflectance using a multi-step calibration process. This process removed the influence of the solar irradiance function, atmospheric absorptions, and residual instrument artifacts, resulting in reflectance spectra that have spectral features that arise from the material composition of the surface. Because of the extreme topographic relief and restricted access to ground-calibration sites, modifications to the standard USGS calibration procedures (Clark and

others, 2003a) were required to calibrate the 2007 Afghanistan HyMap dataset (Hoefen and others, 2010). In the first step of the calibration process, the radiance data were converted to apparent surface reflectance using the radiative transfer correction program Atmospheric CORrection Now (ACORN; ImSpec LLC, Palmdale, Calif.). ACORN was run multiple times for each flight line, using average elevations in 100-m increments, covering the range of minimum to maximum elevation within the flight line. A single atmospherically corrected image was assembled from these elevation-incremented ACORN results. This was done by determining the elevation of each HyMap pixel and selecting the atmospherically corrected pixel from the 100-m increment closest to that elevation.

Each assembled atmospherically corrected image was further empirically adjusted using ground-based reflectance measurements from a ground-calibration site. Five ground-calibration spectra were collected in Afghanistan: field spectra at Kandahar Air Field, Bagram Air Base, and Mazar-e-Sharif Airport, as well as laboratory spectra of soil samples from two fallow fields in Kabul. At each site, the average field spectrum of the ground target was used to calculate an empirical correction factor using the pixels of atmospherically corrected HyMap data in the flight lines that passed over the site. Subsequently, each of the HyMap flight lines was ground-calibrated using the empirical correction from the closest calibration site.

To further improve the data quality, an additional calibration step was taken to address the atmospheric differences caused, in part, by the large distances between the calibration sites and the survey areas. The large distances were a result of the lack of safe access to ground-calibration sites. The duration of the airborne survey and variation in time of day during which flight lines were acquired also resulted in differences in atmospheric conditions between standard flight lines and lines over ground-calibration sites. Over the course of the data collection, the sun angle, atmospheric water vapor, and atmospheric scattering differed for each flight line. To compensate for this, cross-cutting calibration flight lines over the ground-calibration areas were acquired (Kokaly and others, 2008) and used to refine the reflectance calculation for standard data lines. A multiplier correction for standard data lines, typically oriented as north-south flight lines, was derived using the pixels of overlap with the well-calibrated cross-cutting lines, subject to slope, vegetation cover, and other restrictions on pixel selection (Hoefen and others, 2010). As a result, the localized cross-calibration multiplier, derived from the overlap region, reduced residual atmospheric contamination in the imaging spectrometer data that may have been present after the ground-calibration step.

7B.1.4 Materials Maps and Presentation

After undergoing the above calibration process, the georeferenced and calibrated reflectance data were processed. The reflectance spectrum of each pixel of HyMap data was compared to the spectral features of reference entries in a spectral library of minerals, vegetation, water, and other materials (King, Kokaly, and others, 2011; Kokaly and others, 2011). The best spectral matches were determined for each pixel, and the results were clustered into classes of materials discussed below.

HyMap reflectance data were processed using the MICA (Material Identification and Characterization Algorithm), a module of the U.S. Geological Survey PRISM (Processing Routines in Interactive Data Language (IDL) for Spectroscopic Measurements) software (Kokaly, 2011). The MICA analysis compared the reflectance spectrum of each pixel of HyMap data to entries in a reference spectral library of minerals, vegetation, water, and other materials. The MICA spectral comparison technique is partly derived from the Tetracorder spectral identification system (Clark and others, 2003b). The HyMap data were compared to 97 reference spectra of well-characterized mineral and material standards. The resulting maps of material distribution, resampled to 23 × 23 meter square pixel grid, were mosaicked to create thematic maps of surface mineral occurrences over the full dataset covering Afghanistan.

MICA was applied to HyMap data twice to present the distribution of two categories of minerals that are naturally separated in the wavelength regions of their primary absorption features. MICA was applied using the subset of minerals with absorption features in the visible and near-infrared wavelength

region, producing a 1-µm map of iron-bearing minerals and other materials (King, Kokaly, and others, 2011), and again using the subset of minerals with absorption features in the shortwave infrared, producing a 2-µm map of carbonates, phyllosilicates, sulfates, altered minerals, and other materials. For clarity of presentation, some individual classes in these two maps were bundled by combining selected mineral types (for example, all montmorillonites or all kaolinites) and representing them with the same color in order to reduce the number of mineral classes. The iron-bearing minerals map has 28 classes. Iron-bearing minerals with different mineral compositions but similar broad spectral features are difficult to classify as specific mineral species. Thus, generic spectral classes, including several minerals with similar absorption features, such as Fe^{3+} Type 1 and Fe^{3+} Type 2, are depicted on the map. The carbonates, phyllosilicates, sulfates, and altered minerals map has 32 classes. Minerals with slightly different compositions but similar spectral features are less easily discriminated; thus, some identified classes consist of several minerals with similar spectra, such as the chlorite or epidote class. When comparisons with reference spectra provided no viable match, a designation of "not classified" was assigned to a pixel.

7B.2 Geologic Setting of the Haji-Gak Area of Interest

The Haji-Gak area of interest is located in the Bamyan, Wardak, and Parwan Provinces of Afghanistan (fig. 7B–1). A large anomalous crustal block within the central tectonized zone, with deep valleys on all four sides, hosts the AOI. Elevations range from 1,900 to 4,962 m (fig.7B–2). The Haji-Gak area of interest is approximately 2,079.29 km^2 . Within this AOI are three subareas: Haji-Gak Prospect (180 km^2), Northeast Haji-Gak (381 km^2), and Farenjal (557 km^2) subareas (see fig. 7B–5). Numerous faults and fractures of different orientations and extent occur in the AOI (fig. 7B–3). Within the Haji-Gak AOI, the most prominent faults strike northeast to southwest, with younger faults trending north-south and northwest-southeast, which juxtaposed Middle Proterozoic, Late Proterozoic, and late Paleozoic age rocks during the Cretaceous (Kusov and others, 1965).

7B.2.1 Lithology and Structure

The Haji-Gak area of interest contains metavolcanic and metasedimentary rocks of Middle to Late Proterozoic age, as well as Paleozoic and Tertiary age rocks (fig. 7B–4). The Middle Proterozoic Jawkol Formation, consisting of limestones, dolomites, schists, and quartzites, has been metamorphosed to amphibolite grade and is the oldest part of the stratigraphic succession. These rocks outcrop in the northwestern part of the Haji-Gak AOI. Late Proterozoic Kab Formation and the overlying Awband Formation form the Qala Series of metavolcanic and metasedimentary rocks that are interpreted as being deposited within a marine basin (Kusov and others, 1965). According to Kusov and others (1965), the Kab Formation is composed of sericite schists, phyllite, volcanic rocks, and marble. The Awband Formation contains quartz-sericite and quartz-chlorite-sericite schists, along with cherts and marbles. The Awband hosts most of the iron deposits that are postulated as being sedimentary exhalative iron-rich fluids that formed lenses on the sea floor during times of increased volcanic activity (Peters and others, 2007). Above the Qala Series is the Late Proterozoic Green Schist Formation, which comprise chlorite schists and quartz-sericite schists that host lesser iron mineralization. Southeast of the Proterozoic rocks, Devonian to Mississippian limestones, conglomerates, sandstones, and pelagic schists and Permian rocks are in fault contact. The northeast region of the AOI contains Mississippian, Ordovician, and Silurian to Devonian rocks in fault contact with the northeastern extent of the Proterozoic rocks (Abdullah and Chymriov, 1977; Doebrich and others, 2006).

During the Cretaceous, displacement along the Herat fault zone has juxtaposed Middle Proterozoic, Late Proterozoic, and upper Paleozoic rocks, forming the northeast-trending Haji-Gak anticline that hosts the iron deposits on the exposed southeast limb within the Late Proterozoic units (Kusov and others, 1965). The predominant strike at the Haji-Gak deposit is to the northeast with a regional dip of 50° to the southeast. The Haji-Gak iron deposits occur in the southwest region

(Haji-Gak Prospect subarea, fig. 7B–5) and similar mineralization to the known iron deposits is exposed to the northeast along a high ridge (Northeast Haji-Gak subarea, fig. 7B–5; Doebrich and others, 2006; as mapped using HyMap data), and is fault truncated (pinched out) on the northeast end (Farenjal subarea: fig. 7B–5; Doebrich and others, 2006).

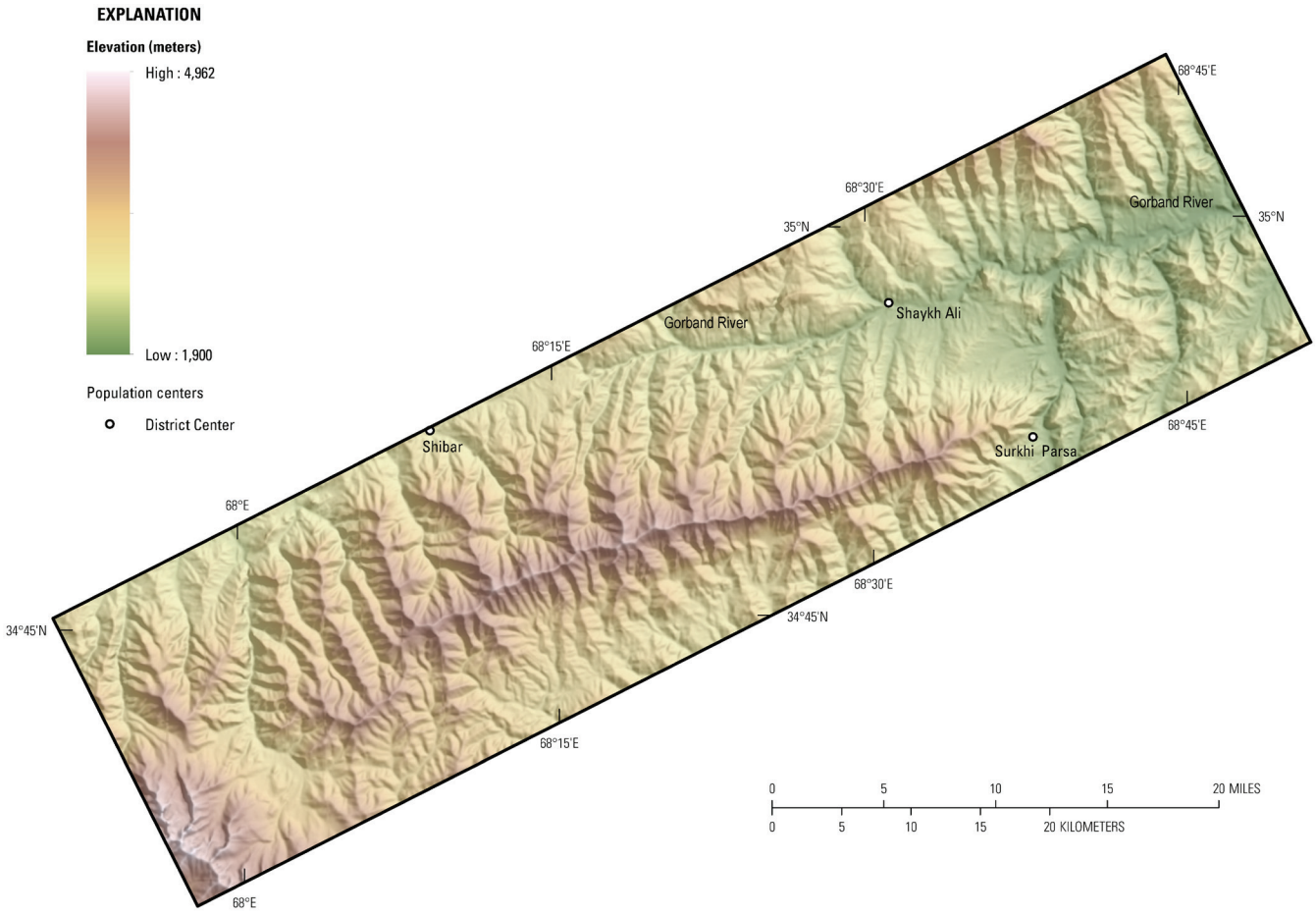

Figure 7B–2. Shaded-relief map showing elevations in the Haji-Gak area of interest (AOI). The darker brown tones indicate the higher elevations, and the lower elevations are represented by the green tones. The AOI is drained by several rivers, principally the Gorband River and its southern tributary.

7B.2.2 Known Mineralization

Table 7B–1. Deposit name, deposit type, mineralogy, and alteration of the known sites of mineralization in the Haji-Gak area of interest.

[unk, unknown]

Name	Deposit type	Mineralogy	Gangue	Alteration
Hajigak	unk stone	No data	No data	–
Haji-Gak Sandstone	unk sandstone	No data	No data	–
Haji-Gak Silica	silica			–
Haji-Gak Barite	vein barite	Barite	Quartz; sericite	Baritization
Haji-Gak Limestone	limestone			
Haji-Gak Iron	unk Fe	Pyrite; magnetite; hydrogoethite; martite; hematite	Carbonate; siderite; quartz; barite	Carbonatization; silicification; sericitization; chloritization
Chapkul	vein barite	Barite	Quartz; sericite	Baritization

Name	Deposit type	Mineralogy	Gangue	Alteration
Harzar	unk Fe	Hematite; magnetite; martite	No data	_
	vein barite	Barite	Quartz; sericite	Baritization
Rokul Khaish	unk Fe	Hematite; magnetite	Sericite; chlorite; carbonate	_
Sausang	unk Fe	Hematite; magnetite	Quartz; chlorite	_
Chuy	unk Fe	Hematite; magnetite	Quartz; chlorite	_
Zarak	vein barite	Barite	No data	Baritization
Unnamed	unk W	Pyrite; galena; scheelite; chalcopyrite; gold native	No data	_
Zerak	unk Fe	Hematite; magnetite	Quartz; dolomite	Dolomitization; silicification
Unnamed	unk Fe	Hematite; magnetite; galena	Barite	_
Surkh-i-Parso	unclassified	Chalcopyrite; uranite	Quartz	Marmorization; silicification
Dara-i-Neel	unk Fe	Martite	No data	_
Tanghi-Loli	unk Ba	Barite	No data	_
Unnamed	unk Ba	Barite	No data	Baritization
Farenjal Talc	ultramafic-hosted talc	Talc; serpentine	No data	Talc alteration; overprinting serpentinization
Farenjal Manganese	unk Mn	Pyrolusite; psilomelane; hematite	No data	_
Farenjal Barite	bedded barite	Barite; witherite; chalcopyrite; pyrite; galena	Quartz; calcite	Baritization
Northern Farenjal	vein barite	Barite	No data	Baritization
Unnamed	unk Ba	Barite; galena	No data	Baritization
Unnamed	unk Ba	Barite	No data	Baritization

7B.3 Mineral Maps of the Haji-Gak Area of Interest

Analysis of the HyMap data of the Haji-Gak AOI using spectral mapping techniques resulted in the identification of a variety of surficial minerals. These minerals have been identified on the presence and wavelength position of absorption features in the 0.45–2.48 μm wavelength region. Two general categories of minerals are recognized: (1) iron-bearing minerals that have characteristic spectral absorption features that occur at wavelengths near 1 μm, and (2) a wide variety of minerals, including carbonates, mica and clay minerals, and sulfates that have diagnostic spectral absorptions near 2 μm. Although the occurrence of certain minerals may suggest mineralization processes may have operated in the area, many of the minerals identified and mapped are also common rock-forming minerals or minerals that can be derived from the weathering of a variety of rock types. Consequently, the distribution patterns of the identified minerals and the geologic content where they occur are extremely important in understanding the causes of the mapped mineral occurrences and assessing the possible potential for related mineral deposits.

Two general types of hyperspectral maps are included: (1) complete AOI maps showing the entire mapped suite of minerals that have absorption in 1-µm and 2-µm wavelengths, and (2) topical maps that are subsets of the mineral classes. The topical maps, which depict selected groups of minerals that are mineralogically related or commonly occur together, are presented to show subtleties in the mineral distribution. A set of maps has been produced for the full Haji-Gak AOI and each of the subareas. It should be noted that geographic registration between various datasets is not always possible, because of differences in collection methods and resolution. A companion report and geodatabase of potential mineral resource anomalies (areas of a potential economic mineral resource occurrence) that were not previously known or where the HyMap data has expanded our knowledge of the region can be found in King, Johnson, and others (2011).

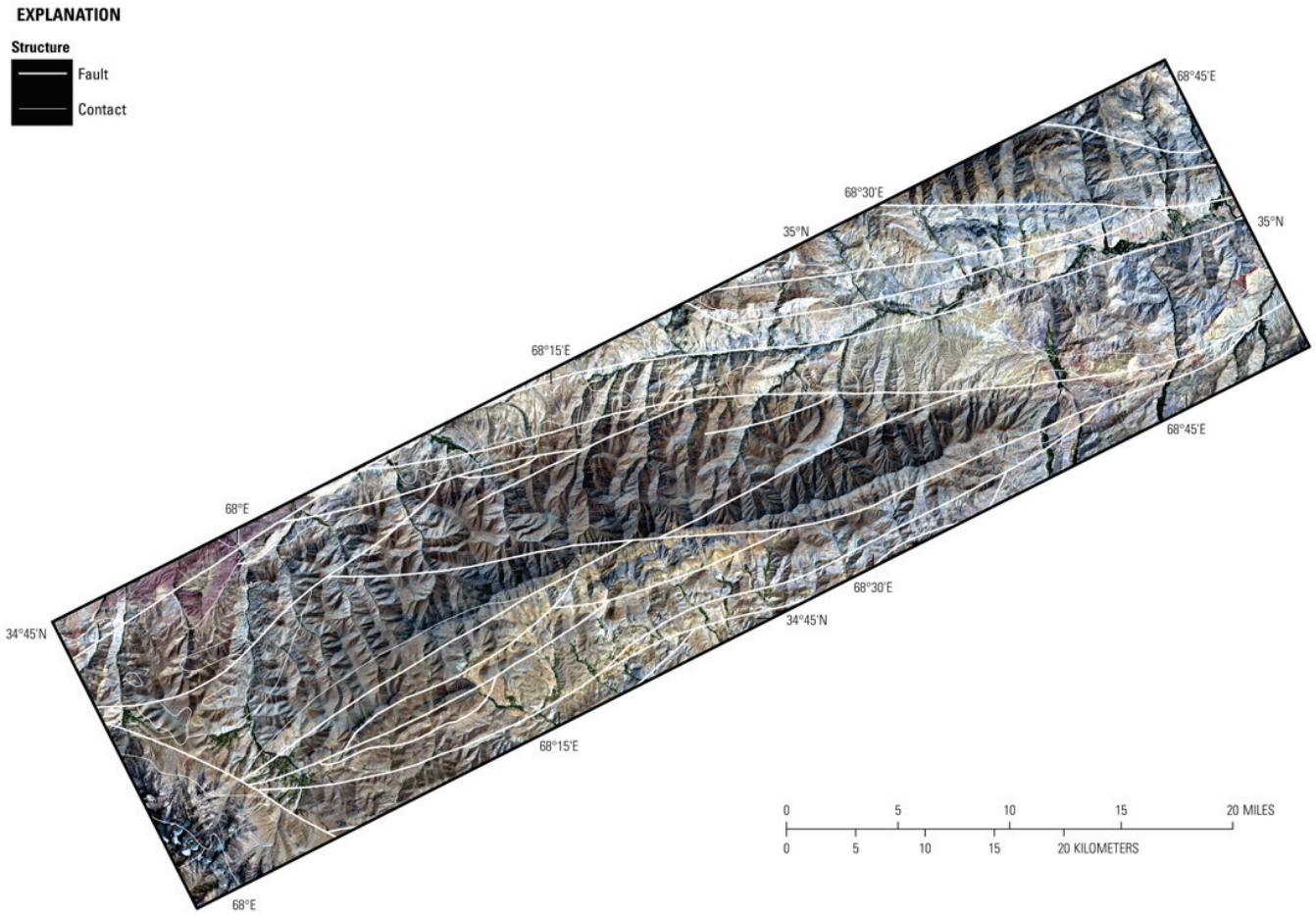

Figure 7B–3. Numerous faults and fractures of different orientations and extent occur within the Haji-Gak area of interest. The fault traces (Doebrich and others, 2006) are placed on a Landsat Thematic Mapper image (Davis, 2007).

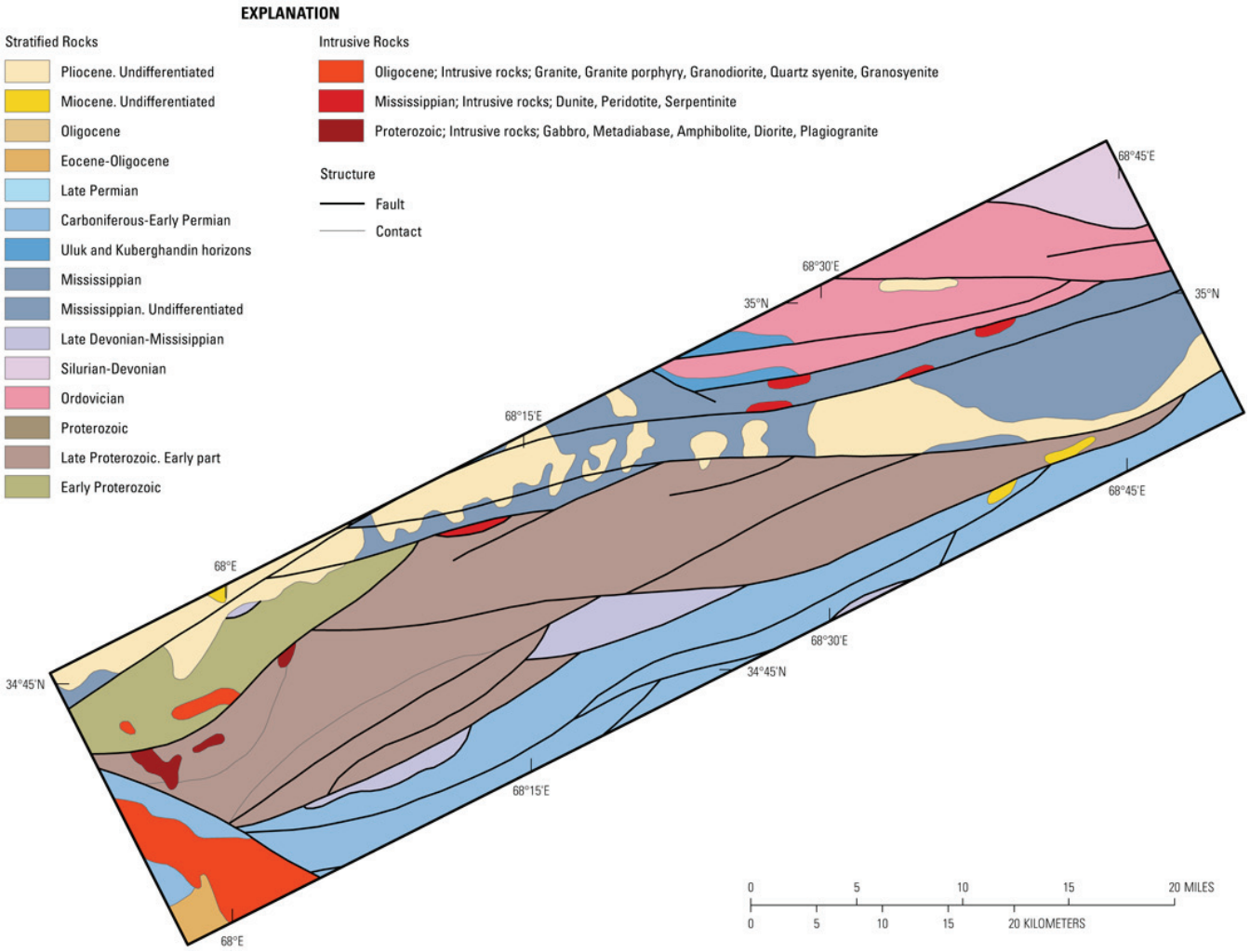

Figure 7B–4. The geologic map of the Haji-Gak area of interest (AOI) is from the 1:500,000-scale geologic map of Afghanistan (Dronov and others, 1972). A series of intrusive rocks are exposed in the northern part of the AOI along the secondary fault traces and also in the southwest adjacent to a major secondary fault.

7B.3.1 Haji-Gak Area of Interest

Figures 7B–6 and 7B–7 shows the distribution of carbonates, phyllosilicates, sulfates, altered minerals, and other materials (30 possible classes) and the Fe-bearing minerals (27 possible classes), respectively, for the entire Haji-Gak AOI. HyMap data are also a powerful tool to use in the identification and mapping of faults and fractures (see fig. 7B–9); note the correlation between mapped minerals and fault traces. Because of the large number of mineral classes represented and the subtleties of the distribution patterns in these maps, it is more instructive to display these results as a series of topical images depicting a group of minerals that are commonly related or occur together in special geologic environments (figs. 7B–8 to 7B–12). Figure 7B–8 shows the distribution of carbonate minerals in the AOI, whereas figure 7B–9 shows where the clays and micas were mapped. The distribution of iron-oxide and iron-hydroxide minerals are displayed in figure 7B–10. Secondary minerals are shown in figure 7B–11, and minerals commonly found in hydrothermally altered rocks are mapped in figure 7B–12.

Spectrally mapped minerals (1- and 2-µm wavelengths; figs. 7B–7 and 7B–6) correlate with the field-mapped lithologies of the Haji-Gak Proterozoic stratigraphic succession that form the diagenetic hanging and footwalls of the sedex iron-oxide deposits (most clearly seen in the mineral maps of the Haji-Gak iron deposit in the Haji-Gak Prospect subarea; fig. 7B–5) located in the southwestern part of the AOI. Upward through the sequence (trending southeast, perpendicular to strike in the image; see

fig. 7B–6), scattered carbonate pixels are associated with regions containing the Middle Proterozoic Jawkol Formation (limestone and dolomite). Ferrous and ferric (goethite) iron (see fig. 7B–7), muscovite (sericite or illite), and possibly kaolinite pixels trend within regions containing the Late Proterozoic Qala Series (Kab and Awband Formations; see fig. 7B–6) that hosts the majority of iron deposits (sericite, quartz-sericite, and quartz-chlorite schists, phyllite, volcanic rocks, and minor chert and marble; Kusov and others, 1965; Renaud and others, chap. 7A, this volume). Stratigraphically higher (to the southeast), the Green Schist Formation (chlorite schists and quartz-sericite schists) also hosts iron deposits, though to a lesser extent, and is mapped using epidote/chlorite and serpentine mineral pixels (see fig. 7B–6 and Haji-Gak Prospect subarea section). Paleozoic limestones are located to the southeast and were identified by the presence of an abundant calcite zone (lat 34°45'N., long 68°12'W.) that trends along strike to the northeast. This sequence of rocks is spectrally mapped trending northeast through the length of the bottom half of the AOI. It forms the southeast limb of the Haji-Gak anticline, along the ridgeline of the host block.

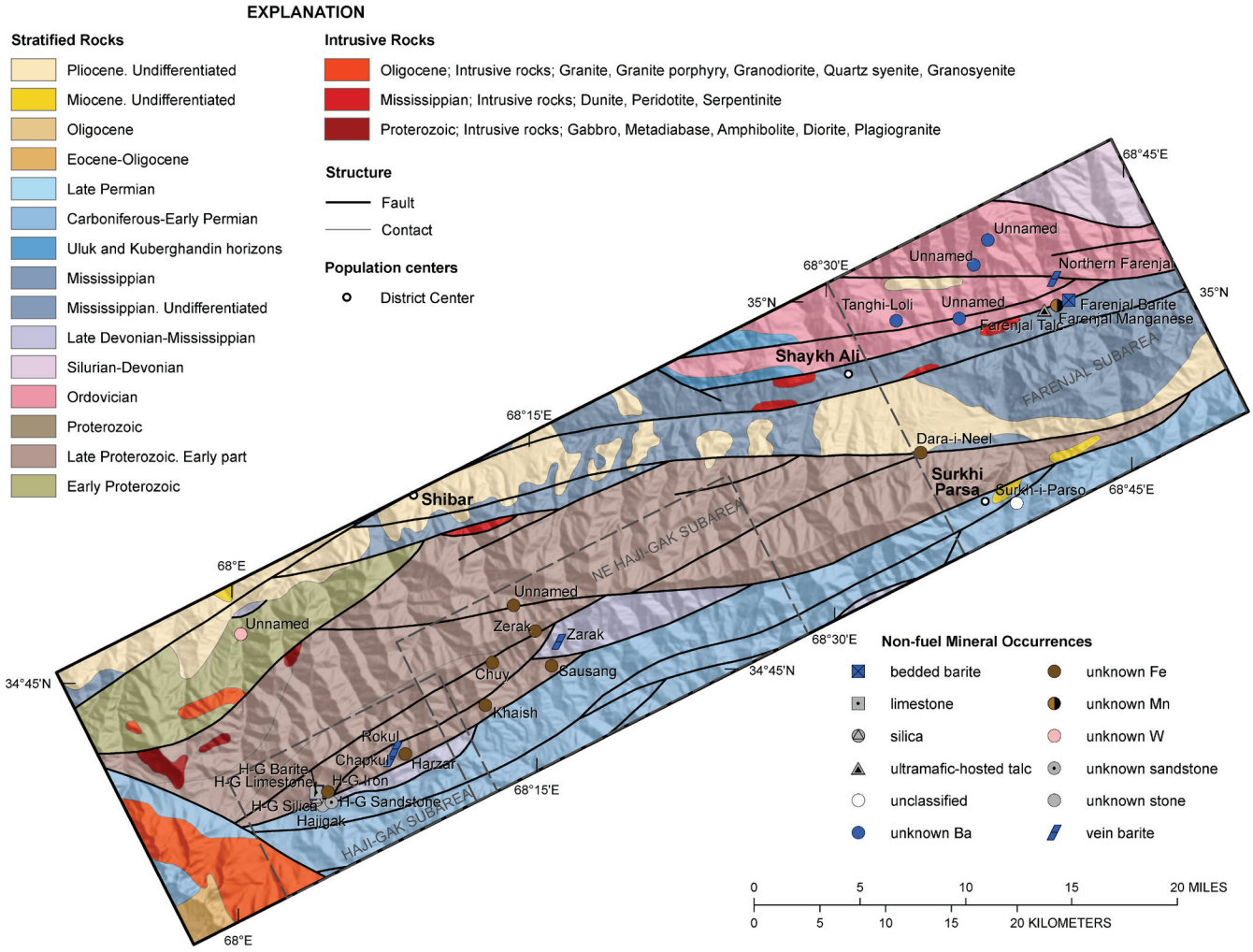

Figure 7B–5. This map shows the location of known mineral occurrences in the Haji-Gak area of interest (AOI). The map consists of four data layers: shaded-relief base map, transparency of the geologic map (Dronov and others, 1972), fault traces (Peters and others, 2007), and known mineral occurrences (Abdullah and others, 1977). The map shows the overall AOI and three subareas: Haji-Gak Prospect, Northeast Haji-Gak, and Farenjal subareas.

7B.3.1.1 Carbonate Minerals

The calcite and calcite + muscovite/illite groups follow the southern edge of the major trend of iron-oxide deposits that occur at the western end of the image and projects eastward throughout the mapped area (fig. 7B–8). These groups potentially define the Paleozoic limestones above the iron-oxide zone that were deposited after the iron was precipitated on the sea floor. Additional calcite was mapped to the far northeast and north, trending within or near Paleozoic rocks, especially within the Uluk and Kuberghandin horizons (fig. 7B–5).

7B.3.1.2 Clays and Micas

The phyllosilicates are the most dominant group of minerals mapped in the AOI (fig. 7B–9). Muscovite (sericite) and illite group minerals are widespread. Chlorite or epidote group minerals, when present, occur primarily in the Proterozoic greenstones (Green Schist Formation) in the western part of the AOI and in Ordovician rocks in the northeastern part of the AOI. Chlorite or epidote are anomalous just northwest of the Haji-Gak deposits, within the Proterozoic sequence.

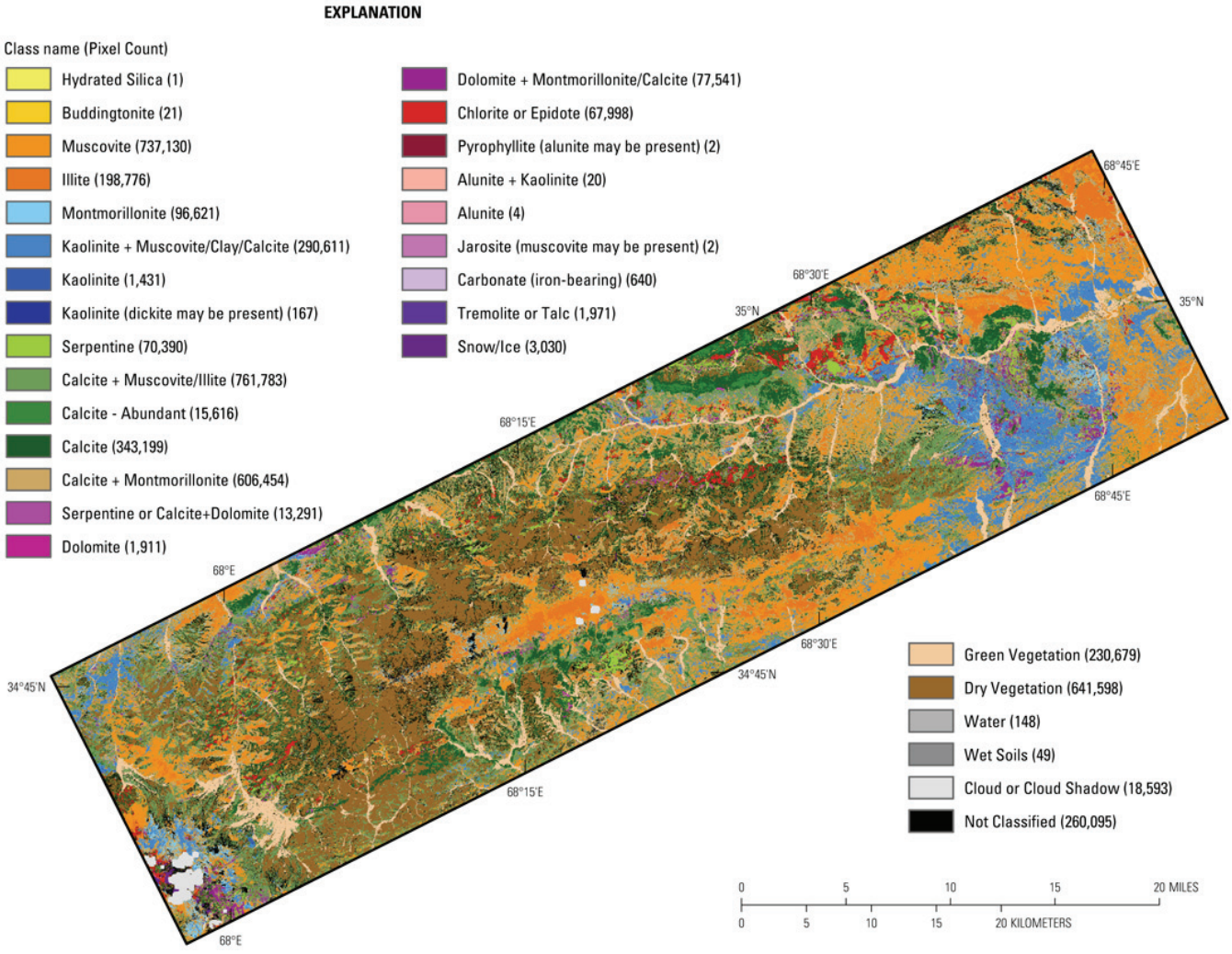

Figure 7B–6. Distribution of clays, carbonates, phyllosilicates, sulfates, altered minerals, and other materials detected in the HyMap data for the entire Haji-Gak area of interest. The identification of the specific minerals is based on the presence of characteristic absorption features resulting from vibrational processes in the mineral. The map area was analyzed to detect the presence of 32 possible specific minerals or groups of minerals.

The kaolinite group of minerals primarily occurs in the far northeast, cutting across Mississippian to Proterozoic age rocks and tend to be located along or near the major drainages. Minor amounts of kaolinite group minerals occur as spatially discrete regions along the iron-oxide trend near the middle of the AOI.

7B.3.1.3 Iron Oxides and Iron Hydroxides

Figure 7B–10 shows the iron-bearing minerals in the Haji-Gak AOI. These iron-bearing minerals can roughly be grouped within three trends. The most important is a discontinuous goethite trend within the Haji-Gak iron-oxide deposits that extends eastward along the projected iron trend with muscovite (sericite; see fig. 7B–9) and ferrous iron, though the ferric iron (goethite) becomes more abundant and quickly broadens in the central region (described in detail within the subareas). Another trend is within the eastern end of the AOI, overlaying and extending past the kaolinite zone, cutting across lithologic boundaries. The third trend is a hematite-rich zone within Tertiary rocks at the northwestern corner of the AOL. Minor hematite also occurs at the easternmost part of the AOI.

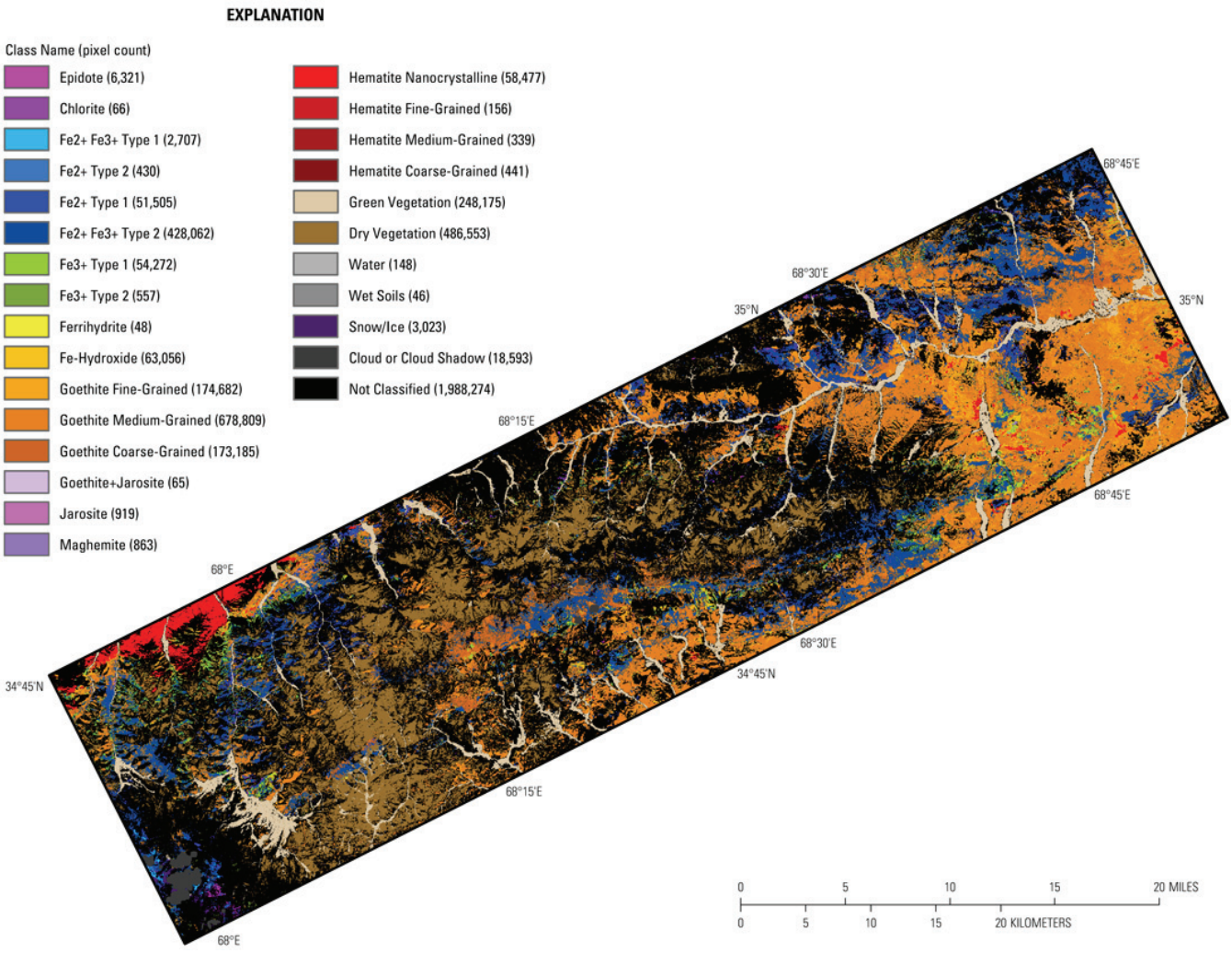

Figure 7B–7. This image shows the iron-bearing minerals and other materials in the Haji-Gak area of interest detected in the HyMap data.

7B.3.1.4 Common Secondary Minerals

The occurrence and distribution of common secondary minerals for the AOI are shown in figure 7B–11. This map shows information taken from both the 1-µm and 2-µm datasets. The chlorite or

epidote group minerals, as described within the Clays and Mica section standout within the Proterozoic rocks near the Haji-Gak iron deposit. A discontinuous trend of chlorite or epidote group minerals also follows the northern contact of Proterozoic-Paleozoic rocks (between the village of Shibar and the Dara-i-Neel mineral occurrence). Serpentine-bearing rocks are associated with carbonate-bearing units, especially in the northeast part of the AOI. Importantly, small, local serpentine-rich rocks are associated with the Haji-Gak iron deposits (see fig. 7B–11). A strong zone of serpentine-bearing rock (fig 7B–11) occurs near the Sausang mineral occurrence within a region of spatially coherent calcite.

7B.3.1.5 Common Alteration Minerals

Most of the minerals in this group are commonly present in hydrothermally altered rocks associated with epithermal processes. Consequently, where they occur in distinct clusters is of great interest in terms of potential mineral deposits. However, the only association of chlorite or epidote group minerals and kaolinite (fig. 7B–9) with Oligocene intrusive rocks occurs on the southwestern edge of the area (fig 7B–12). All other occurrences are as described within the Clays and Micas section above.

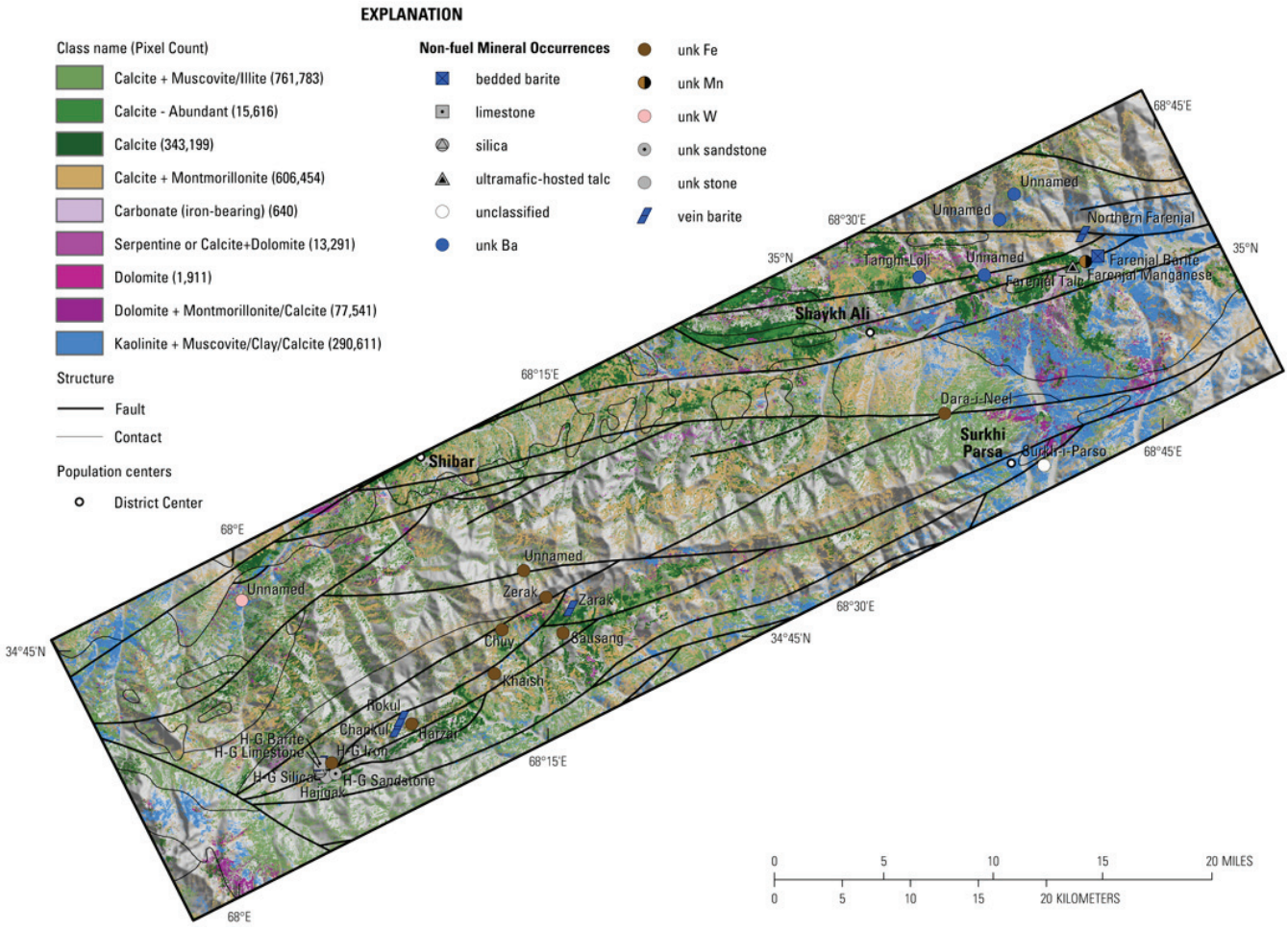

Figure 7B–8. Distribution of carbonate-bearing minerals detected by the HyMap data in the Haji-Gak area of interest detected in the HyMap data.

7B.3.2 Haji-Gak Prospect Subarea

The known mineral occurrence map (semi-transparent geologic map overlain on a shaded-relief image) shows the position of reported mineral occurrences in the Haji-Gak Prospect subarea (fig. 7B–13),

including the Haji-Gak iron deposit, with associated barite, limestone, silica, sandstone, Harzar iron, and Chapkul and Rokul vein-barite occurrences. Iron-oxide deposits at Haji-Gak Prospect subarea make up the most important iron resource presently known in Afghanistan. The structurally controlled mineralization is estimated by Russian scientists to have a mining reserve of 85 million metric tons (Abdullah and others, 1977; Peters and others, 2007). Primary ore consists of magnetite and pyrite with minor chalcopyrite. Oxidized ores are composed of three hematitic types, whereas altered-rock mineralization from the ore-forming event includes sericitization, silicification, and carbonization. The Harzar iron occurrence is hosted by greenschist containing 300-m-thick hematitic lenses grading to as much as about 63-weight-percent iron.

The topography in the area ranges from 2,874 to 4,324 m (fig. 7B–14). The Haji-Gak Prospect subarea deposits and mineralization trends northeast along the topographic ridge on the southeast-facing slope.

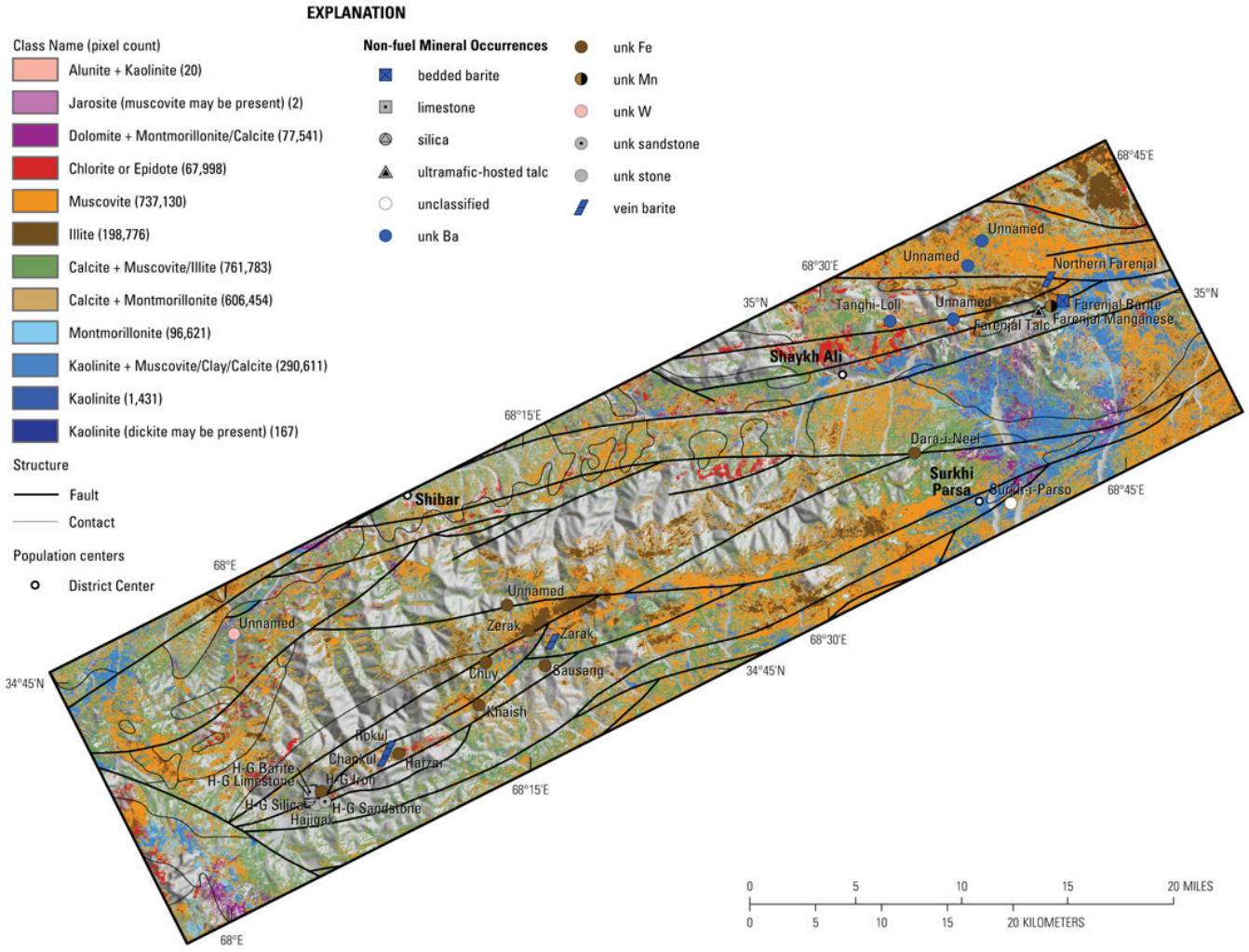

Figure 7B–9. Distribution of clays and micas identified in the HyMap data for the Haji-Gak area of interest detected in the HyMap data.

The geologic map of the area (fig. 7B–15) shows stratified rocks ranging in age from Late Proterozoic to Early Permian, with Oligocene age intrusive rocks in fault contact with the Permian age rocks in the southwest corner of the AOI. The known mineral occurrences in the Haji-Gak Prospect subarea occur within the upper part of the Late Proterozoic rocks, near the contact with Paleozoic rocks (can be seen in detail within the Haji-Gak Prospect subarea on the Russian geologic map of Kusov and others, 1965; Renaud and others, chap. 7A, this volume). These iron deposits form large outcrops along

the upper south-facing side of the main northeast-trending ridge of the subarea, as seen throughout the center of the Landsat Thematic Mapper (TM) image (fig. 7B–16).

Mapped minerals (figs. 7B–17 and 18) correlate well within this subarea with lithology, especially when compared with the Renaud and others (chap. 7A, this volume) modified Russian geologic map (after Kusov and others, 1965). The Middle Proterozoic Jawkol Formation, containing limestone and dolomite, shows spatially distinct pixels of calcite. The iron-oxide-bearing Late Proterozoic Qala Series is composed of tuffites, argillaceous rocks, and minor chert and marble (Kusov and others, 1965); ferrous-and ferric-iron oxides, muscovite (sericite or illite), and lesser amounts of kaolinite are mapped using the HyMap data. Stratigraphically above the mineralized units, the Green Schist Formation consisting of chlorite schists and quartz-sericite schists have regions of mapped epidote/chlorite and serpentine (and mobilized iron occurrences). The overlying Paleozoic limestones are mapped with abundant calcite (linear, green calcite unit trending northeastward throughout the center of the subarea).

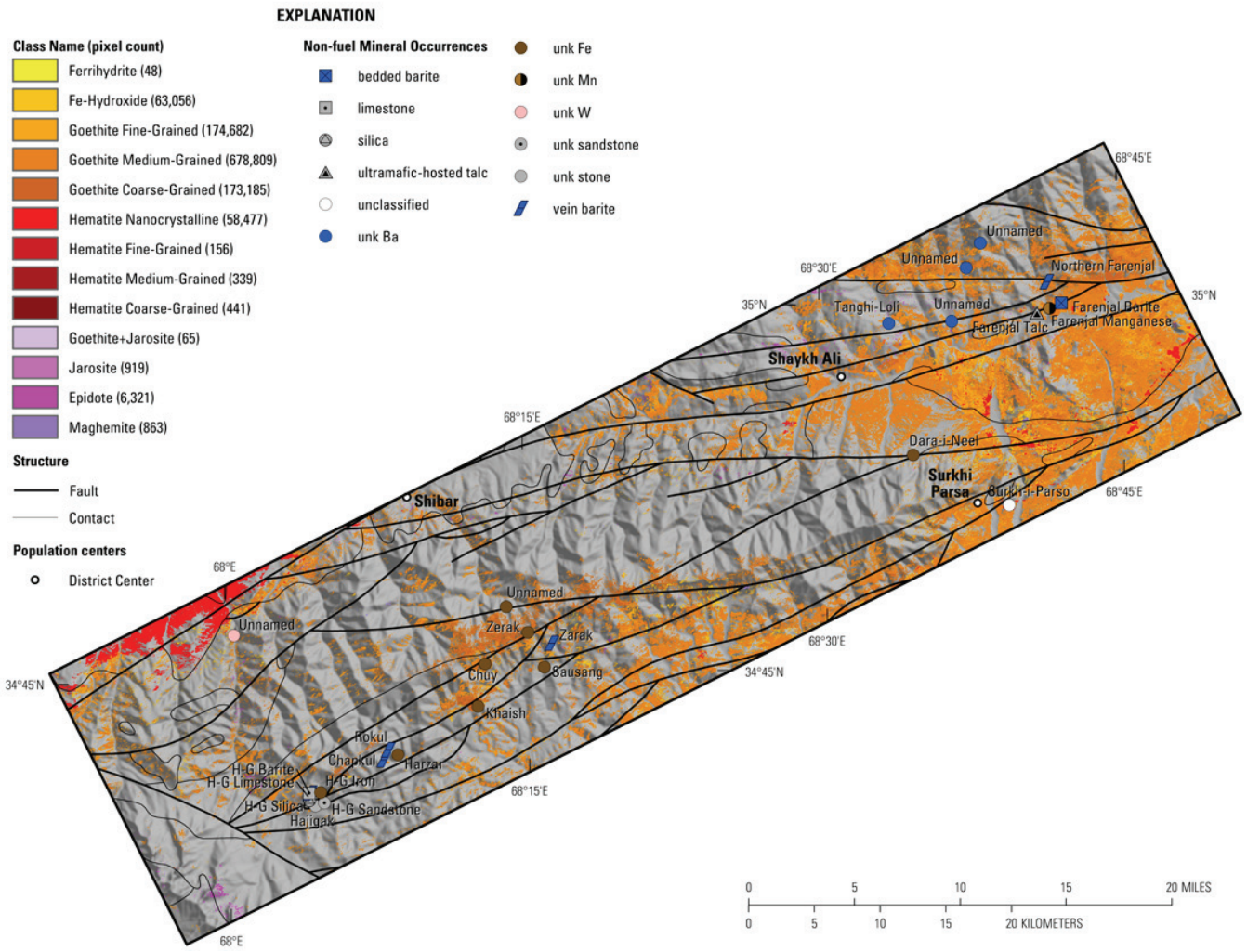

Figure 7B–10. Distribution of iron hydroxides and iron oxides mapped using the HyMap data for the Haji-Gak area of interest detected in the HyMap data.

Figure 7B–17 shows the distribution of Fe-bearing minerals and figure 7B–18 shows carbonate, sulfate, phyllosilicate and altered minerals. The map of Fe-bearing minerals (fig. 7B–17) displays the Haji-Gak Prospect iron-oxide deposit and nearby mineralization as a southwest to northeast linear trend through the center of the image. Ferrous- and ferric-iron oxide dominates the area with goethite on the

fringes. Muscovite (sericite or illite) pixels shown in figure 7B–18 are highly correlated with the iron-oxide pixels.

The strike of the lithology is mapped by linear trending pixels of calcite, muscovite, chlorite/epidote, and calcite-bearing rock units (oldest to youngest, dipping to the southeast). There is an area of mapped minerals (iron oxide, chlorite/epidote, serpentine, and calcite) at the upper northwest corner of the image that is a separate region not associated with the main Haji-Gak mineralization.

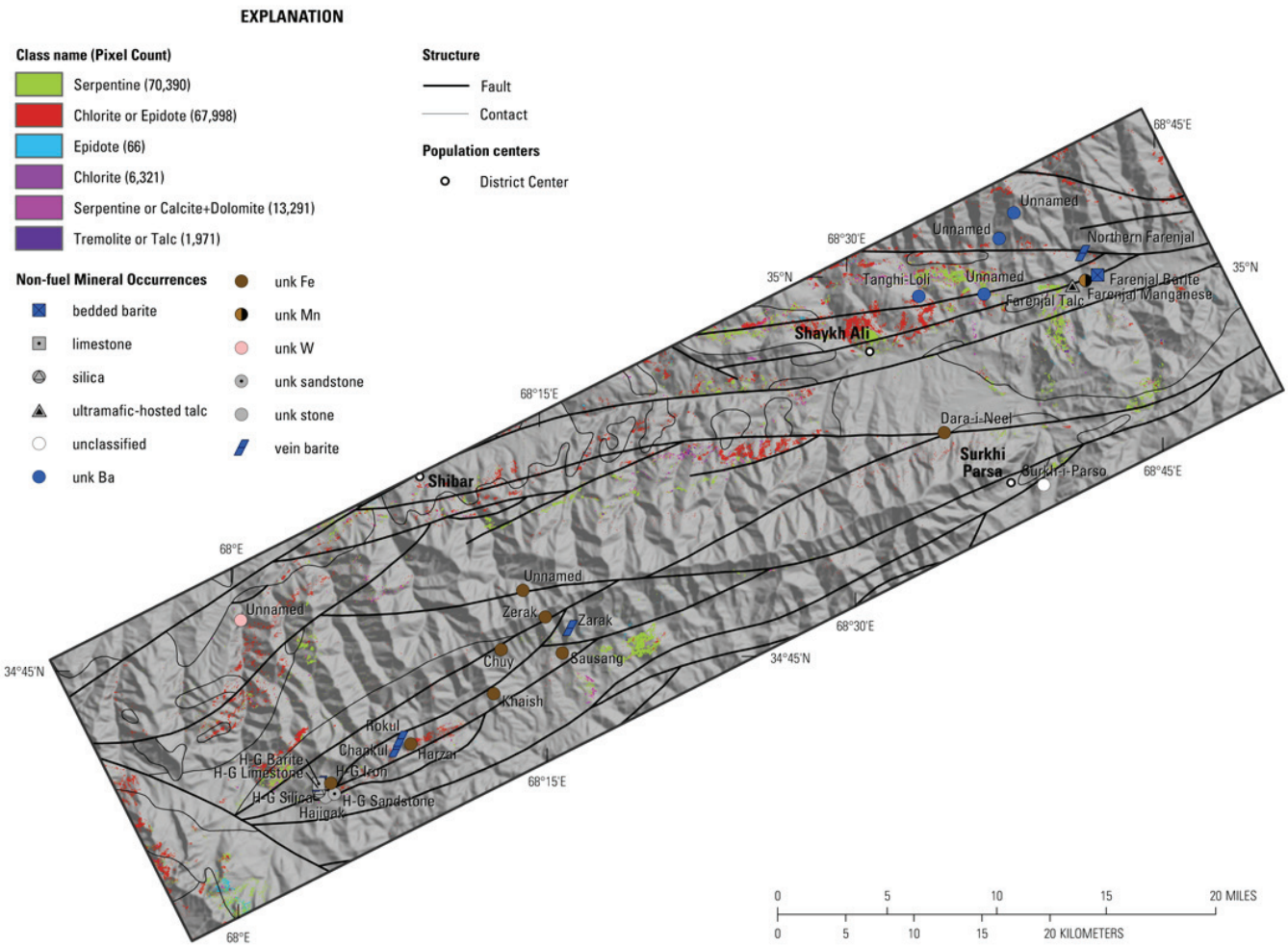

Figure 7B–11. Occurrence and distribution of common secondary minerals detected in the HyMap data for the Haji-Gak area of interest detected in the HyMap data.

7B.3.2.1 Haji-Gak Prospect Subarea: Carbonate Minerals

Calcite-rich rocks are widespread over the entire subarea (fig.7B–19). The iron-mineralization trend in the center of the image contains a moderate abundance of carbonate minerals in a southwest to northeast zone that follows the iron-mineralization trend. A strong trend of calcite, parallel, but southeast (up dip) of the iron mineralization occurs within areas containing Paleozoic limestones (the strong, green linear trend through the center of the image). Pixels spectrally matched to calcite mixed with montmorillonite in the HyMap data may in actuality contain calcite mixed with clay and mica; the clay and mica is a mixture that could include sericite and possibly illite.

7B.3.2.2 Haji-Gak Prospect Subarea: Clays and Micas

A southwest-northeast trend of muscovite (sericite or illite) minerals is present in the central part of the image along the iron-mineralization trend (fig. 7B–20). This pixel trend of pod-like occurrences spectrally matched to muscovite is along the topographic divide and shows variability in surficial abundance (along the ridge between Haji-Gak and Rokul mineral occurrences). South of this zone, chlorite/epidote are the dominant minerals spectrally mapped in the Green Schist Formation. Farther to the southeast (stratigraphically upward) discontinuous calcite group minerals occur in Phanerozoic rocks.

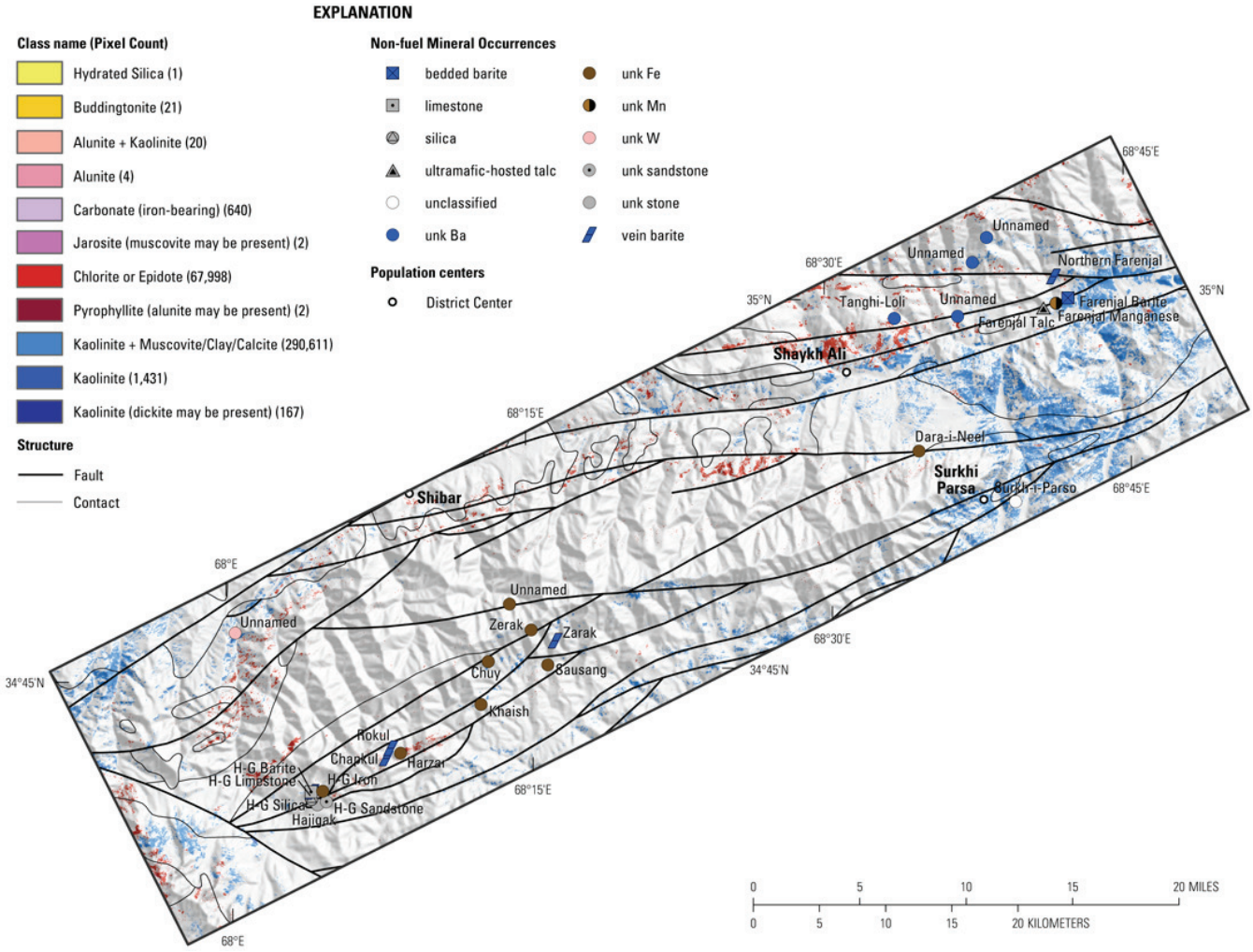

Figure 7B–12. Distribution of common alteration minerals in the Haji-Gak area of interest detected in the HyMap data.

7B.3.2.3 Haji-Gak Prospect Subarea: Iron Oxide and Iron Hydroxide Minerals

Figure 7B–21 shows the distribution of Fe-oxides and Fe-hydroxides in the Haji-Gak Prospect subarea. The ferric iron (goethite) minerals are mapped as discontinuous pixels along the iron-oxide trend between the Haji-Gak and Rokul mineral occurrences. An anomalous area in the northwest corner (northwest of the Haji-Gak deposit) shows abundant goethite distal to Haji-Gak deposit mineralization. The easternmost border of the subarea continues the iron-oxide trend to the northeast, and a spatially distinct concentration of goethite pixels is seen within Phanerozoic rocks in the southeast part of the AOI.

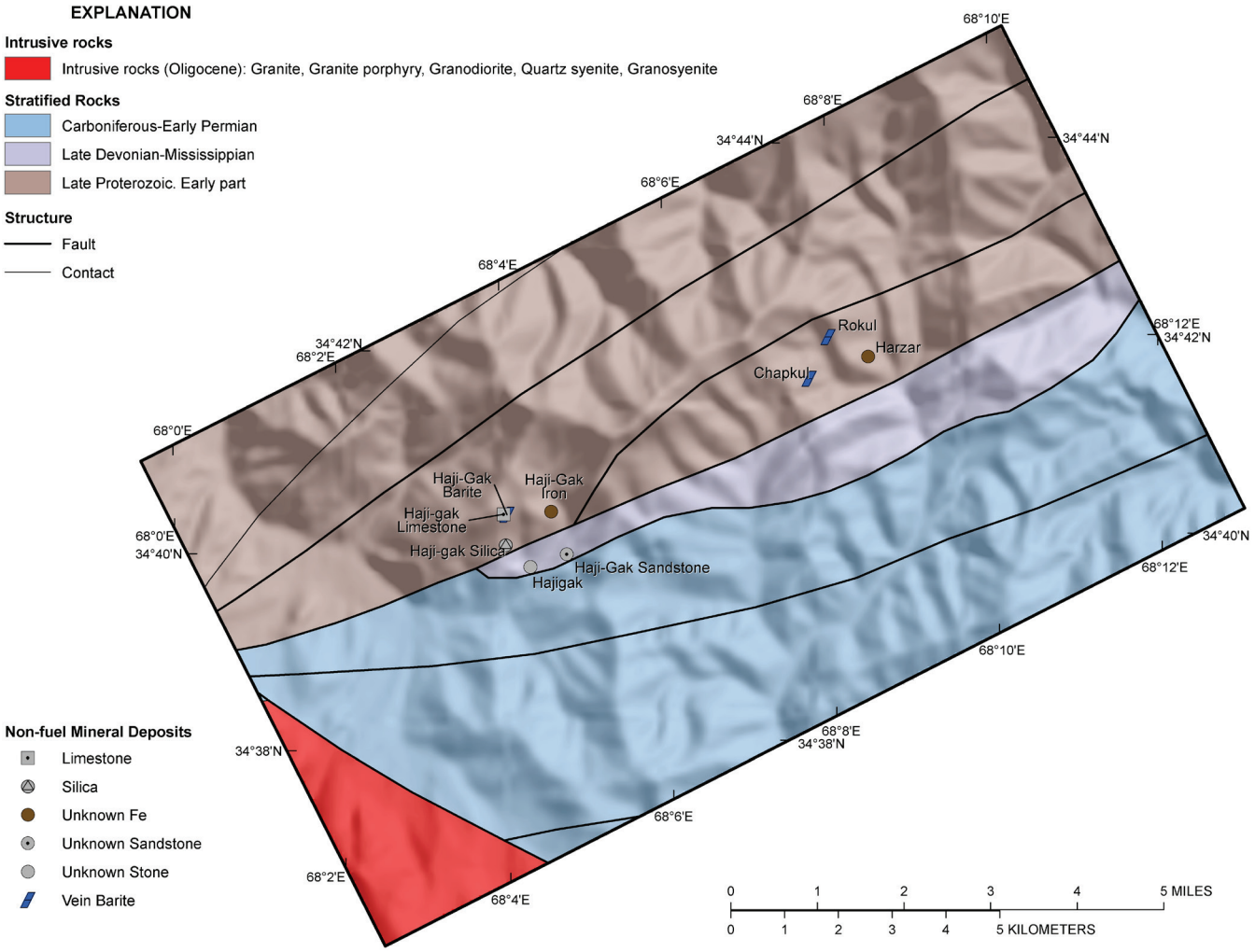

Figure 7B–13. Map showing the known mineral occurrences in the Haji-Gak Prospect subarea of the Haji-Gak area of interest.

7B.3.2.4 Haji-Gak Prospect Subarea: Common Secondary Minerals

There are few occurrences and scattered distribution of common secondary minerals (fig.7B–22) in the area. The northeast-trending Green Schist Formation is spectrally mapped as containing chlorite and (or) epidote group minerals (southeast of the Haji-Gak-Rokul iron-oxide mineral-occurrence trend). The Harzar iron and Chapkul and Rokul barite deposits are located in the Haji-Gak Prospect subarea. Of note, an anomalous region in the northwest corner (northwest of the Haji-Gak deposit) shows abundant chlorite/epidote and serpentine occurrences (King, Johnson, and others, 2011).

7B.3.2.5 Haji-Gak Prospect Subarea: Common Alteration Minerals

Similar to the common secondary minerals map above (fig. 7B–22), common alteration materials detected in the HyMap data (fig. 7B–23) within the area are primarily chlorite/epidote group minerals that are mapped in the regions described in the previous section. A small, spatially coherent group of calcite-clay mineral pixels occur in the west-central part of image (Haji-Gak deposit area) and within Phanerozoic age rocks at the southeast corner of the subarea.

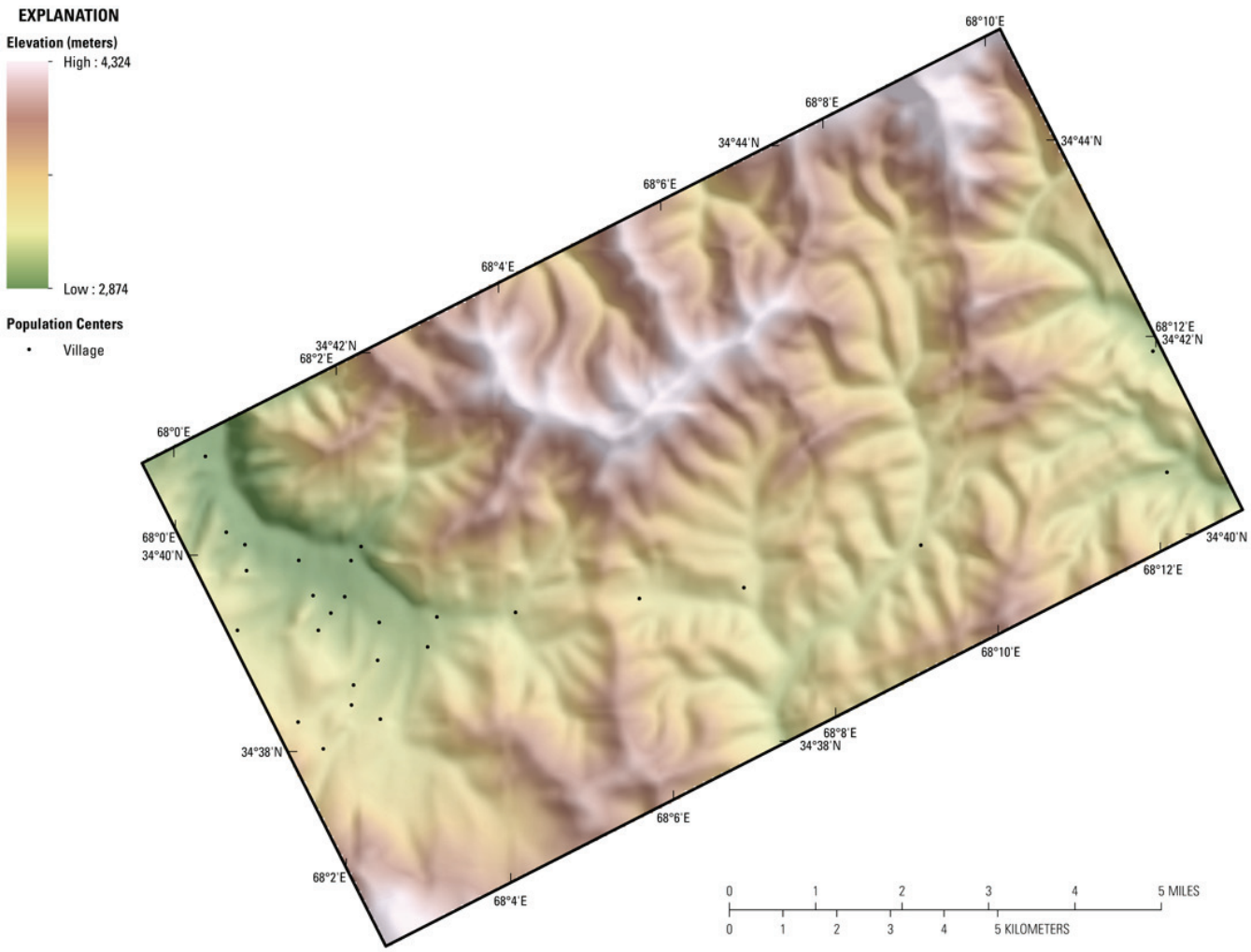

Figure 7B–14. Shaded-relief map showing elevation in the Haji-Gak Prospect subarea of the Haji-Gak area of interest. The darker brown tones indicate higher elevations, and lower elevations are represented by the green tones.

7B.3.3 Northeast Haji-Gak Subarea

The known mineral occurrence map (semi-transparent geologic map overlain on a shaded-relief image) shows the position of reported mineral occurrences in the Northeast Haji-Gak subarea (fig. 7B–24). Iron-mineral occurrences include the Khaish, Chuy, Zerak, and Sausang deposits, along with the Zarak vein barite. Khaish, the largest iron prospect, located near Haji-Gak, is hosted within the same rock units as the Haji-Gak deposit. Chuy occurs within a quartz-chlorite schist host rock with hematite-magnetite mineralization. Zerak also contains hematite-magnetite mineralization (Abdullah and others, 1977; Peters and others, 2007).

The topography in the subarea ranges from 2,686 to 4,600 m and trends southwest-northeast (fig. 7B–25). Figure 7B–26 shows the distribution of Late Proterozoic rocks along the northern side and younger Paleozoic units on the south side of the subarea. Fault-bounded wedges of Late Devonian to Mississippian age rocks occur in the middle of the subarea. All units have a northeast-trending strike parallel to the ridge crest.

In the Landsat TM data (Davis, 2007), the Paleozoic age rocks occur within moderate topographic relief in the southern half of the subarea and older Proterozoic rocks form the steeper sloping southern ridge area and the north slope (fig.7B–27). The majority (five of six) of the known

mineral occurrences in the Northeast Haji-Gak subarea occur in rocks of Late Proterozoic age (see fig. 7B–24).

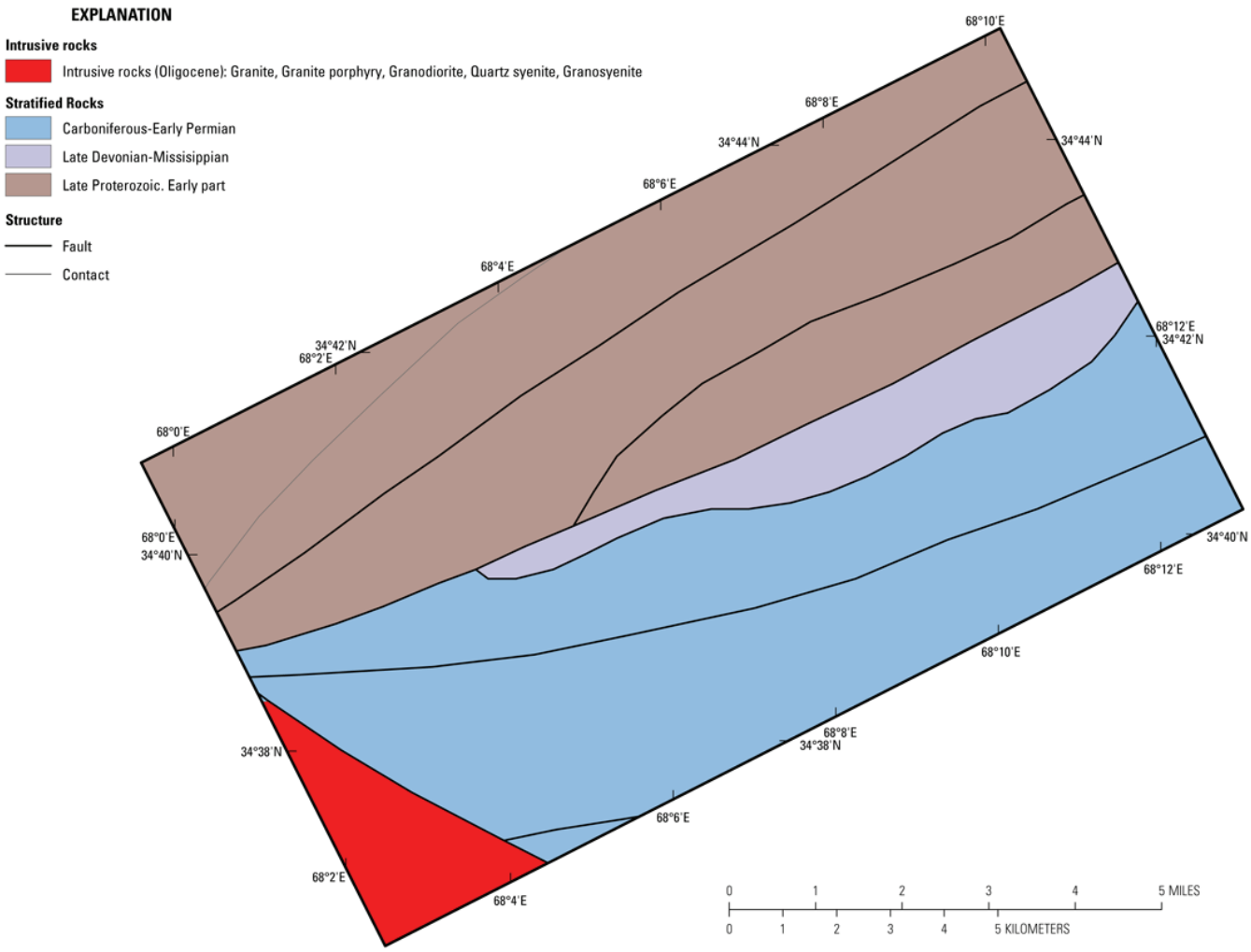

Figure 7B–15. Geologic map of the Haji-Gak Prospect subarea of the Haji-Gak area of interest (AOI) taken from the Russian 1:500,000-scale geologic map of Afghanistan (Dronov and others, 1972). The intrusive rocks are exposed in the southwestern part of the AOI.

The overall-inclusive HyMap data for the area show the distribution of iron-bearing (fig. 7B–28) and carbonate, phyllosilicate, sulfate, alteration minerals, and other materials (fig. 7B–29). Dry vegetation (brown pixels, figs. 7B–28 and 7B–29) is abundant throughout the entire subarea, but is most pervasive on the north-sloping rock faces. The presence of the dry vegetation masks much of the north-facing surface and reduces the mineral identification in these areas. Known mineralization (iron and barite) occur within regions of abundant ferrous and ferric iron, muscovite (sericite or illite), other clay, and calcite. This group of minerals, mixed with dispersed zones of ferrihydrite (and calcite as shown in fig. 7B–29), occurs on the ridgeline and top of the southern slope. A circular-like feature of ferrous iron (blue) is situated within another discontinuous northeast trend of ferrous-iron-bearing minerals south of the ridgeline. Much of the Paleozoic rock on the southeastern side of the subarea also contains abundant ferric iron and a small zone of hematite occurs to the southeast (fig. 7B–28).

7B.3.3.1 Northeast Haji-Gak Subarea: Carbonate Minerals

Figure 7B–30 shows widespread distribution of carbonate-rich rocks over the entire AOI. Calcite group minerals are by far the dominant mineral groups mapped in the HyMap data. The Paleozoic age

rocks contain abundant calcite pixels in the central part of the image, whereas kaolinite occurs to the east and west, near the Proterozoic-Paleozoic contact (see blue areas in fig. 7B–30 and fig. 7B–24). Calcite with mica and clay and zones of kaolinite occur along the southern border of the subarea.

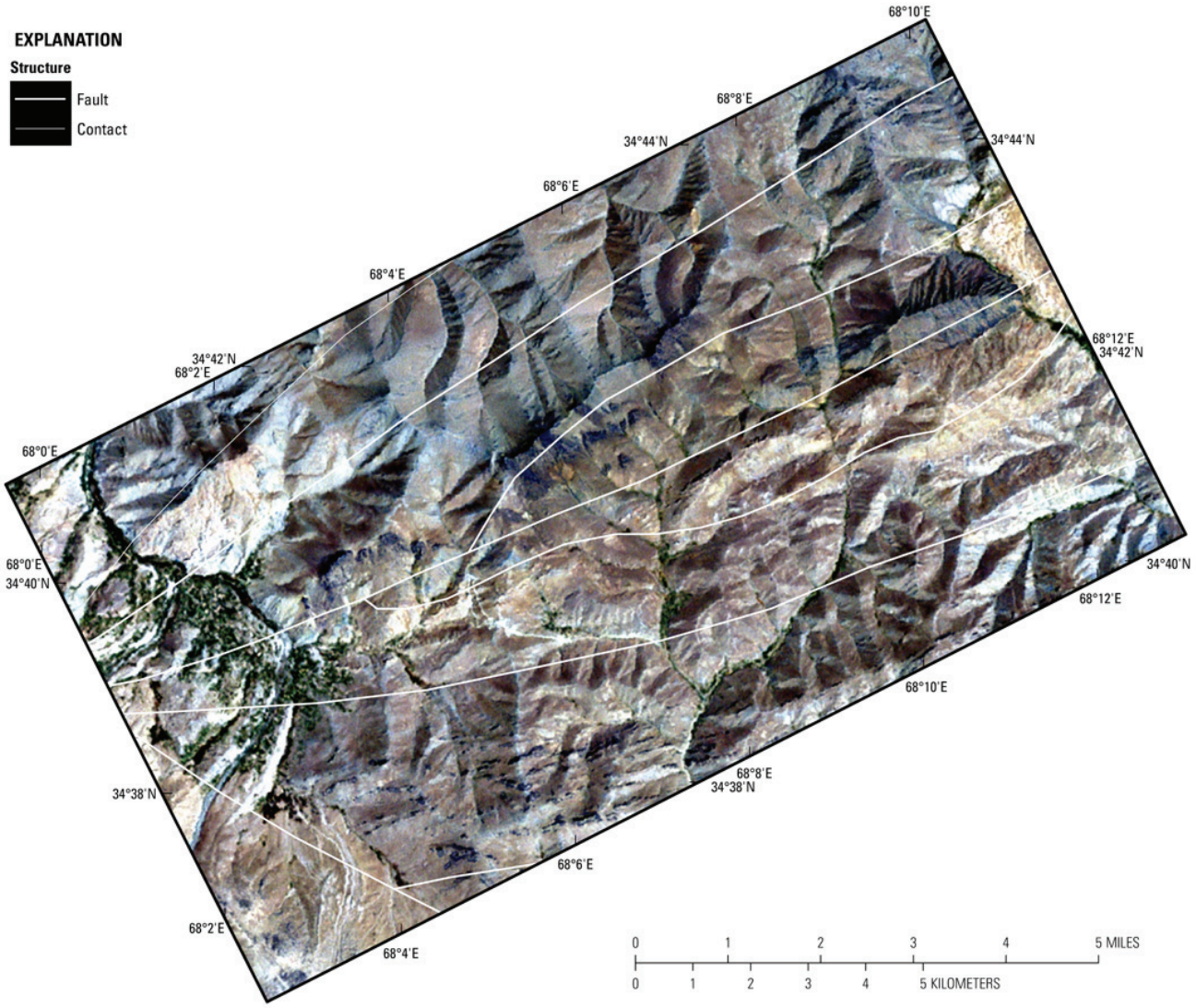

Figure 7B–16. Numerous faults and fractures of different orientations and extent occur in the Haji-Gak Prospect subarea of the Haji-Gak area of interest. The fault traces (Peters and others, 2007) are placed on Landsat Thematic Mapper (TM) images (Davis, 2007). Marked color differences in the TM data are associated with rocks of different ages.

7B.3.3.2 Northeast Haji-Gak Subarea: Clays and Micas

Figure 7B–31 shows the enrichment of phyllosilicates in the Northeast Haji-Gak subarea. Muscovite (light-orange pixels) with zones of kaolinite (blue pixels) and other clay minerals are mapped as a band following the ridgeline. A second discontinuous band of similar composition parallels the first to the south. Both bands are located over areas that host known iron prospects (fig. 7B–24). The early Paleozoic age rock (fig. 7B–24) in the central part of the clay/mica image is associated with calcite-clay, and the younger Paleozoic rocks to the southeast are characterized by a mixture of calcite-clay group minerals, muscovite, and kaolinite. Within this subarea, regions of Proterozoic rock mapped as

muscovite (sericite/illite) and minerals containing ferrous and ferric iron, with possibly kaolinite and calcite, suggest permissible lithologies for sed-ex hosted iron deposits.

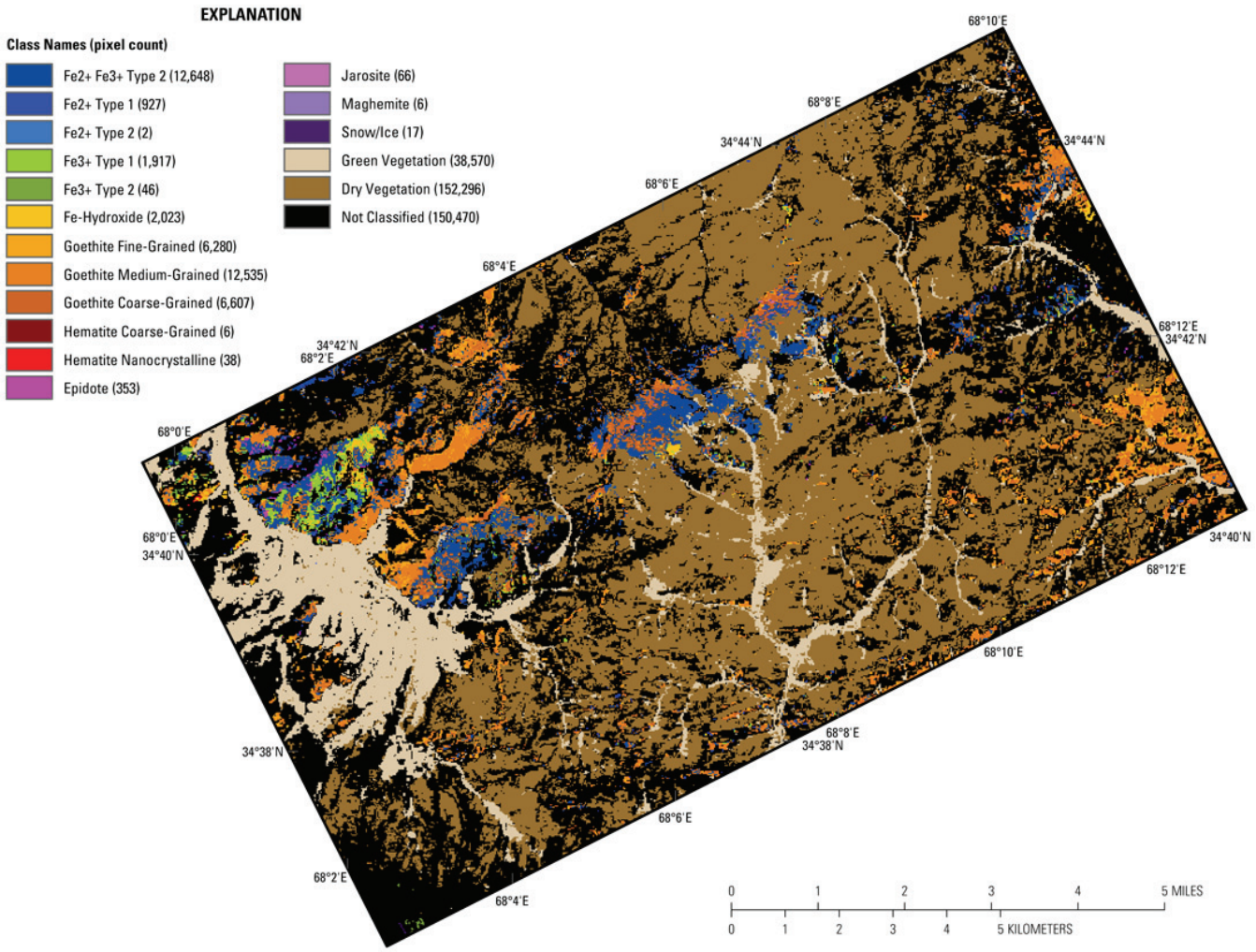

Figure 7B–17. Image showing iron-bearing and other alteration minerals detected in the HyMap data for the Haji-Gak Prospect subarea of the Haji-Gak area of interest.

7B.3.3.3 Northeast Haji-Gak Subarea: Iron Oxides and Iron Hydroxides

The distribution of Fe-oxides and Fe-hydroxides is shown in figure 7B–32. Goethite dominates the subarea and defines regions of weathered rock abundant in iron-bearing minerals. The contact zone between the goethitic minerals along the southwest-northeast trending ridgeline and the Proterozoic and Paleozoic age rocks defines an important zone of potential iron mineralization. Grain size of the goethite may be important along this iron-mineralization trend (along the ridgeline); the crystallinity of goethite is coarse-grained. Abundant goethite is also mapped in the Paleozoic rocks to the southeast, along with a small zone of hematite. Minor occurrences of ferrihydrite are located south of the goethite trending near the ridgeline that increase eastward in abundance.

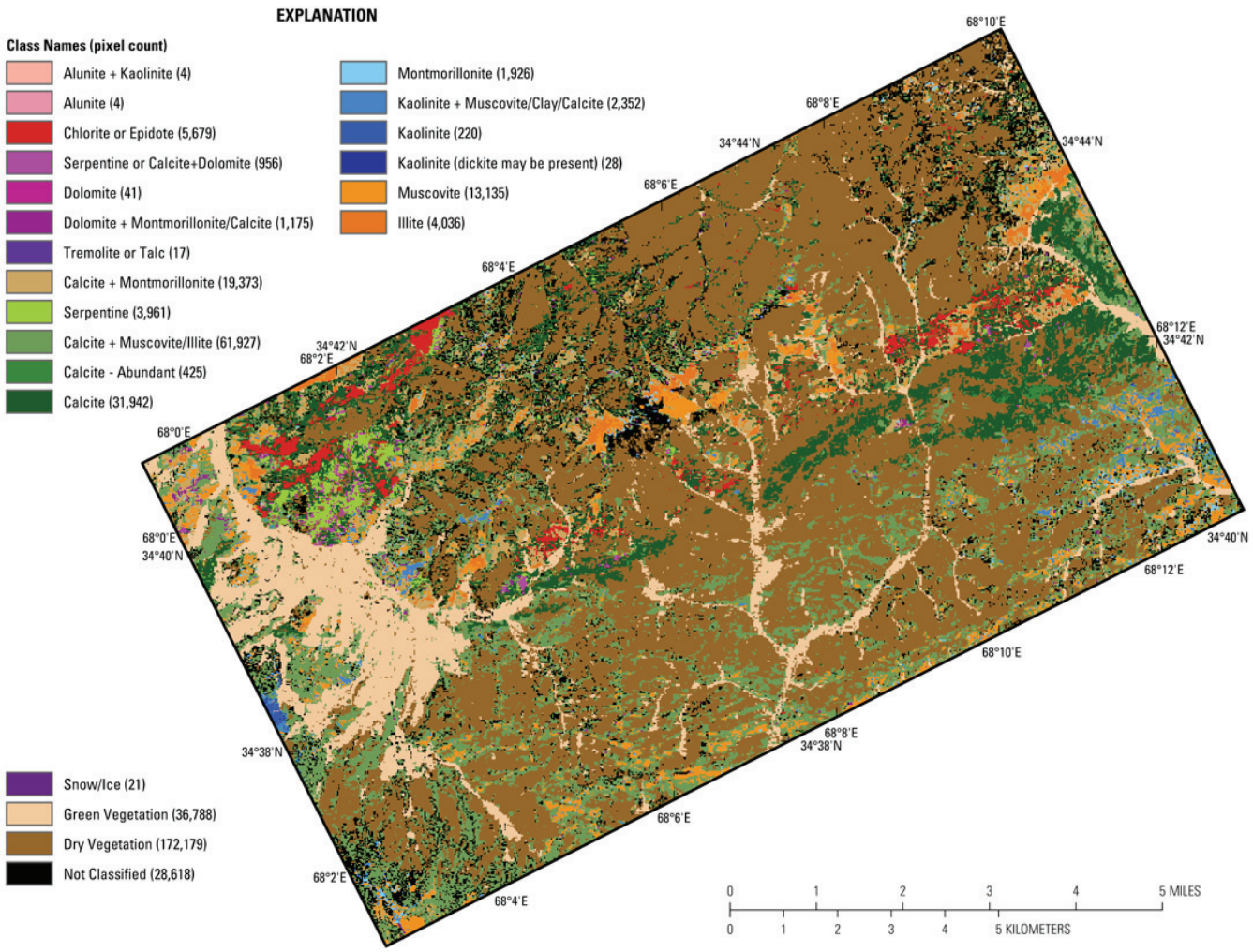

Figure 7B–18. Map showing distribution of clays, carbonates, phyllosilicates, sulfates, altered minerals, and other materials for the Haji-Gak Prospect subarea of the Haji-Gak area of interest based on the HyMap data.

7B.3.3.4 Northeast Haji-Gak Subarea: Common Secondary Minerals

There are few occurrences of common secondary minerals (fig.7B–33), with the exception of serpentine and the chlorite or epidote group that are mapped in two small concentrated regions within upper Paleozoic rocks. These minerals, combined with the structure and geomorphology expressed within the Landsat TM image (fig. 7B–27),suggest potential mineral alteration of the country rock through weathering, skarn formation, or hydrothermal fluid flow.

7B.3.3.5 Northeast Haji-Gak Subarea: Common Alteration Minerals

The only significant common alteration minerals mapped in the imaging spectrometer data are the kaolinite group minerals and the previously mentioned chlorite or epidote group minerals (fig. 7B–34). Local areas of spatially abundant kaolinite is present at or near the northern edge of calcite-rich rocks and appear to be positioned close to the contact of older Proterozoic rocks with younger Paleozoic limestones (about lat 34°48' N., long. 68° 22' E). The kaolinite maps as strings of small, spatially distinct pixel groups with well-defined cores. Kaolinite is also common as a discontinuous dispersed band of pixels along the southern edge of the subarea.

Figure 7B–19. Map showing the distribution of carbonate-bearing minerals in the Haji-Gak Prospect subarea detected in the HyMap data.

7B.3.4 Farenjal Subarea

The known mineral occurrence map (semi-transparent geologic map overlain on a shaded-relief image) shows the position of reported mineral occurrences in the Farenjal subarea (fig. 7B–35), including the Dara-i-Neel iron, Farenjal talc, Farenjal bedded barite, Northern Farenjal vein barite, Tanghi-Loli, three unnamed occurrences of barite (unknown type), Farenjal manganese (unknown type), and Surkh-i-Parso (unknown mineral and type). All the known barite occurrences are hosted in Ordovician age rock, with the Farenjal bedded barite, manganese, and talc mineralization occurring near a contact zone between Ordovician and Mississippian age rocks (fig. 7B–35). The Dara-i-Neel iron occurrence comprises martite float (Kusov and others, 1965).

The topography in the subarea ranges from 1,900 to 3,832 m with the Gorband River flowing eastward through its center. A second river flows northward into the Gorband River with the confluence at the center of the subarea (fig. 7B–36). The Proterozic rock that hosts the Haji-Gak iron-bearing deposits is fault bounded and pinches out within this subarea; younger lithologies dominate this region (fig. 7B–37). Of note, the Dara-i-Neel iron occurrence is located on the northern edge of the Proterozoic rock in (or near) fault contact with upper Paleozoic rocks (fig. 7B–35).

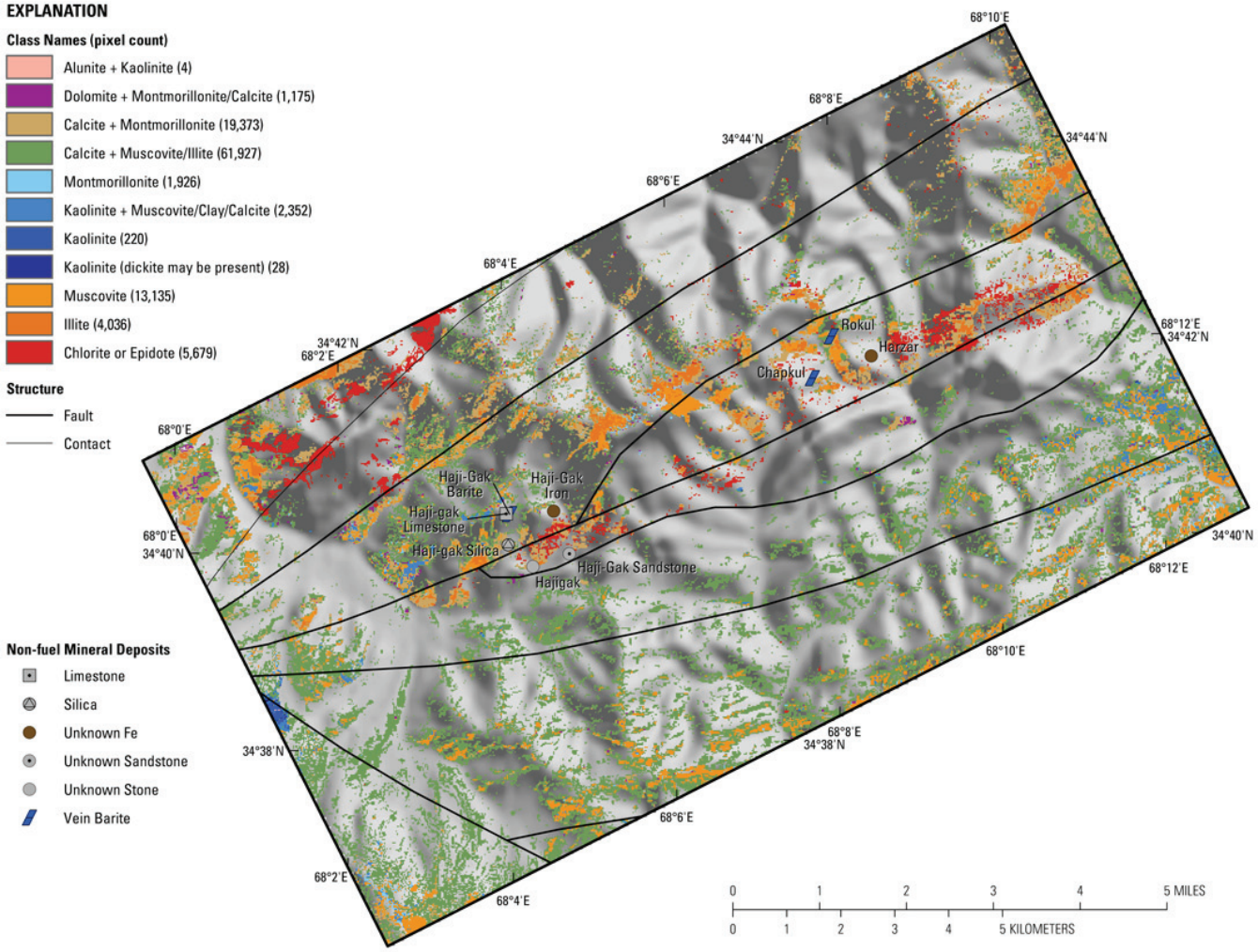

Figure 7B–20. Mapped distribution of clays and micas detected using the HyMap data. The figure shows the occurrence of muscovites and illites, chlorite and (or) epidote, and kaolinite group minerals along the southwest-northeast lithologic trend.

In the Landsat TM data (Davis, 2007), the Proterozoic and Paleozoic rocks occur within areas of moderate topographic relief and can usually be traced by color within their fault-bounded blocks that are defined by the fault traces shown in fig. 7B-38. Changes in surface color represent spectral differences in surface mineralogy.

The overall-inclusive imaging spectrometer data for the area show the distribution of iron-bearing minerals (fig. 7B–39) and carbonate, phyllosilicate, sulfate, alteration minerals, and other materials (fig. 7B–40). Dry vegetation (brown pixels) is sparse in the subarea. Known mineralization (iron and barite) occurs in the northern part of the image within regions of spatially well-defined pixels of ferrous iron, muscovite, and calcite.

A complex mixture of minerals are mapped in the subarea. Abundant ferrous-iron-group minerals along with calcite, serpentine, chlorite or epidote are mapped in the northwest part of the subarea (above and to the west of the confluence of the Gorband River with the second primary river flowing in from the south). Muscovite occurs in the northern one-third of the image, north of the Gorband River, and is commonly associated with Ordovician age rocks that host the barite deposits (in the north-central part of the subarea; fig. 7B–35). In the southern part of the image, the Proterozoic rocks host ferrous-iron minerals and associated dolomite with spatially isolated pods of hematite and other

ferric-iron minerals in contact zones with Paleozoic strata. Goethite minerals dominate the rest of the subarea. Kaolinite group minerals with dolomite dominate the south-central region of the image.

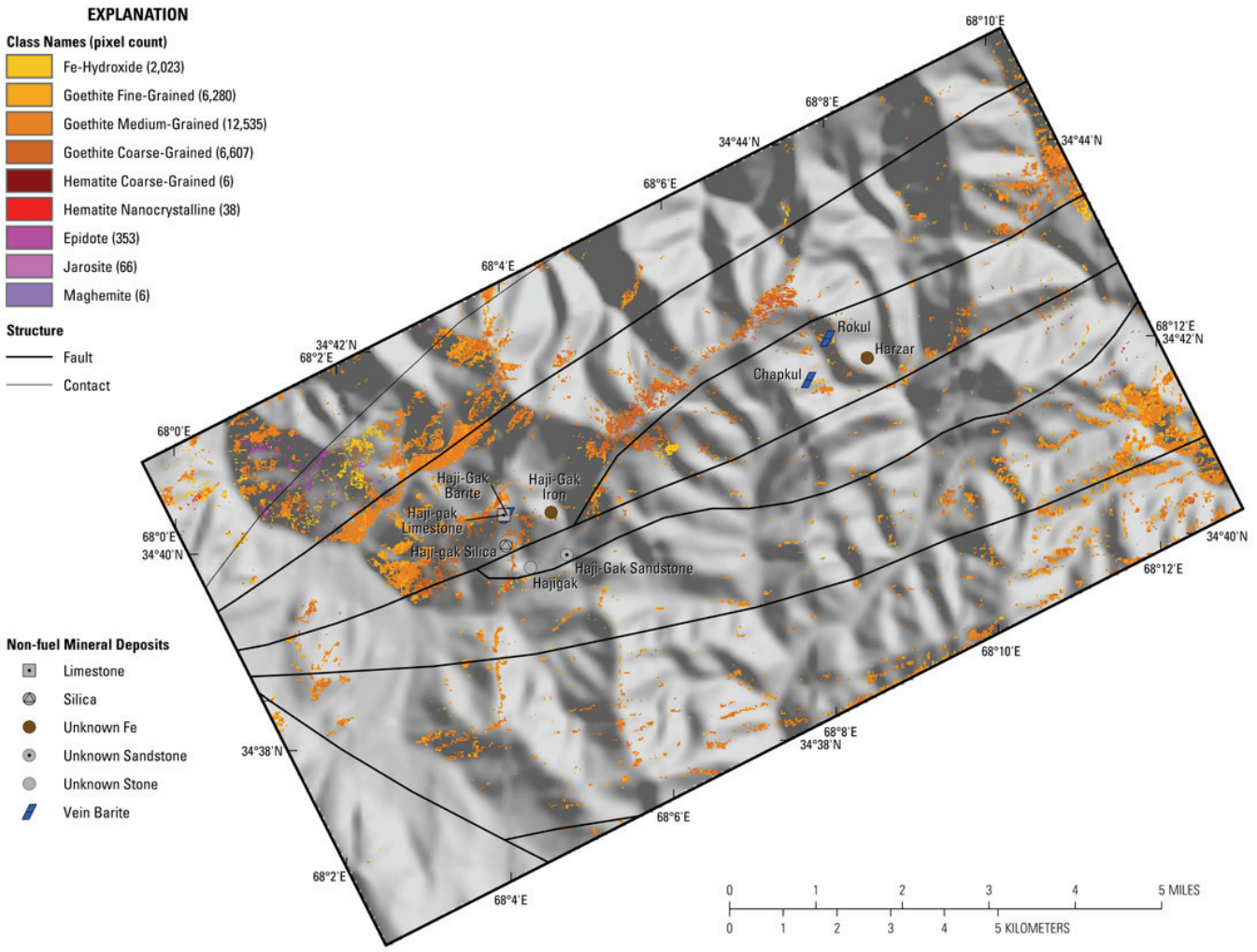

Figure 7B–21. Map showing the distribution of iron hydroxides and iron oxides for the Haji-Gak Prospect subarea.

7B.3.4.1 Farenjal Subarea: Carbonate Minerals

Figure 7B–41 shows widespread distribution of minor, discontinuous carbonate and carbonate group mineral-bearing rocks over the entire Farenjal subarea. An abundant zone of calcite pixels trends west to east through most of the image along the northern edge of the Gorband River, looping and cutting across Ordovician and Mississippian age lithologies. This calcite is mapped together with ferrous-iron minerals, serpentine, chlorite or epidote, and known barite prospects (see locations within fig. 7B–41) on the northwestern side of the subarea. Dolomite with kaolinite and other clay (and with ferrous iron and chlorite (or) epidote) is mapped in Proterozoic age terrain east of Dara-i-Neel, as well as northward within Mississippian age units (see fig. 7B–35).

7B.3.4.2 Farenjal Subarea: Clays and Micas

Figure 7B–42 shows the enrichment of phyllosilicates in the Farenjal subarea. Abundant muscovite (lighter orange pixels) occurs in much of the subarea. The kaolinite-, dolomite-, and chlorite- or epidote-bearing areas are described above with the carbonate minerals.

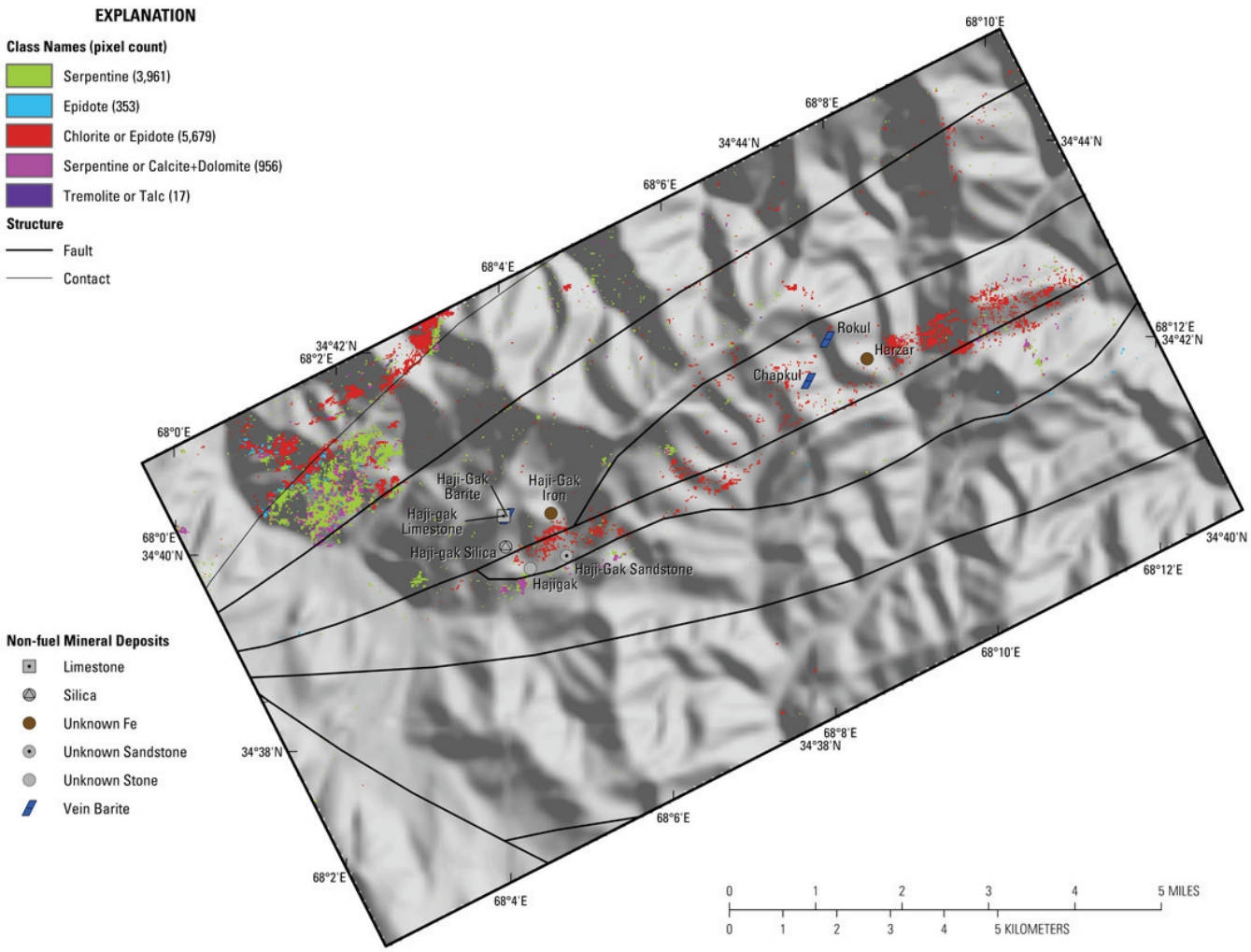

Figure 7B–22. Image showing the very limited occurrence and scattered distribution of common secondary minerals detected in the HyMap data. A coherent grouping of secondary minerals occurs along the lithologic trend in the center of the image and in the northwestern part of the AOI.

7B.3.4.3 Farenjal Subarea: Iron Oxides and Iron Hydroxides

The distribution of Fe-oxides and Fe-hydroxides is shown figure 7B–43. Goethite dominates the subarea and is mapped in regions of weathered rock abundant in iron-bearing minerals. Goethitic group minerals are less abundant in the northeast edge of the image and are not mapped in the western one-third of the image, because (undisplayed) ferrous-iron pixels are dominant and occupy these pixel sites. Hematite and ferrihydrite occur near and along contacts of Proterozoic and Paleozoic rocks with Pliocene deposits in the southern part of the subarea.

7B.3.4.4 Farenjal Subarea: Common Secondary Minerals

There are few occurrences of common secondary minerals (fig.7B–44), with the exception of serpentine and chlorite or epidote group minerals. A prominent zone of these minerals occur along the northern edge of the Gorband River near the Tangi-Loli mineral occurrence and southeast of the Gorband River confluence. Chlorite is also located within or near faulted rock contacts to the northeast (near and north of the barite occurrences). Proterozoic age rocks containing serpentine (along with ferrous-iron minerals, dolomite, and clay) occur in the southern region of the image (see carbonate minerals section above).

7B.3.4.5 Farenjal Subarea: Common Alteration Minerals

The only significant common alteration minerals mapped are the previously mentioned (carbonate minerals section) kaolinite and chlorite or epidote group minerals (fig. 7B–45). Chlorite occurrences are abundant to the north, whereas kaolinite group minerals dominate the central and southern regions.

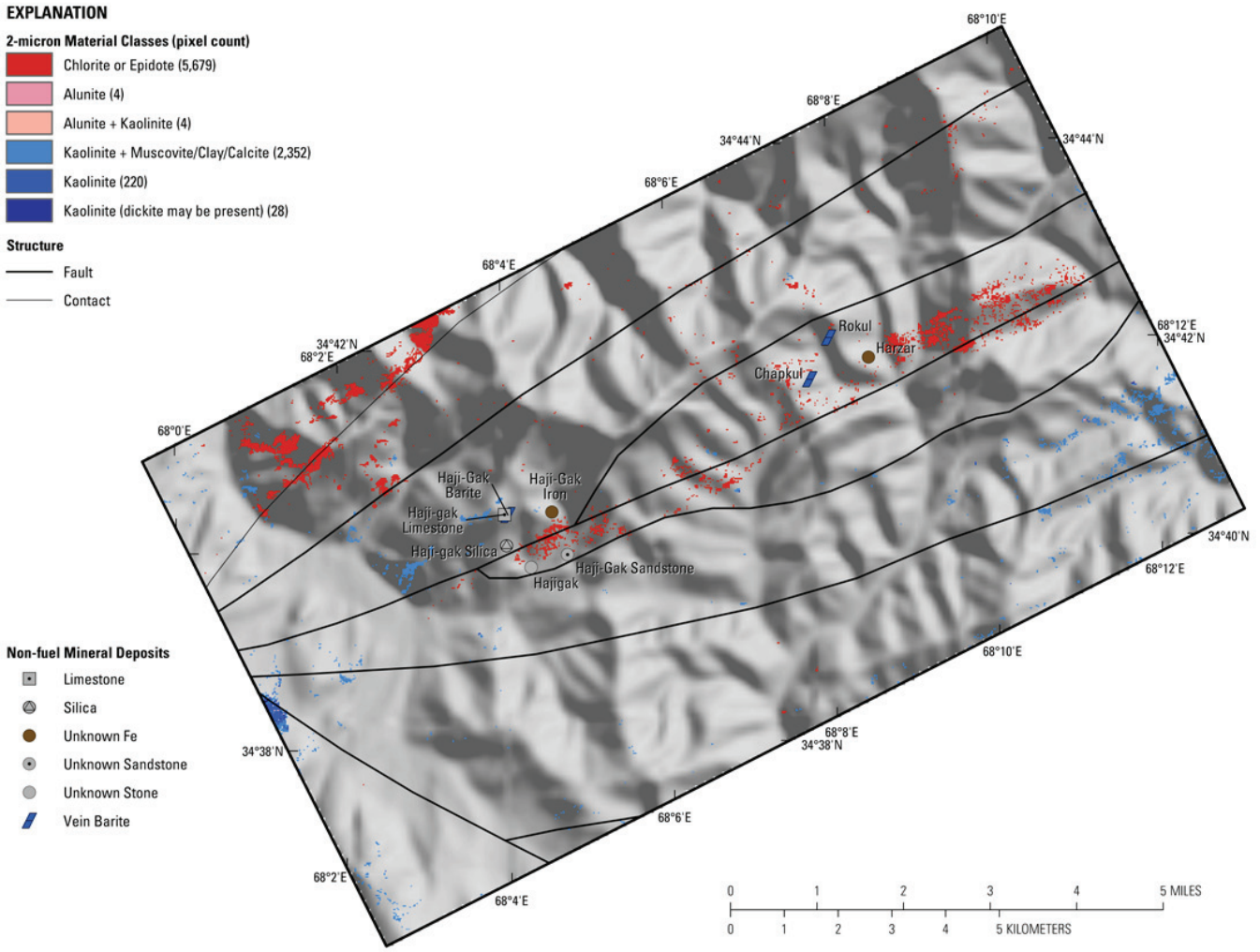

Figure 7B–23. Common alteration materials detected in the HyMap data are limited primarily to chlorite or epidote and kaolinite group minerals. A coherent grouping of secondary minerals occurs along the lithologic trend in the center of the image and in the northwestern part of the AOI.

7B.4 Summary

The Haji-Gak area of interest (AOI) is well-exposed and is readily mapped using HyMap imaging spectrometer data. The HyMap data mapped the well-defined lithologic sequence in the AOI and supports the previous field mapping (Kusov and others, 1965), especially in the important ore deposit area at the western side of the AOI. Permissive areas of iron mineralization and sericitic wallrock alteration trend northeastward through the Northeast Haji-Gak subarea and terminate at the eastern side of the AOI within the Farenjal subarea (as seen within HyMap data analysis).

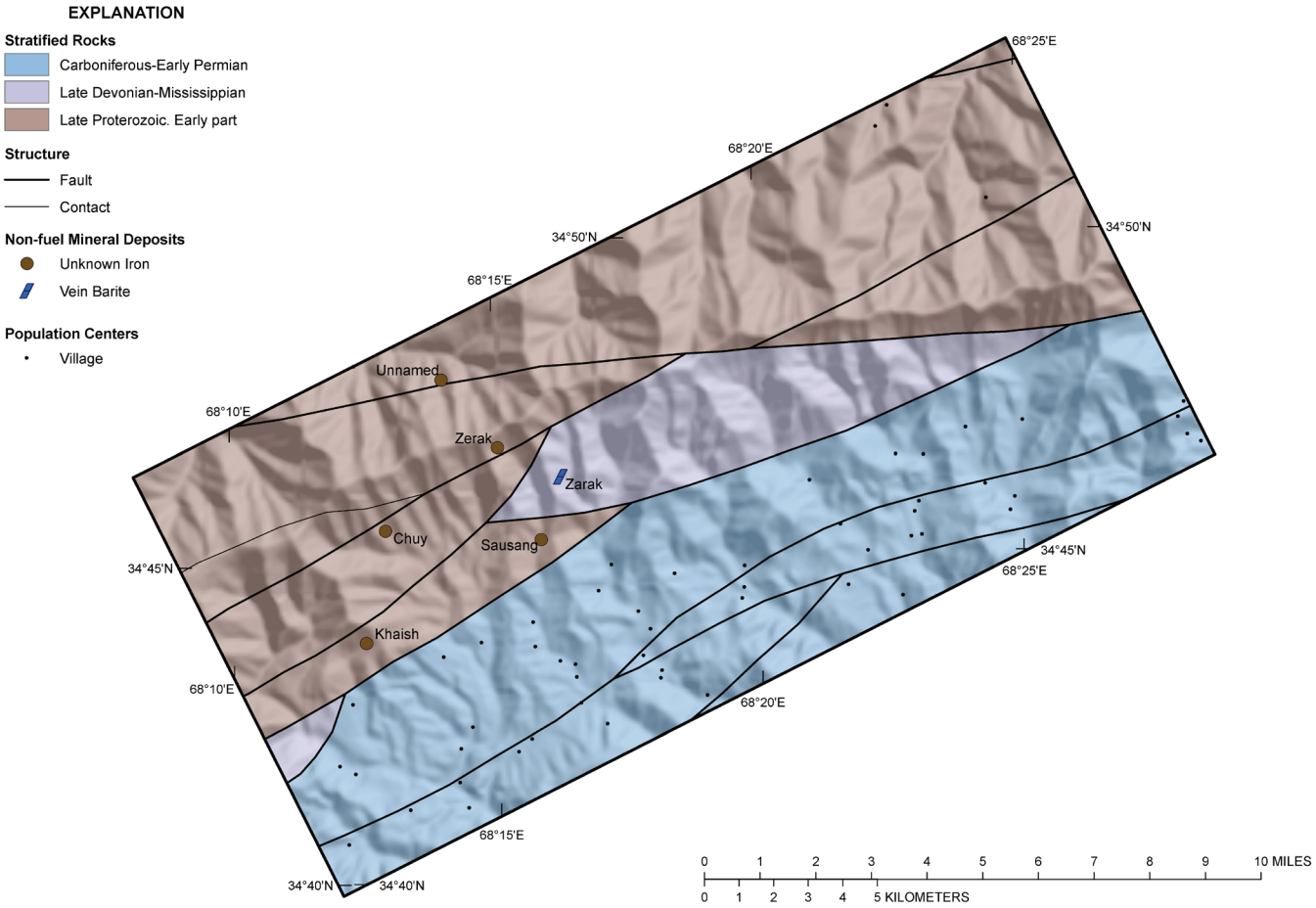

Figure 7B–24. Map showing the known mineral occurrences in the Northeast Haji-Gak subarea of the Haji-Gak area of interest. The subarea includes five iron deposits and one vein-barite deposit.

Within the Northeast Haji-Gak subarea, known mineralization (iron and barite) occurs within The Haji-Gak Prospect subarea contains well-exposed iron deposits hosted within Late Proterozoic rocks on the southeast flank of an anticline. The stratigraphic succession is mapped within the HyMap data, and additional iron mineralization is mapped as ferrous-iron minerals, goethite, sericite, and lesser amounts of ferric minerals and chlorite or epidote group minerals.

regions of abundant ferrous and ferric iron, clays and mica (sericite or illite), and calcite. A linear trend of this mineral group follows the major topographic ridgeline northeast into the Farenjal subarea. Zones of kaolinite may be associated with this trend.

The Farenjal subarea marks the termination of the iron-bearing trend described above. Known barite mineralization occurs that appears to be associated with internal faulting of Ordovician age rocks near areas containing abundant ferrous-iron minerals and calcite, serpentine, chlorite and (or) epidote and with or without muscovite.

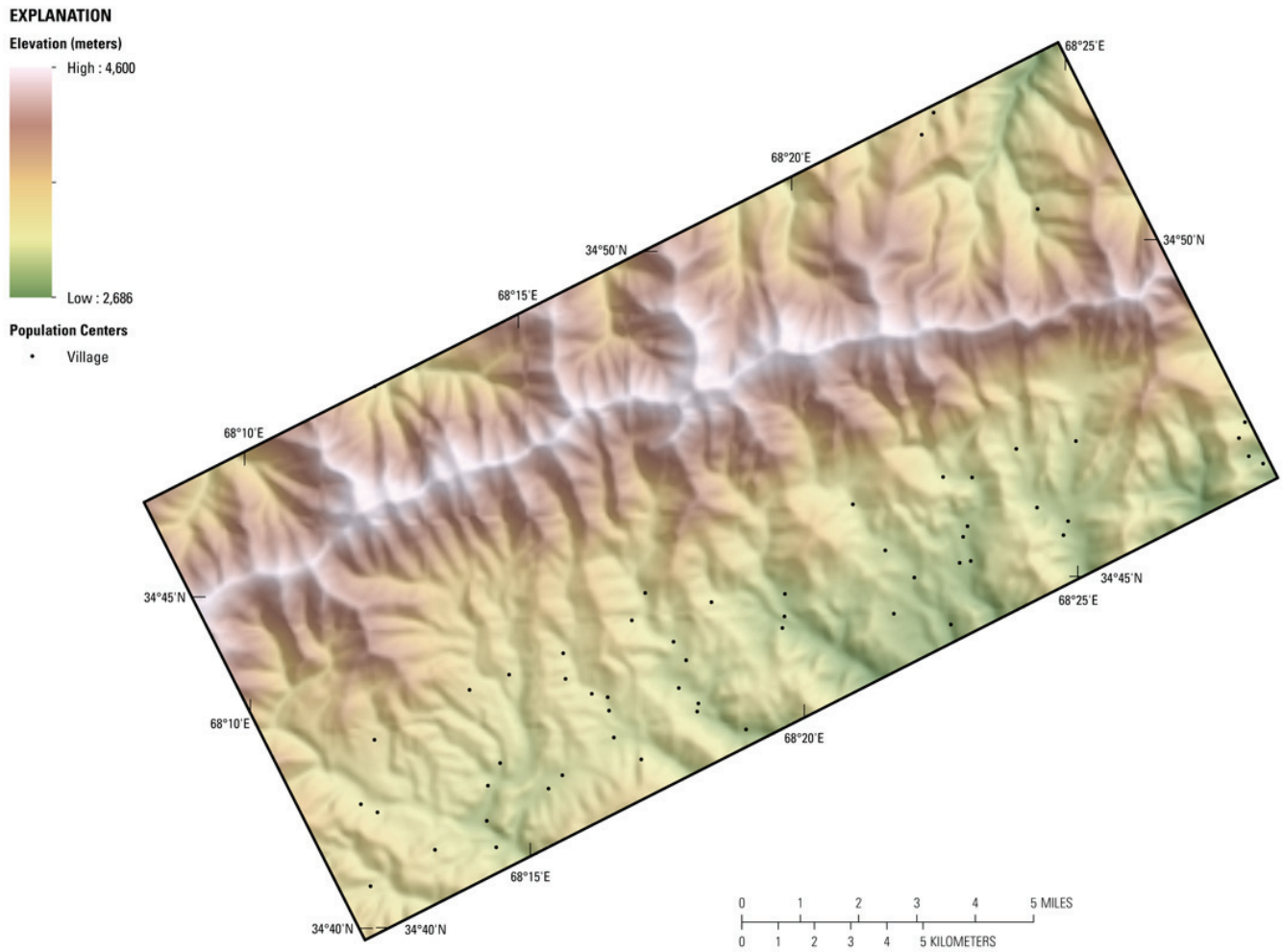

Figure 7B–25. Shaded-relief map showing the elevation of the Northeast Haji-Gak subarea. The darker brown tones indicate the higher elevations and the lower elevations are represented by the green tones. Two rivers bound the area outside the subarea; both rivers flow in the southwest-northeast direction with tributaries draining into them from the northwest and southeast.

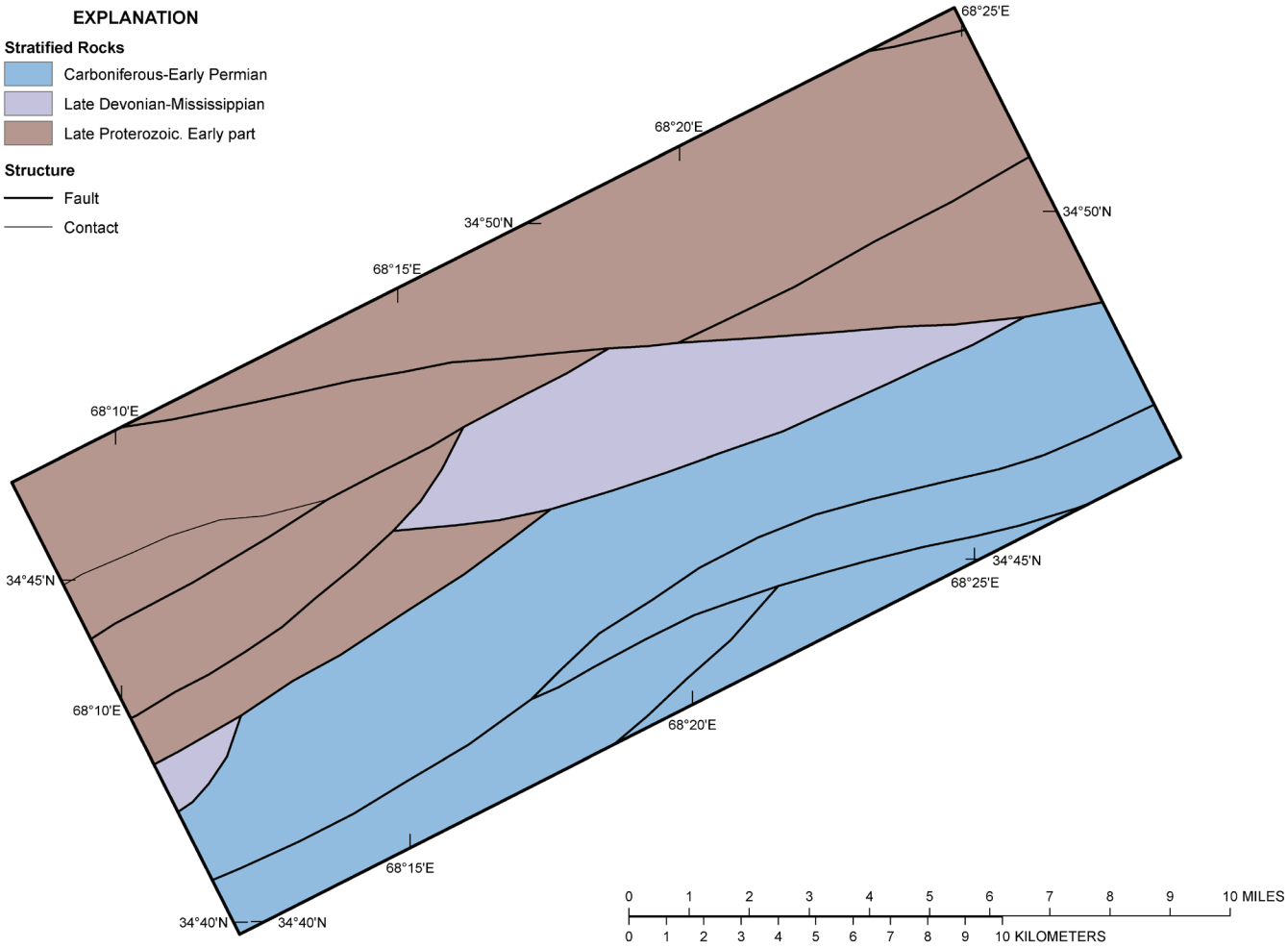

Figure 7B–26. Geologic map of the Northeast Haji-Gak subarea of the Haji-Gak area of interest taken from the 1:500,000-scale geologic map of Afghanistan (Dronov and others, 1972).

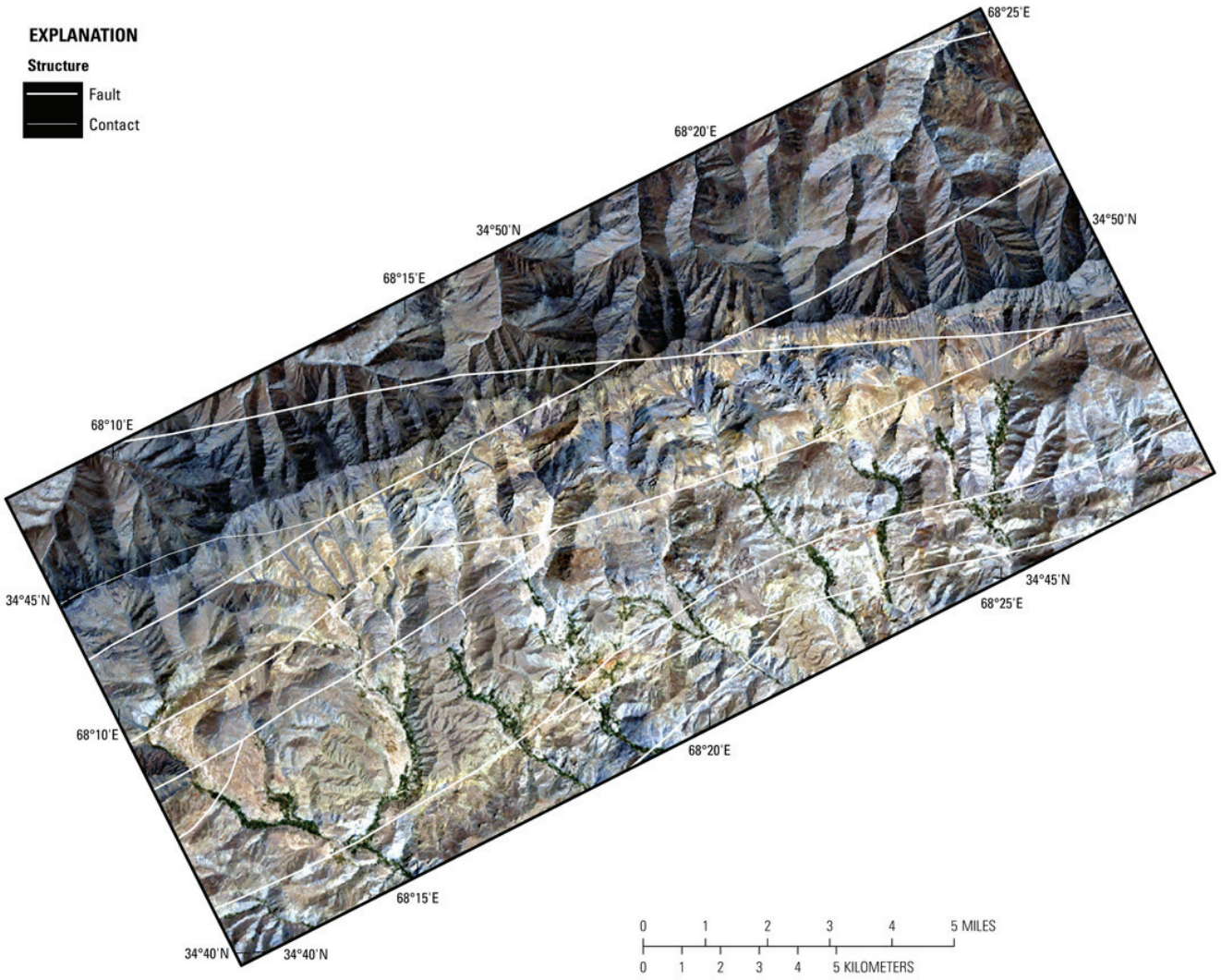

Figure 7B–27. The fault traces (Peters and others, 2007) are placed on Landsat Thematic Mapper (TM) images (Davis, 2007). Color difference in the TM data correlate with different geologic units.

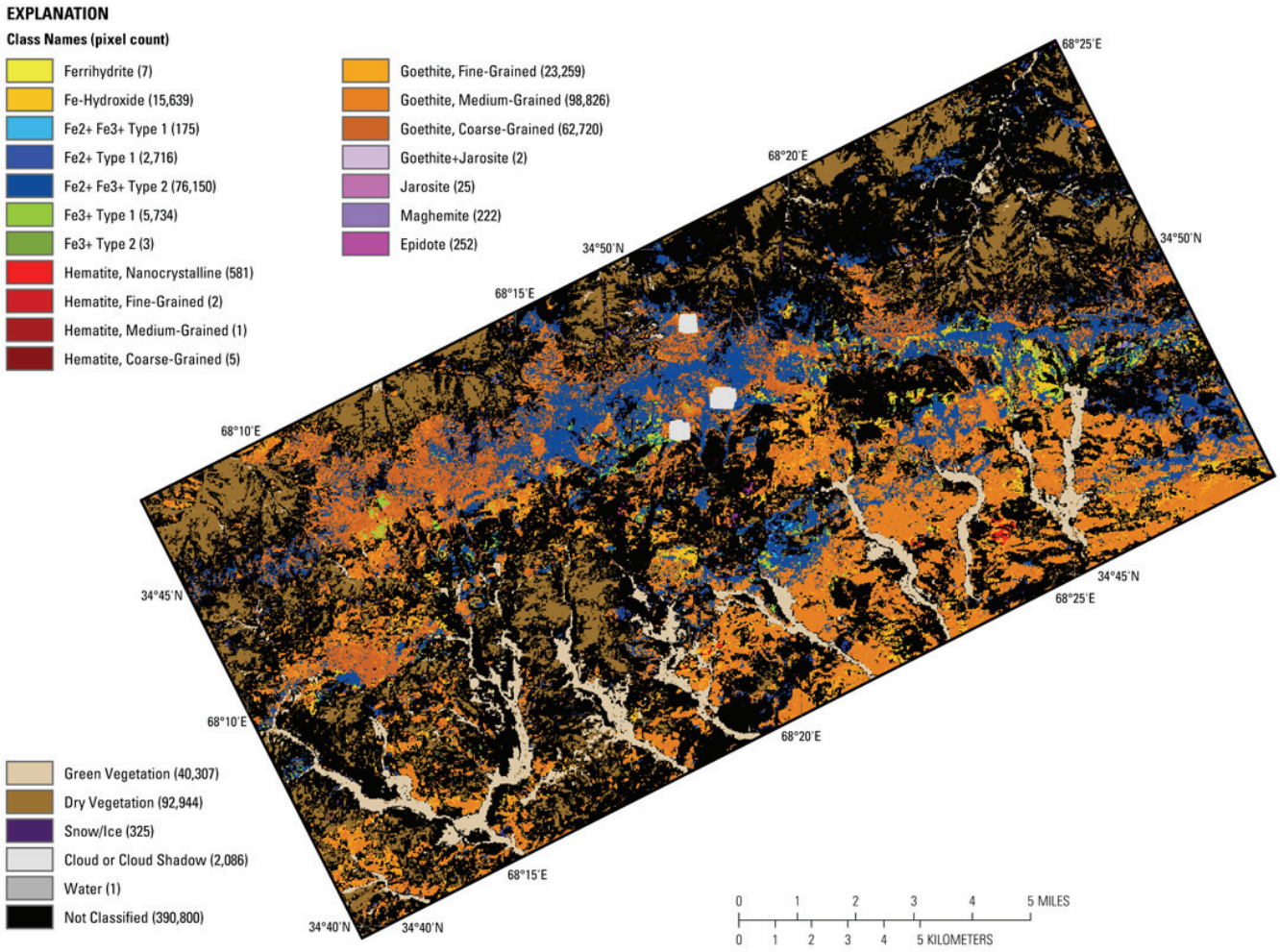

Figure 7B–28. The iron-bearing and other alteration minerals detected in the HyMap data of the Northeast Haji-Gak subarea are shown in this image.

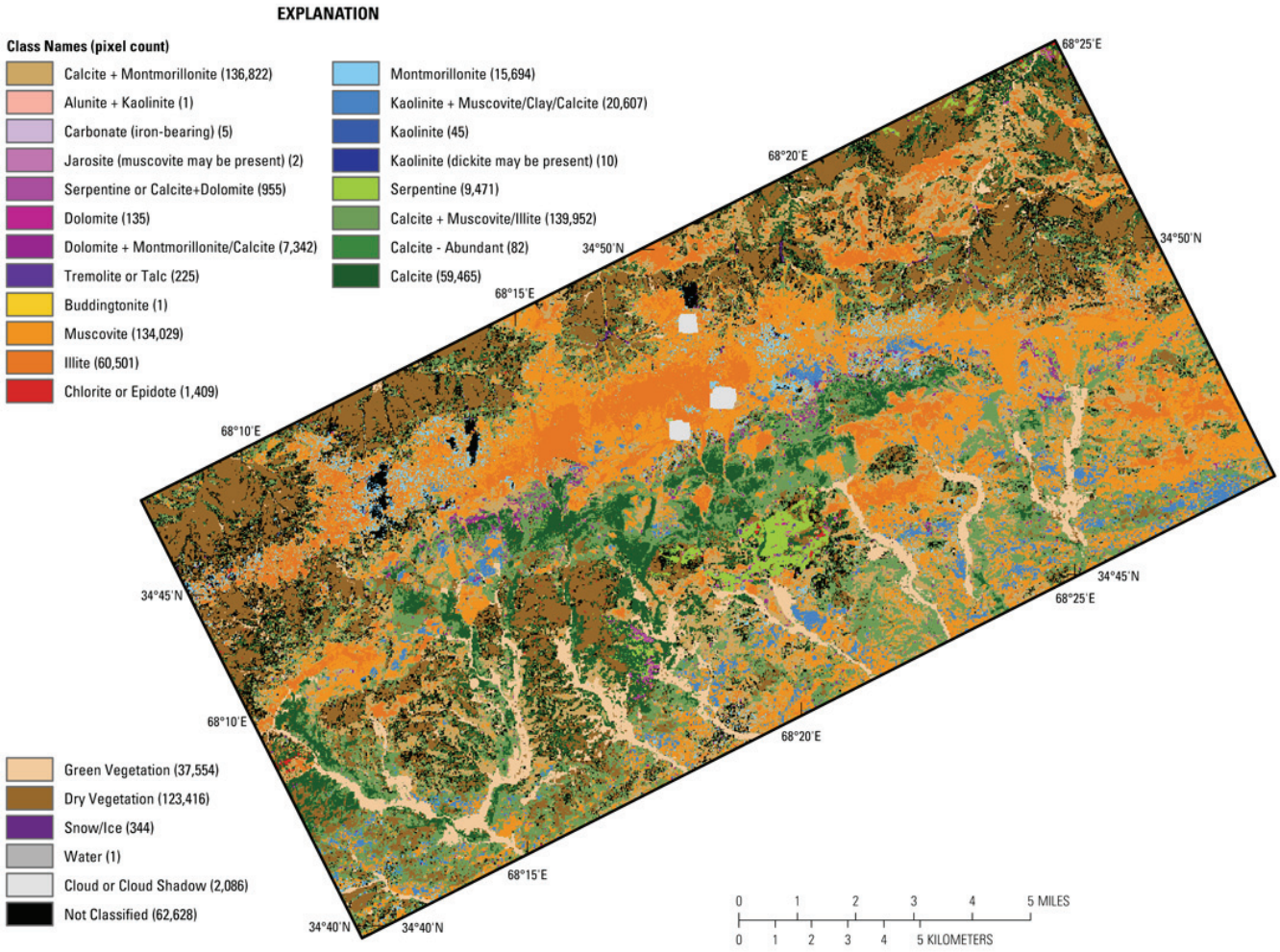

Figure 7B–29. Map showing the distribution of clays, carbonates, phyllosilicates, sulfates, altered minerals, and other materials for the Northeast Haji-Gak subarea of the Haji-Gak area of interest using the HyMap data.

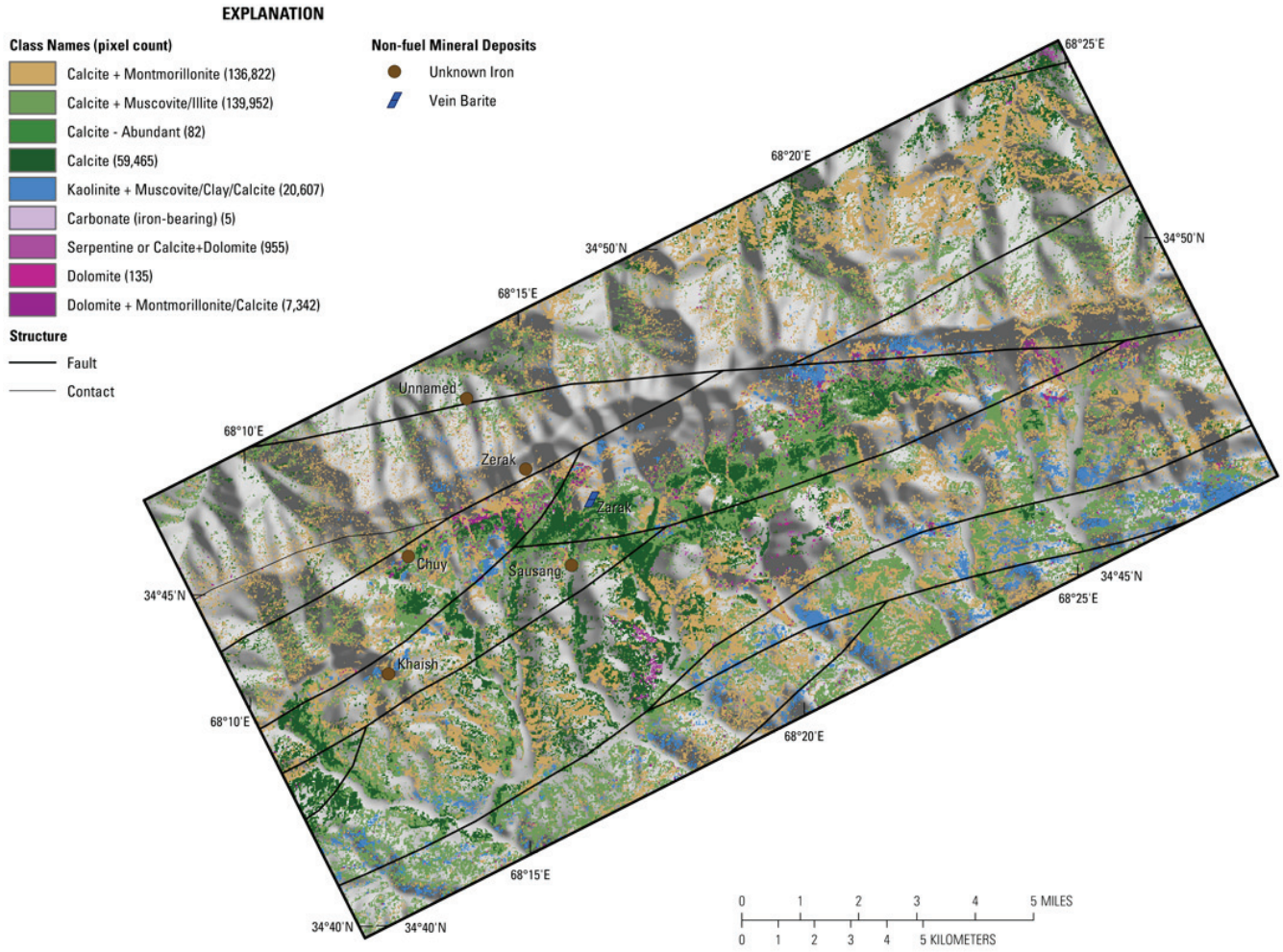

Figure 7B–30. Map showing the distribution of carbonate-bearing minerals in the Northeast Haji-Gak subarea detected in the HyMap data. The figure shows calcite, kaolinite, and dolomite within Paleozoic rocks in the southern half of the image.

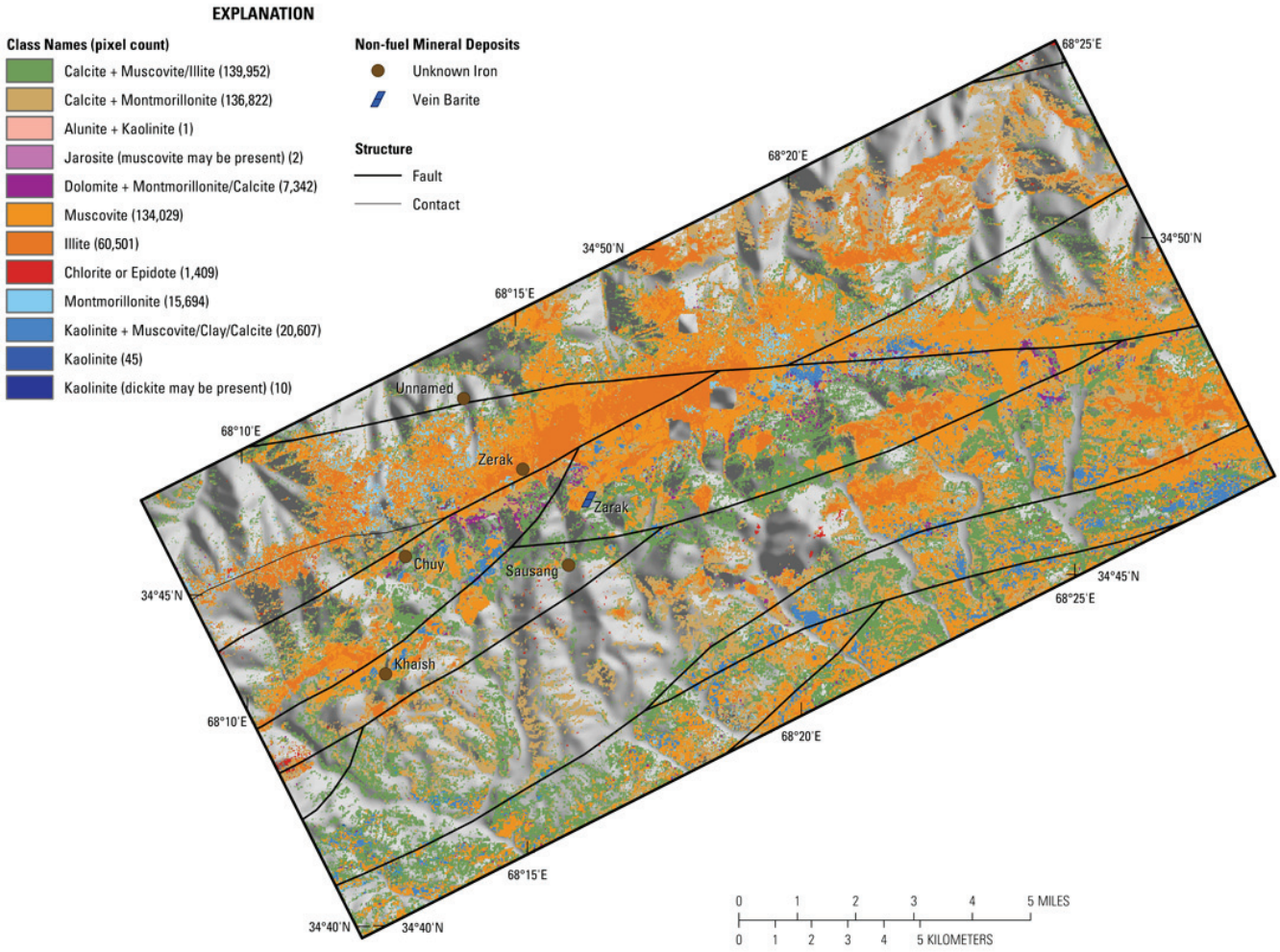

Figure 7B–31. Map showing the distribution of clays and micas in the Northeast Haji-Gak subarea that were mapped using the HyMap data. The figure shows the occurrence of muscovites and illites, chlorite or epidote, and kaolinite group minerals.

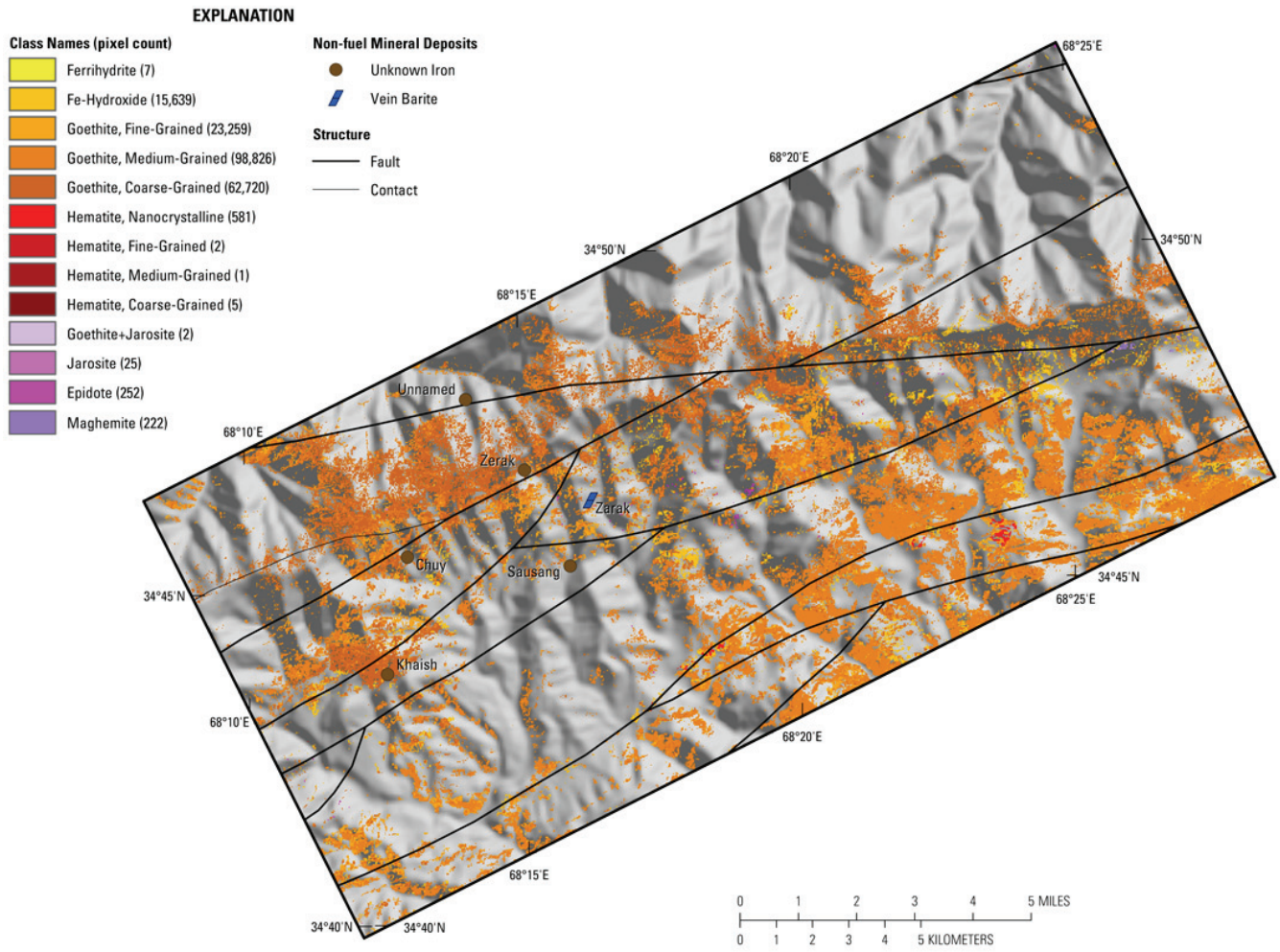

Figure 7B–32. Map showing the distribution of iron hydroxides and iron oxides for the Northeast Haji-Gak subarea.

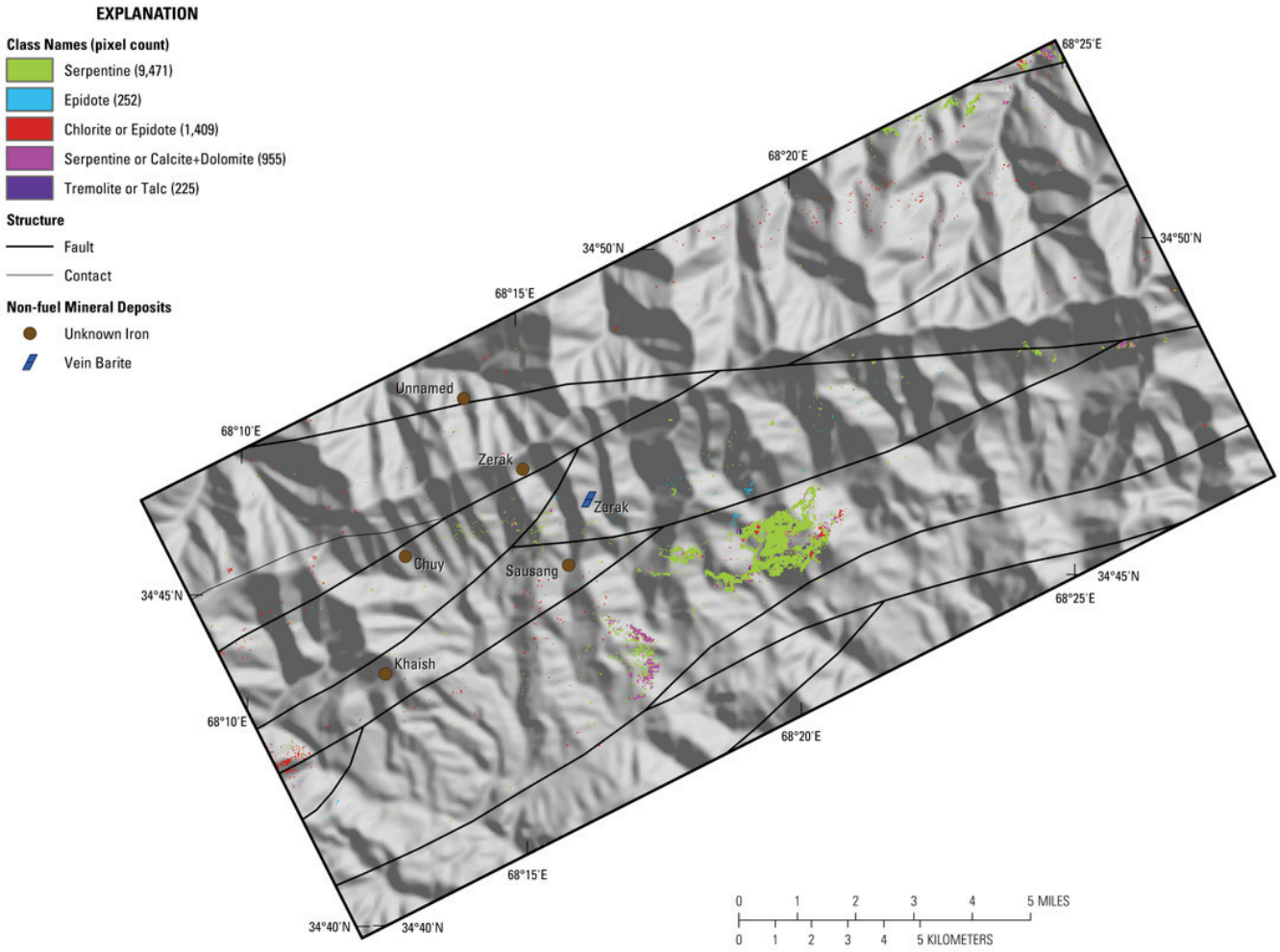

Figure 7B–33. Image showing the very limited occurrence of common secondary minerals detected in the HyMap data for the Northeast Haji-Gak subarea.

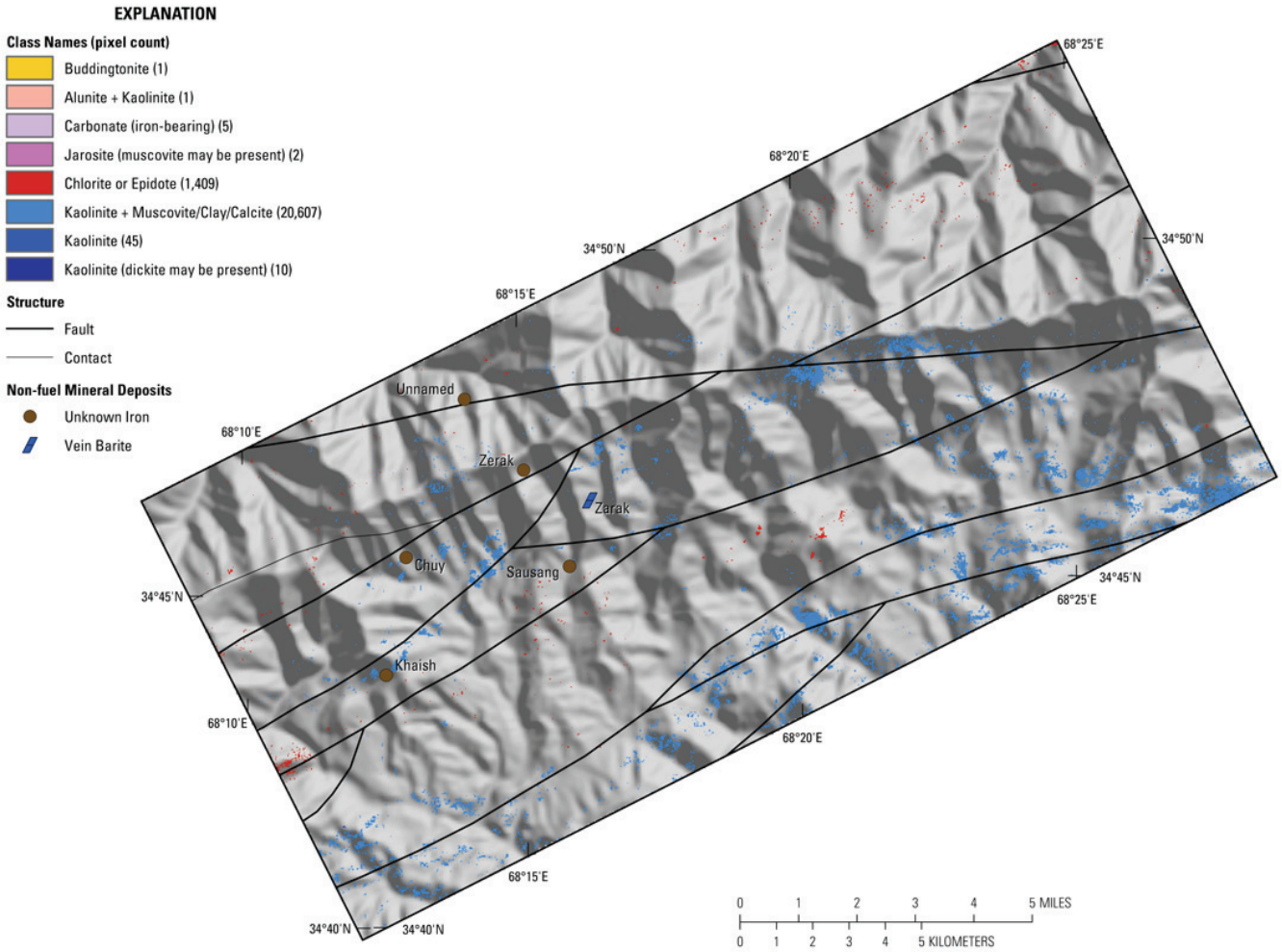

Figure 7B–34. Common alteration materials detected in the HyMap data are shown on this map.

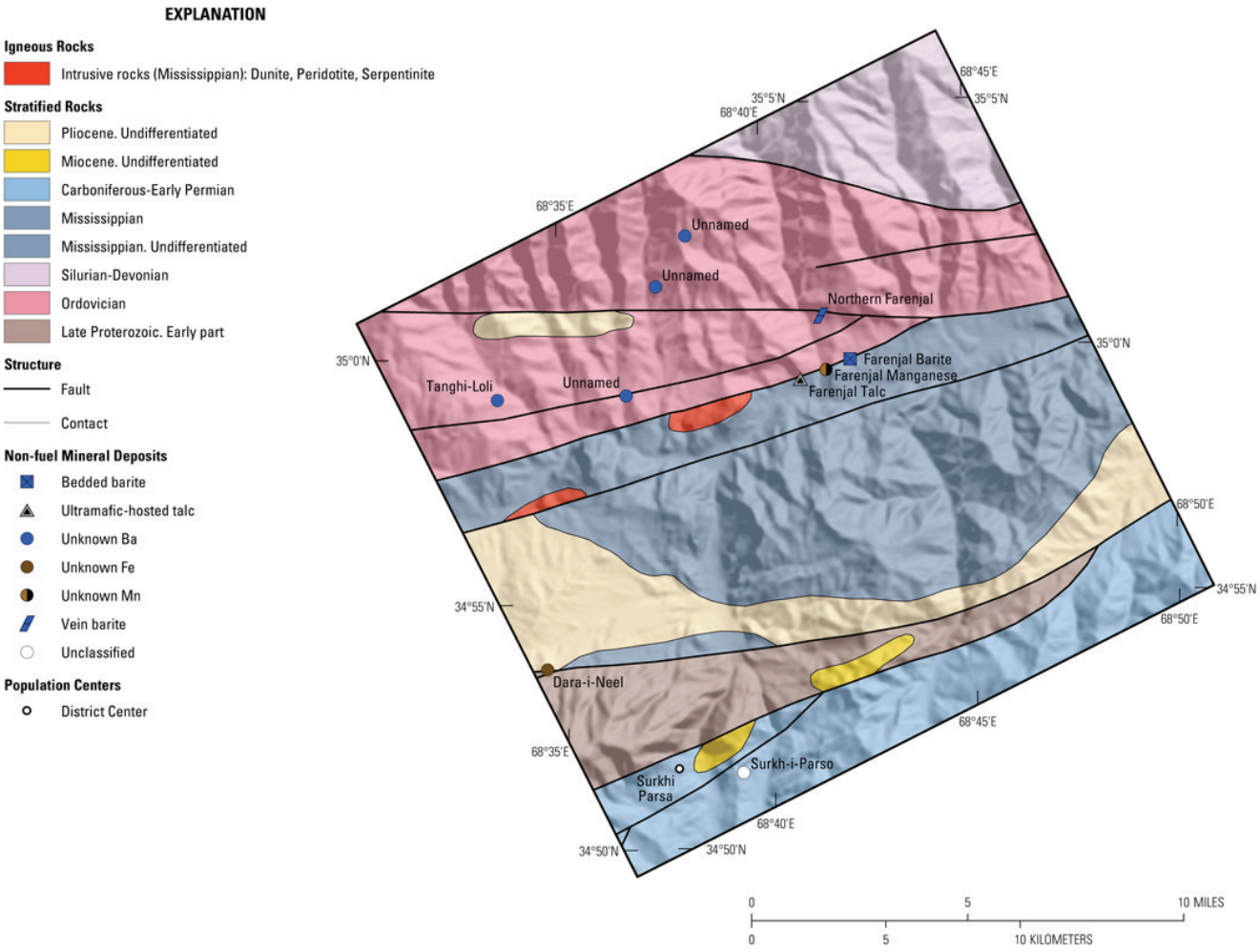

Figure 7B–35. Map showing the known mineral occurrences in the Farenjal subarea of the Haji-Gak area of interest. The subarea includes iron, barite, manganese, and talc deposits.

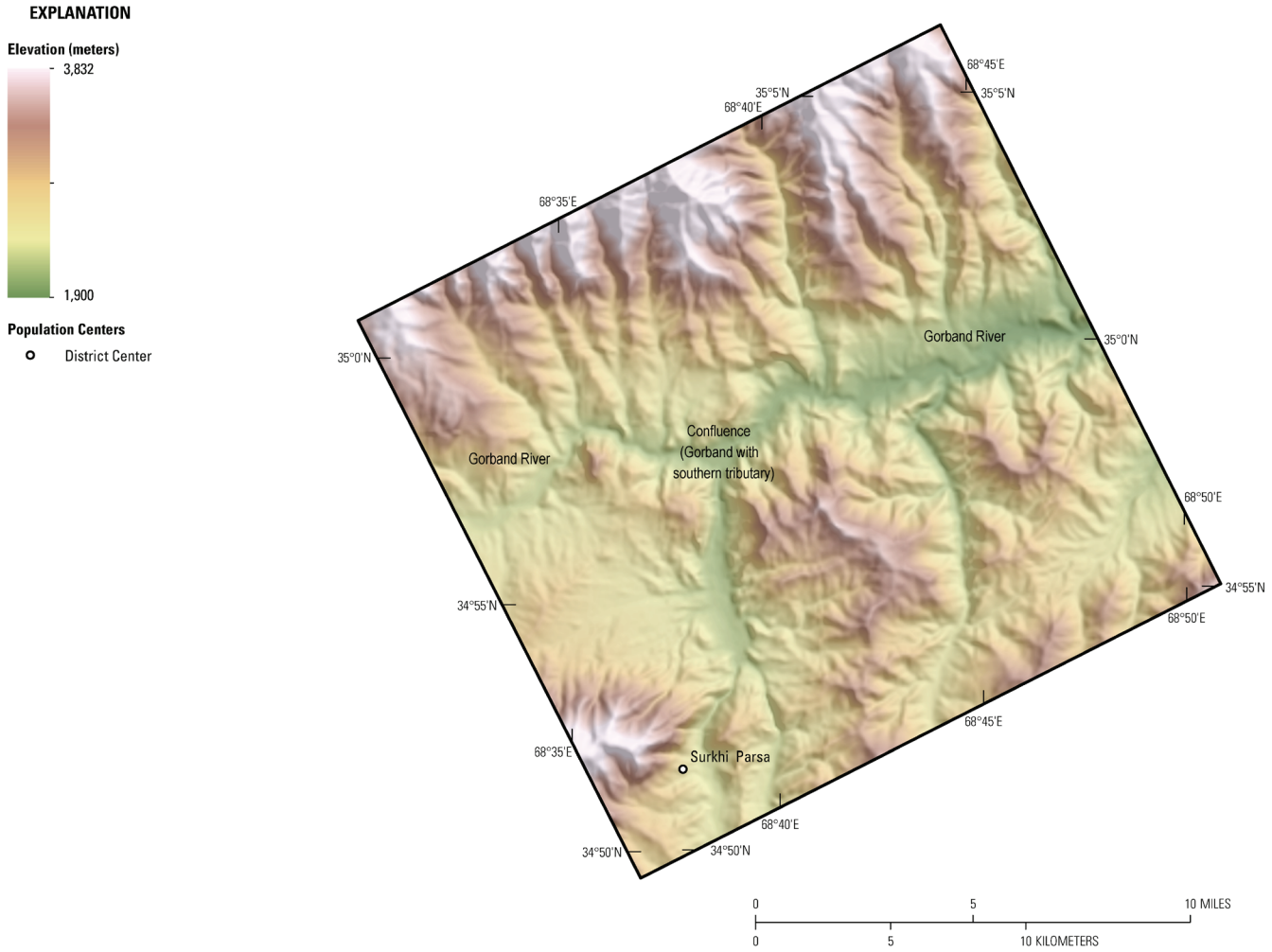

Figure 7B–36. Shaded-relief map showing the elevation of the Farenjal subarea. The darker brown tones indicate the higher elevations and the lower elevations are represented by the green tones. The Gorband River flows west to east through the middle of the subarea, where it is joined by tributaries flowing from the north and south.

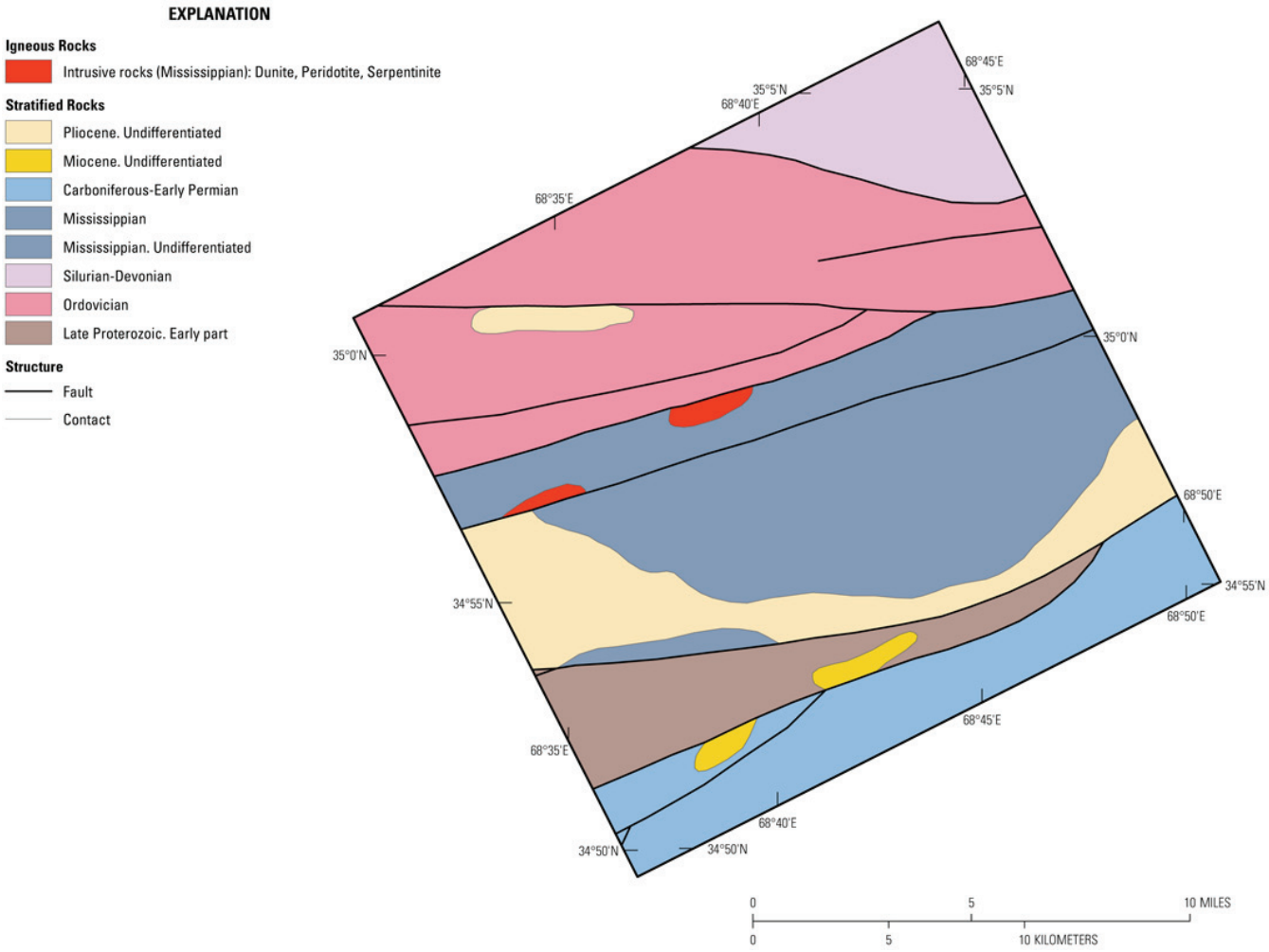

Figure 7B–37. Geologic map of the Farenjal subarea of the Haji-Gak area of interest is taken from the Russian 1:500,000-scale geologic map of Afghanistan (Dronov and others, 1972.)

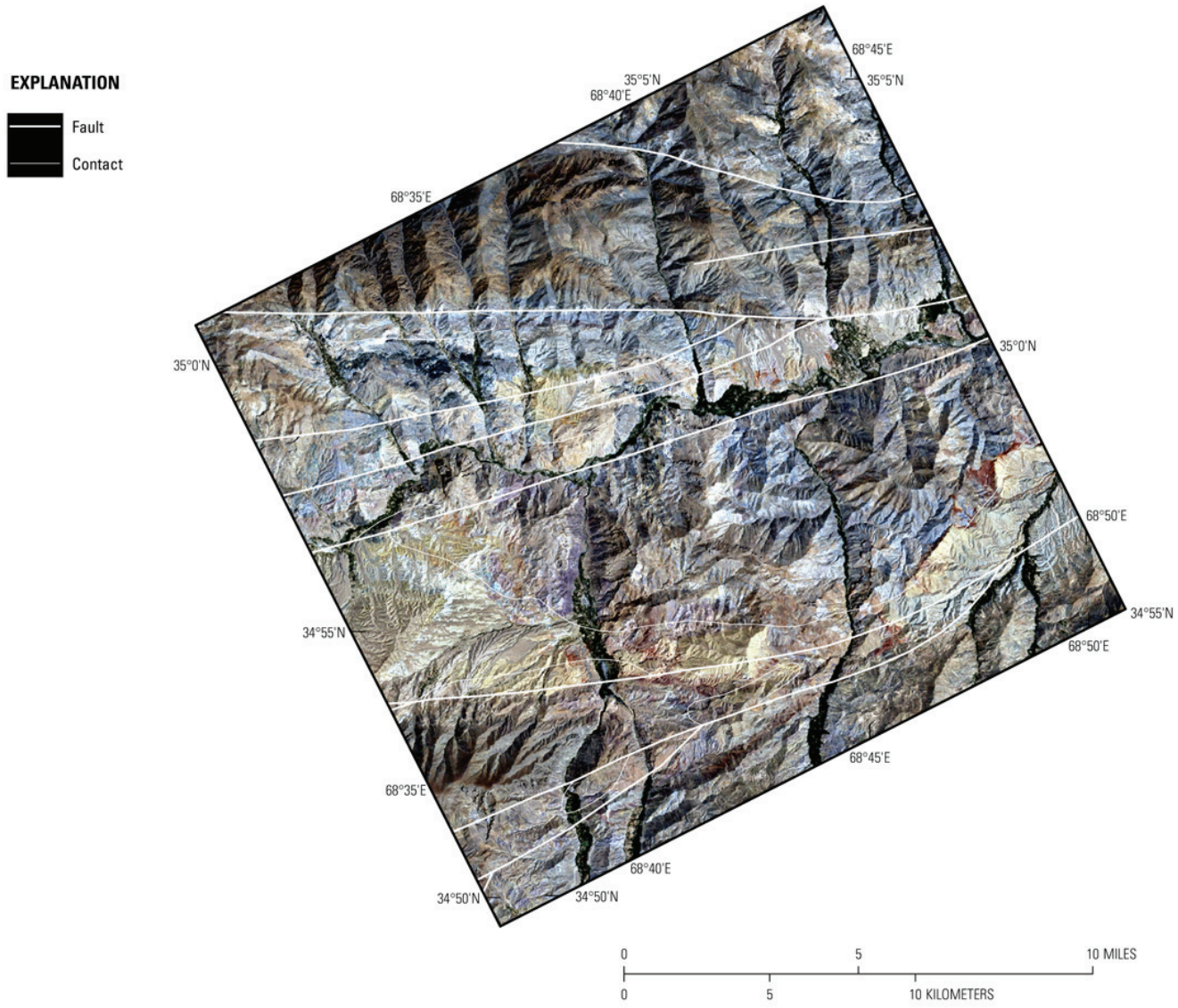

Figure 7B–38. The fault traces (Peters and others, 2007) are placed on a Landsat Thematic Mapper (TM) image (Davis, 2007). Color difference in the TM data correlate with different geologic units.

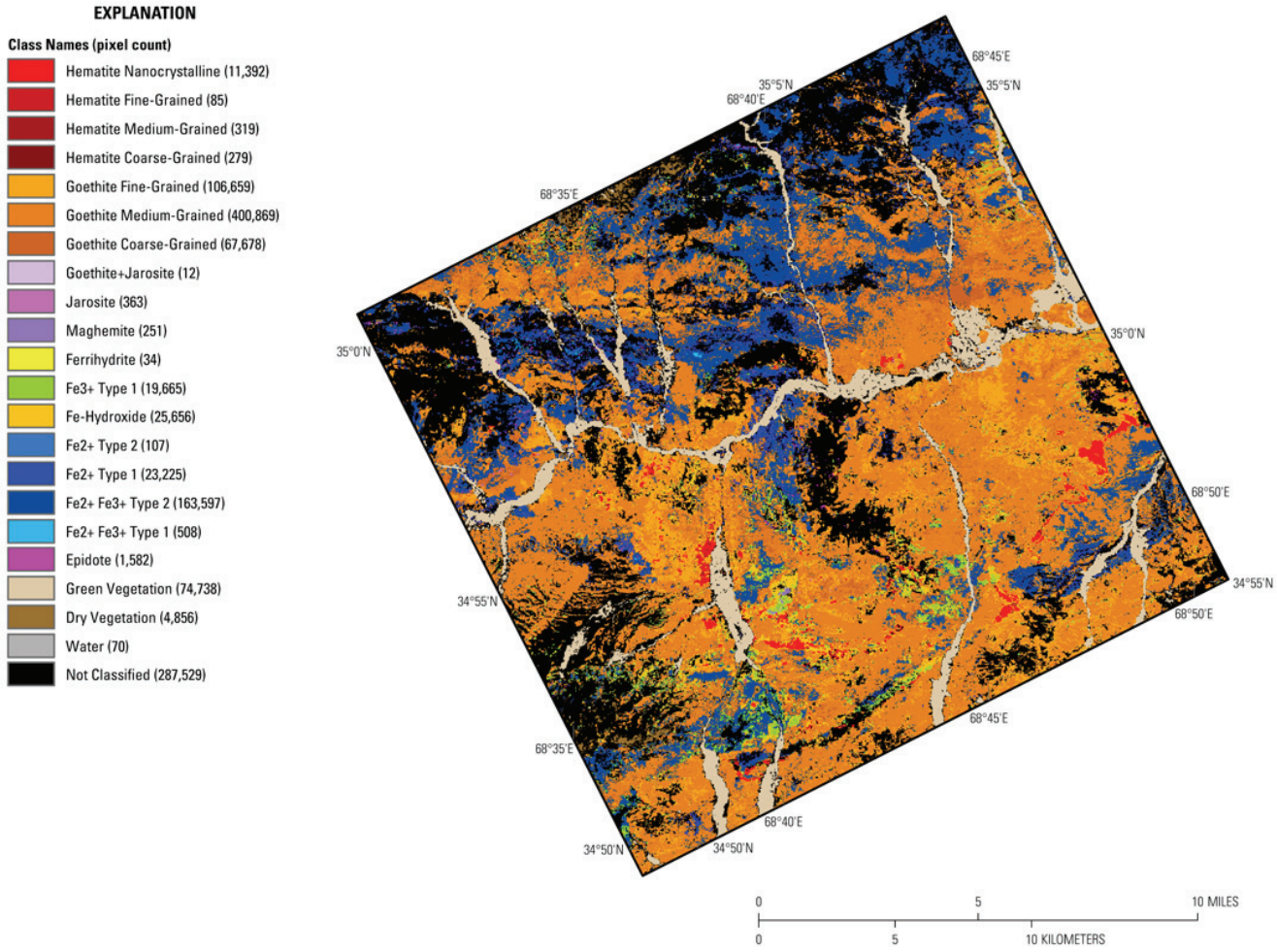

Figure 7B–39. Map showing the iron-bearing and other alteration minerals detected in the HyMap data for the Farenjal subarea.

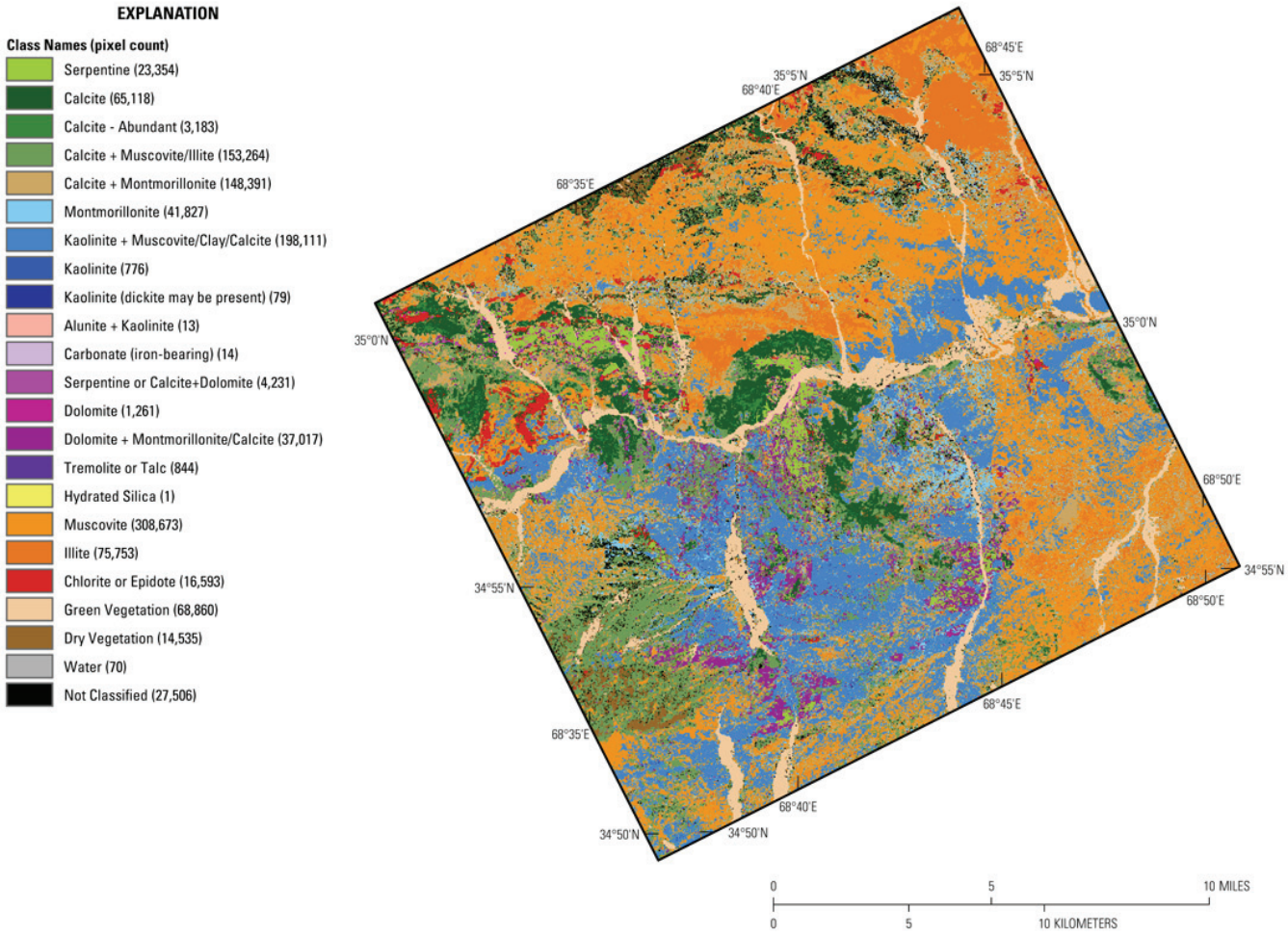

Figure 7B–40. Map showing the distribution of clays, carbonates, phyllosilicates, sulfates, altered minerals, and other materials for the Farenjal subarea of the Haji-Gak area of interest using the HyMap data.

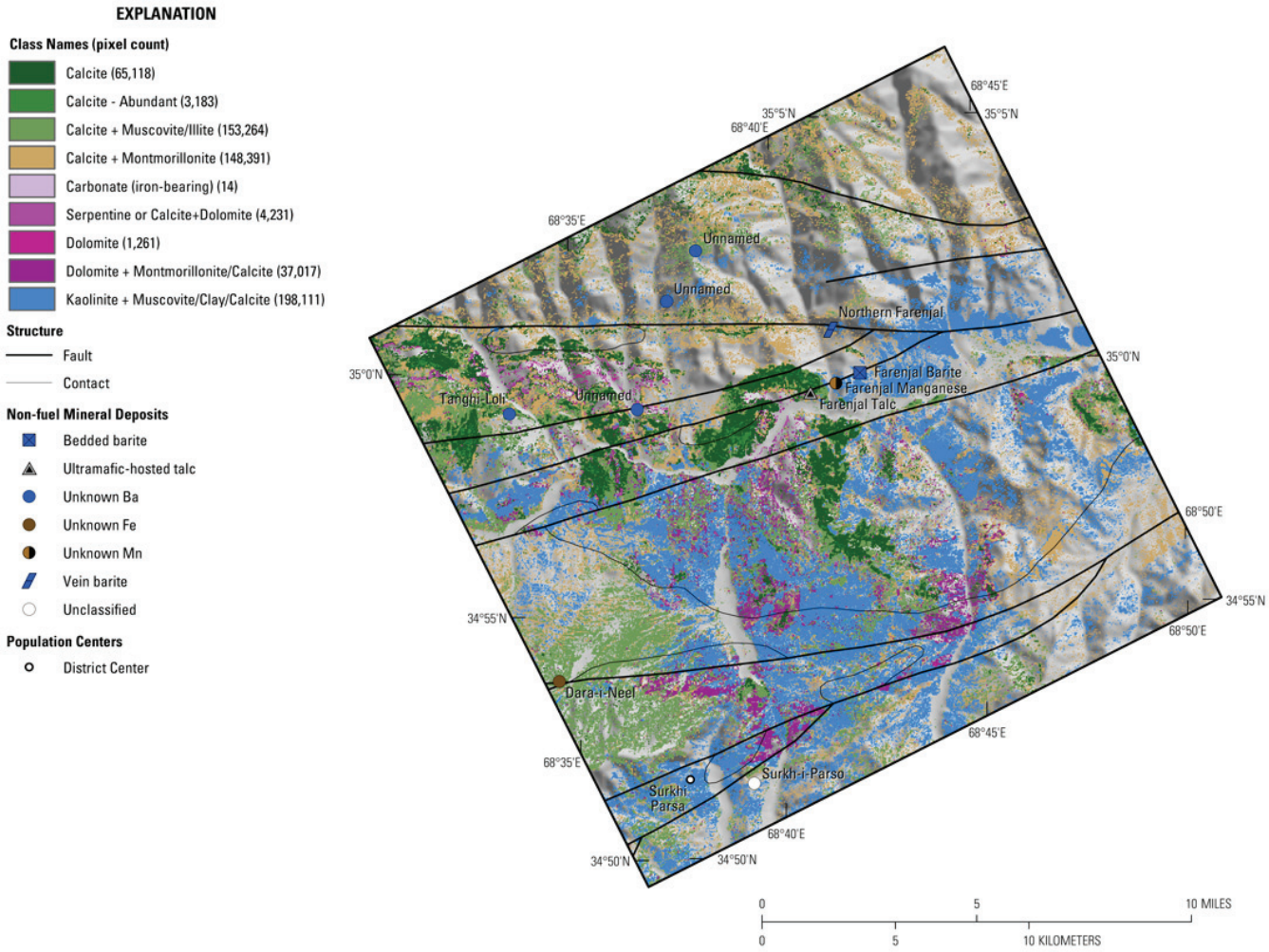

Figure 7B–41. Map showing the distribution of carbonate-bearing minerals in the Farenjal subarea detected in the HyMap data. The figure shows zones of abundant calcite, kaolinite, and dolomite.

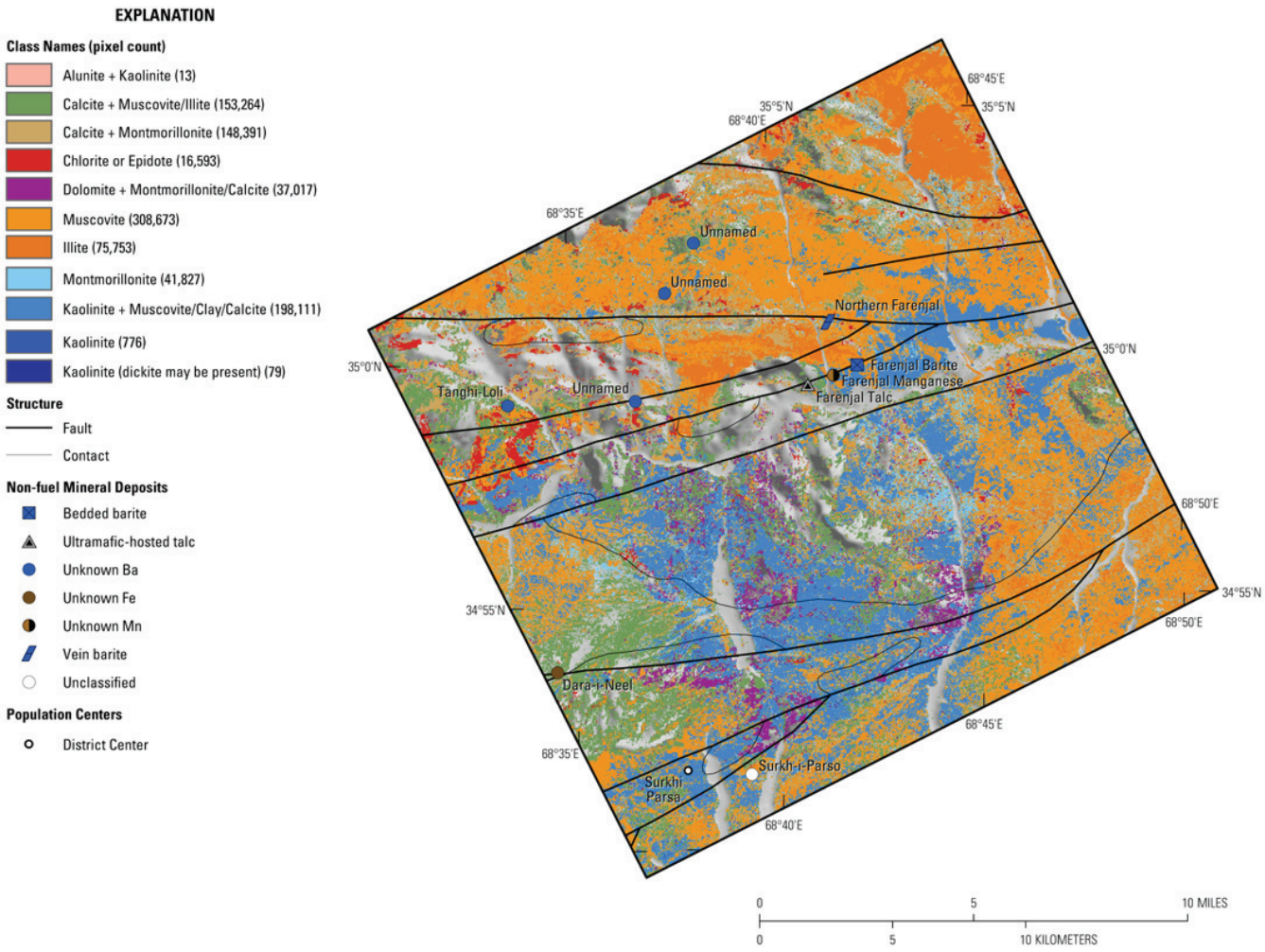

Figure 7B–42. Map showing the distribution of clays and micas in the Farenjal subarea that were mapped using the HyMap data. The figure shows the occurrence of muscovites and illites, chlorite or epidote, dolomite, and kaolinite group minerals.

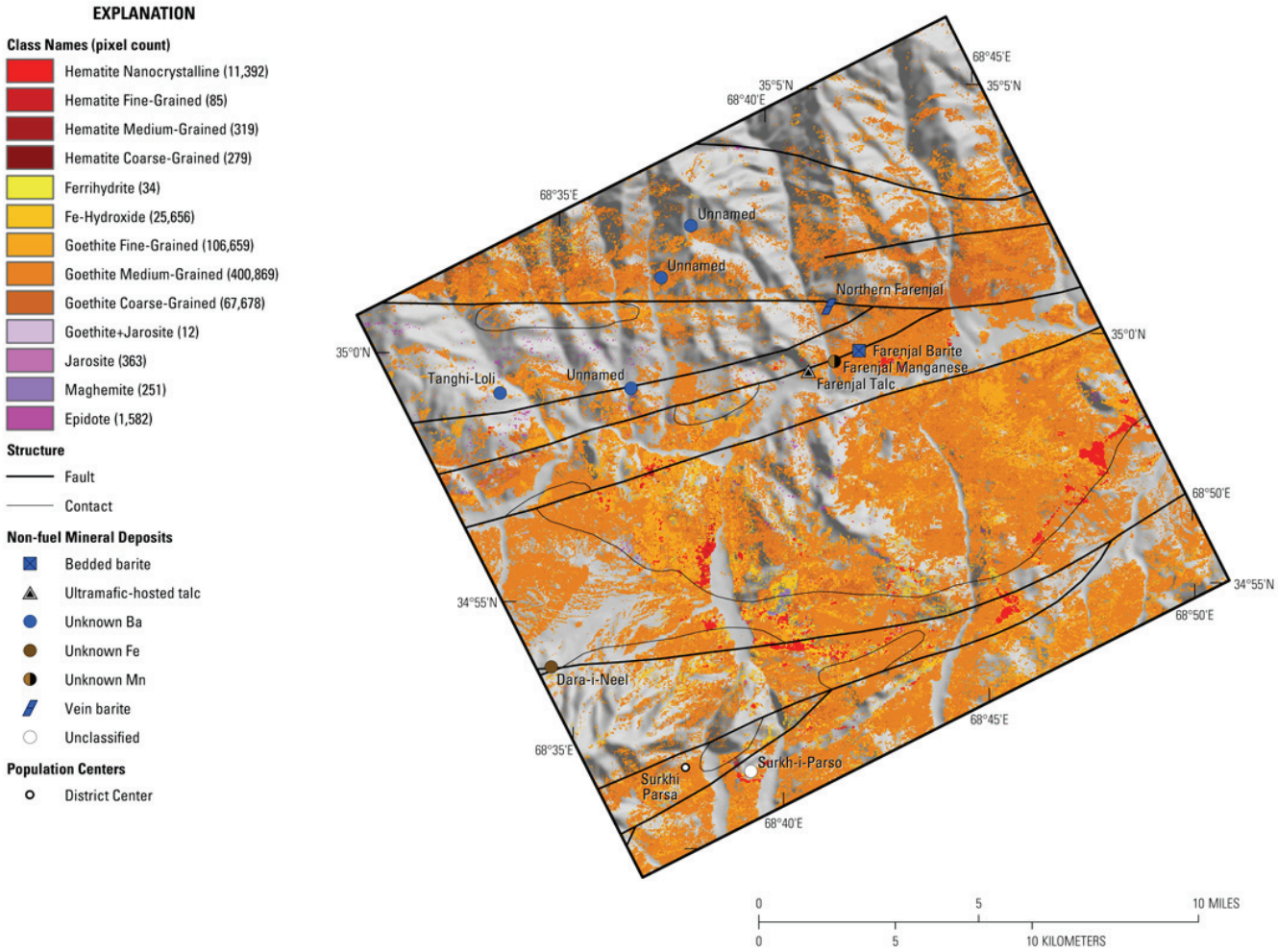

Figure 7B–43. Map showing the distribution of iron hydroxides and iron oxides for the Farenjal subarea.

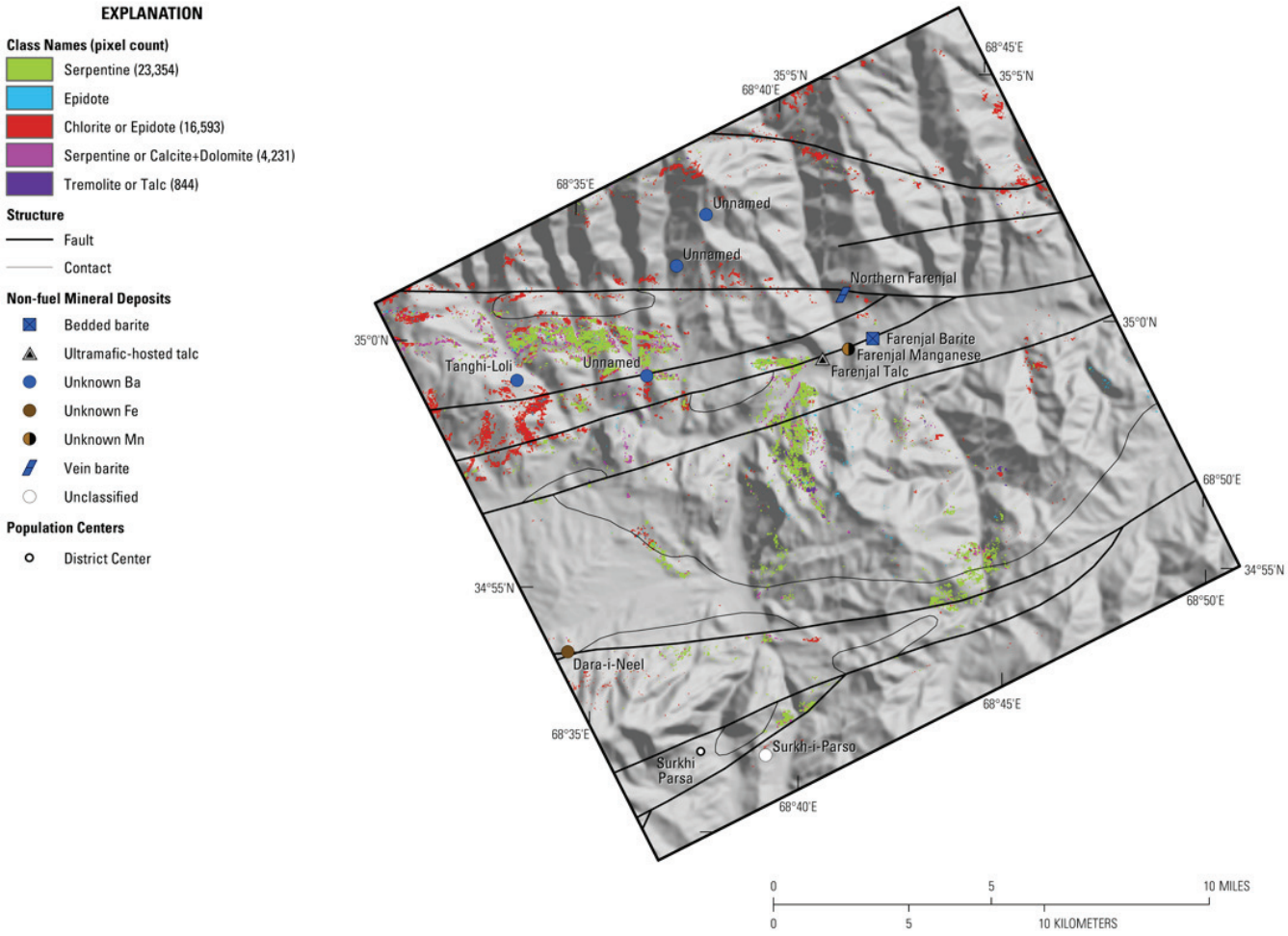

Figure 7B–44. Map showing the very limited occurrence of common secondary minerals detected in the HyMap data for the Farenjal subarea of the Haji-Gak area of interest.

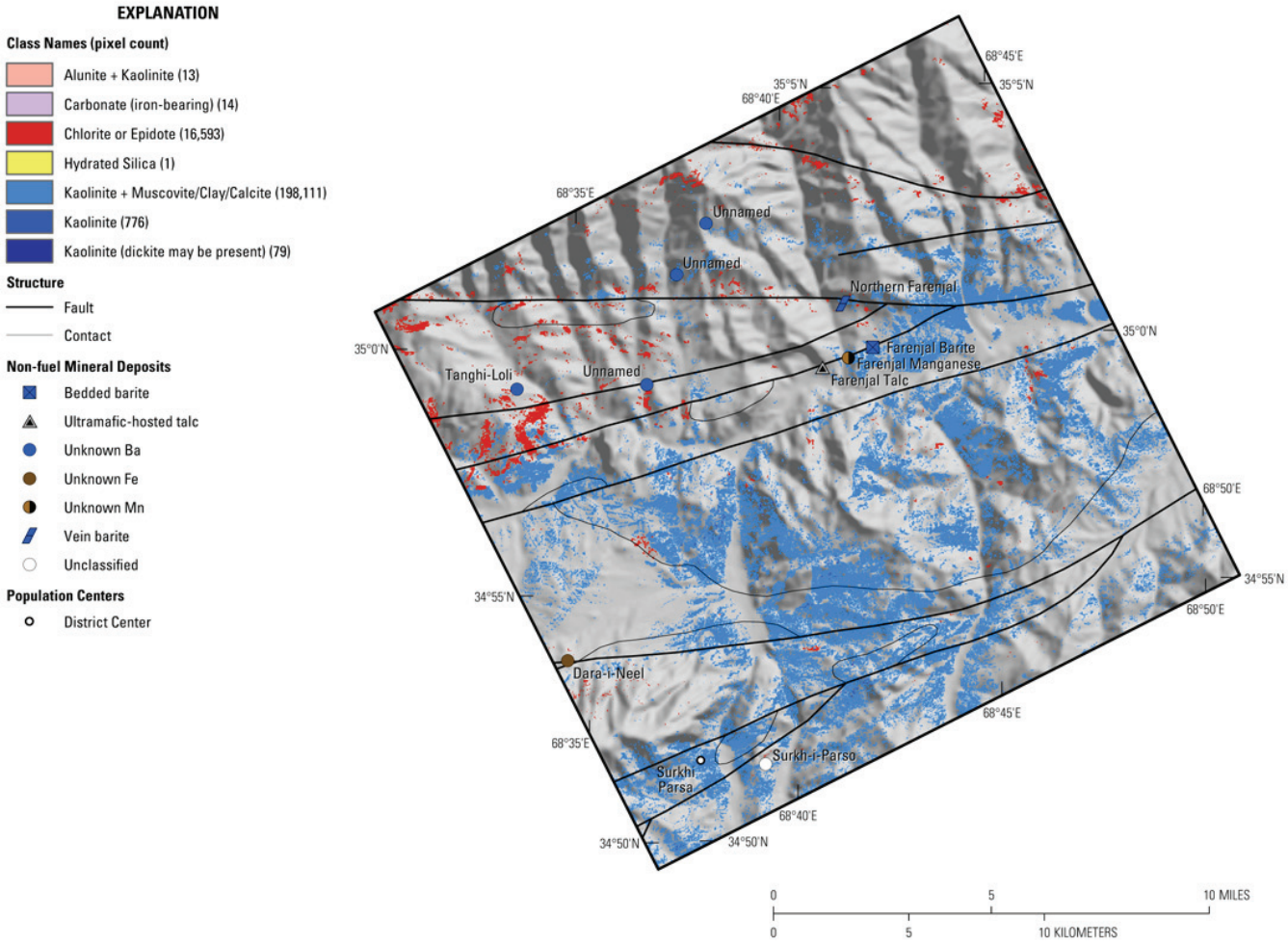

Figure 7B–45. Map showing the common alteration materials detected in the HyMap data for the Farenjal subarea.

7B.5 References Cited

Abdullah, Sh., and Chmyriov, V.M., 1977, Geological map of Afghanistan: Kabul, Afghanistan, Ministry of Mining and Industry of Democratic Republic of Afghanistan, 1:500,000 scale.

Abdullah, Sh., Chmyriov, V.M., Stazhilo-Alekseev, K.F., Dronov, V.I., Gannan, P.J., Rossovskiy, L.N., Kafarskiy, A.Kh., and Malyarov, E.P., 1977, Mineral resources of Afghanistan (2nd edition): Kabul, Afghanistan, Republic of Afghanistan Geological and Mineral Survey, 419 p.

Clark, R.N., Swayze, G.A., Livo, K.E., Kokaly, R.F., King, T.V.V., Dalton, J.B., Vance, J.S., Rockwell, B.W., Hoefen, T., and McDougal, R.R., 2003a, Surface reflectance calibration of terrestrial imaging spectroscopy data: A tutorial using AVIRIS, *in* Green, R.O., ed., Proceedings of the 11th JPL Airborne Earth Science Workshop: JPL Publication 03-4, p. 43-63.

Clark, R.N., Swayze, G.A., Livo, K.E., Kokaly, R.F., Sutley, S.J., Dalton, J.B., McDougal, R.R., and Gent, C.A., 2003b, Imaging spectroscopy: Earth and planetary remote sensing with the USGS Tetracorder and Expert Systems: Journal of Geophysical Research, v. 108, no. E12, 5131, doi:10.1029/2002JE001847, 44p.

Cocks, T., Jenssen, R., Stewart, A., Wilson, I., and Shields, T., 1998, The HyMap airborne hyperspectral sensor—The system, calibration and performance, *in* Schaepman, M., Schlapfer, D., and Itten, K.I., eds., Proceedings of the 1st EARSeL Workshop on Imaging Spectroscopy, 6–8 October 1998, Zurich: Paris, European Association of Remote Sensing Laboratories, p. 37–43.

Davis, P.A., 2007, Landsat ETM+ false-color image mosaics of Afghanistan: U.S. Geological Survey Open-File Report 2007–1029, 22 p.

Doebrich, J.L., and Wahl, R.R., comps., with contributions by Doebrich, J.L., Wahl, R.R., Ludington, S.D., Chirico, P.G., Wandrey, C.J., Bohannon, R.G., Orris, G.J., Bliss, J.D., and ____, 2006, Geologic and mineral resource map of Afghanistan: U.S. Geological Survey Open File Report 2006-1038, scale 1:850,000, available at *http://pubs.er.usgs.gov/usgspubs/ofr/ofr2005103*.

Dronov, V.I., Kalimulin, S.M., Sborshchikov, I.M., Svezhentsov, V.P., Chistyakov, A.N., Zelensky, E.D., and Cherepov, P.G., 1972, The geology and minerals of North Afghanistan (parts of map sheets 400-II and 500-I, the Kaysar-Hari Rod Interfluve area): Kabul, DGMS, 44.

Hoefen, T.M., Kokaly, R.F., and King, T.V.V., 2010, Calibration of HyMap data covering the country of Afghanistan, *in* Proceedings of the 15th Australasian Remote Sensing and Photogrammetry Conference, Alice Springs, Australia, September 12–17, 2010, p. 409, available at *http://dl.dropbox.com/u/81114/15ARSPC-Proceedings.zip/*.

King, T.V.V., Kokaly, R.F., Hoefen, T.M., and Knepper, D.H., 2010, Resource mapping in Afghanistan using HyMap data, *in* Proceedings of the 15th Australasian Remote Sensing and Photogrammetry Conference, Alice Springs, Australia, September 12–17, 2010, p. 500, available at *http://dl.dropbox.com/u/81114/15ARSPC-Proceedings.zip/*.

King, T.V.V., Johnson, M.R., Hoefen, T.M., Kokaly, R.F., and Livo, K.E., 2011, Mapping potential mineral resource anomalies using HyMap data, *in* King, T.V.V., Johnson, M.R., Hubbard, B.E., and Drenth, B.J., eds, Identification of mineral resources in Afghanistan—Detecting and mapping resource anomalies in prioritized areas using geophysical and remote sensing (ASTER and HyMap) data in Afghanistan: U.S. Geological Survey Open-File Report 2011–1229, available at *http://pubs.usgs.gov/of/2011/1229/*.

King, T.V.V., Kokaly, R.F., Hoefen, T.M., Dudek, K. and Livo, K.E., 2011, Surface materials map of Afghanistan—Iron-bearing minerals and other materials: U.S. Geological Survey Scientific Investigations Map 3152–B.

Kokaly, R.F., King, T.V.V., and Livo, K.E., 2008, Airborne hyperspectral survey of Afghanistan 2007—Flight line planning and HyMap data collection: U.S. Geological Survey Open-File Report 2008–1235, 14 p.

Kokaly, Ray, 2011, PRISM—Processing routines in IDL for spectroscopic measurements: U.S. Geological Survey Open-File Report 2011–1155, available at *http://pubs.usgs.gov/of/2011/1155/*.

Kokaly, R.F., King, T.V.V., Hoefen, T.M., Dudek, K. and Livo, K.E., 2011, Surface materials map of Afghanistan—Carbonates, phyllosilicates, sulfates, altered minerals, and other materials: U.S. Geological Survey Scientific Investigations Map 3152–A.

okaly, R.F., 2010, Spectroscopic remote sensing for material identification and mapping, *in* Proceedings of the 15th Australasian Remote Sensing and Photogrammetry Conference, Alice Springs, Australia, September 12–17, 2010, p. 409, available at *http://dl.dropbox.com/u/81114/15ARSPC-Proceedings.zip/*.

Kusov, I.K., Smirnov, M.S., and Reshetniak, V.V., 1965, Report of the results of prospecting-survey and reconnaissance works for iron ores in central Afghanistan with reserve calculation of Hajigak Deposit for 1963-1964: USSR v/o Technoexport, contract no. 640, 3 volumes with English translation, Royal Government of Afghanistan, Ministry of Mines and Industries internal report, contract No. 640, Kabul, unpub. data, 269 p.

Peters, S.G., Ludington, S.D., Orris, G.J., Sutphin, D.M., Bliss, J.D., and Rytuba, J.J., eds., and the U.S. Geological Survey-Afghanistan Ministry of Mines Joint Mineral Resource Assessment Team, 2007, Preliminary non-fuel mineral resource assessment of Afghanistan: U.S. Geological Survey Open-File Report 2007–1214, 810 p., 1 CD–ROM. (Also available at *http://pubs.usgs.gov/of/2007/1214/*.)